Morphodynamics of Barrier Island Systems

Dissertation zur Erlangung des Doktorgrades der Naturwissenschaften

im Fachbereich Geowissenschaften der Universität Bremen

vorgelegt von

Gerald Herrling

Bremen, 23. Oktober 2014

Gutachter:

PD Dr. Christian Winter

Prof. Dr. Tobias Mörz

Tag des Dissertationskolloquiums:

6. März 2015

Prüfungsausschuss:

PD Dr. Christian Winter

Prof. Dr. Tobias Mörz

Prof. Dr. Dierk Hebbeln

Prof. Dr. Andrés Fernando Osorio Arias

Dr. Marius Becker

BSc. Markus Benninghoff

Gerald Herrling
MARUM
Leobenerstr.
28359 Bremen

23.10.2014

Erklärung

Hiermit versichere ich, dass ich die Arbeit ohne unerlaubte fremde Hilfe angefertigt habe, keine anderen als die von mir angegebenen Quellen und Hilfsmittel benutzt habe und die den benutzten Werken wörtlich oder inhaltlich entnommenen Stellen als solche kenntlich gemacht habe.

Gerald Herrling

Bremen, den 23.10.2014

Contents

Acknowledgements

This study is funded by and associated with the research project WIMO (www.wimo-nordsee.de) and is financed in equal parts by two ministries in Lower Saxony: the Ministry of Environment, Energy and Climate Protection, and the Ministry of Science and Culture. Additional funding for the participation in three international conferences and an international summer school was received through the WIMO project's support program for young researchers.

I am very thankful to my supervisor, P.D. Dr. Christian Winter, who gave me the chance to freely develop the research questions and approaches of this thesis. I greatly appreciate his steady availability and openness to listening to new ideas and the ability to discuss with him my findings in an open, pleasant and fruitful atmosphere. I am grateful for his encouragement and guidance throughout the manuscript writing.

I would also like to express my gratitude to Prof. Dr. Tobias Mörz, the second reviewer.

The coastal dynamic research group is a team of inspiring young coastal researchers and friends who made the everyday working atmosphere productive and enjoyable. I am especially thankful to Dr. Marius Becker for his openness, feedback and all of the stimulating discussions on a variety of scientific topics.

Finally, I would like to express my warm thanks to my mother who always supported me. Unfortunately, my father was not able to witness my path into science that is actually so close to his lifetime's work.

Special thanks go to Anne who indulged my every whim during the last period of my finalizing thesis work.

Summary

Barrier island systems, also referred to as multiple-inlet systems, are coastal environments with shallow, interconnected tidal basins that are fringed by a chain of elongated islands. Their geomorphology and tidal habitats encompass numerous transitional zones between the land and the sea that are rich in species specially adapted to the varying hydrodynamic conditions. Morphodynamics at mixed-energy barrier island coasts have been studied for several decades on the basis of aerial photographs, field observations and numerical or analytical models. A process-based understanding of the morphological response to the driving hydrodynamic forces, however, has still not been achieved. The aim of this study is to assess the system morphodynamics in response to the interaction of tidally- and wave-induced currents, wind stress and the availability of mobile sediments. The study area is the East Frisian Wadden Sea (Germany), a lagoon-type environment with intertidal flats that are sheltered by seven inhabited barrier islands; it belongs to the Wadden Sea extending along the southern North Sea coast.

A state-of-the-art process-based model is applied as a hindcasting and experimental tool for the evaluation of relevant processes at short term (tidal cycle) to medium term (annual) time scales. The spatial scales encompass sand shoals (meso-scale) as typical morphological features at ebb-tidal deltas, to the entire system covering the upper shoreface, the barrier islands and the back-barrier basins (large-scale). The main results of the investigations are shown in three manuscripts:

1. Relevant hydrodynamic drivers of tidal inlet morphology and sedimentology are identified at an exemplary study area, the mixed-energy tidal inlet Otzumer Balje between the East Frisian barrier islands Spiekeroog and Langeoog. The morphological and sedimentological response to high-energy wave-dominated storm conditions is compared to mid-term tide-dominated fair-weather conditions. A multi-fractional approach with five grain-size fractions allows the explanation of corresponding surface sediment grain-size distributions and the evaluation of residual sediment fluxes in response to distinct hydrodynamic drivers (paper I).

2. The littoral sediment drift along barrier island coasts involves sediment bypassing at tidal inlets. Morphological evolution and sediment fluxes in response to real-time forcing conditions of tides, wind and waves are simulated at two East Frisian tidal inlets for a representative mid-term period (two years). Tidal inlet bypassing is studied by identifying residual transport pathways of three sediment grain-size fractions. Common tidal inlet

bypassing schemes which were typically assessed on the basis of aerial photographs or sedimentological surveys are discussed in view of the detailed model results (paper II).

3. The residual circulation into and through barrier island systems is primarily driven by the non-linear interaction of tidal and meteorological forcings. This study is a first attempt to quantify the residual discharges through tidal inlets and across tidal divides between interconnected basins in the East Frisian Wadden Sea by the application of a hydrodynamic model. The response of residual water fluxes to varying boundary conditions is evaluated including representative wind forcing, different bottom frictions and an imposed sea level rise. A substantial surplus of water flows into the multiple-inlet system from the lateral margins, which may cause relevant implications for the accumulation of fine-grained sediments, flushing capacities and nutrient cycles in the Wadden Sea area (paper III).

The main method applied in this study is process-based numerical modeling. Generally, models incorporate uncertainties when natural processes are simplified through numerical schematizations and reduction methods. To justify the applicability of a model to a specific domain, simulated parameters are thus verified against observations, e.g. water levels, wave heights, sediment compositions and morphological changes. The pursued approach to comparatively evaluate model scenarios, e.g. storm versus fair-weather, further improves the confidence in the model as the comparison may cancel out relative errors and uncertainties. It is shown that the two-way-coupling of wave and hydrodynamic models and the consideration of sediment transport of multiple grain-sizes nowadays permits the schematization and simulation of coastal processes in environments that are as complex as mixed-energy tidal inlets. The model outcome, i.e. the reproduction of the interacting natural processes, gets increasingly complex which then made a well-considered differentiation of the imposed forcings and relevant parameters necessary in order to decipher and evaluate the governing processes.

Zusammenfassung

Lagunenartige Küstengewässer sind oftmals gesäumt von langgestreckten Barriereinseln, die der Festlandsküste parallel vorgelagert sind. Gezeitenöffnungen zwischen den Inseln, sogenannte Seegatten, ermöglichen den Wasseraustausch zwischen den flachen Tidebecken und der offenen See. Ein lateraler Austausch benachbarter Tidebecken kann dabei über die Wattwasserscheiden erfolgen. Die Geomorphologie dieses zusammenhängenden, marinen Ökosystems umfasst zahlreiche Lebensräume, die sich im Übergangsbereich zwischen Festlandsküste und offener See befinden und reich an Tier- und Pflanzenarten sind, welche sich den besonderen hydrodynamischen Bedingungen angepasst haben. Die Morphodynamik dieses gemischt-energetischen Systems ist vorwiegend durch den Gezeitenstrom und Seegang beeinflusst und ist über Jahrzehnte hinweg erforscht worden. Frühere Studien beschreiben die morphologische Entwicklung anhand von Luftbildaufnahmen sukzessiver morphologischer Zustände oder Feldmessungen sowie durch numerische und analytische Modelluntersuchungen. Ein prozessbasiertes Verständnis der Wirkung unterschiedlicher hydrodynamischer und meteorologischer Einflüsse auf die Morphodynamik dieses Systems wurde jedoch noch nicht erreicht. Das Ziel dieser Studie ist die Analyse und Bewertung der morphodynamischen Prozesse sowie der morphologischen Veränderungen und sedimentologischen Verteilungsmuster unter der Wechselwirkung interagierender Strömungskomponenten gesteuert durch die Gezeiten, Wind und Seegang sowie der Verfügbarkeit mobiler Sedimente. Das Untersuchungsgebiet umfasst das Ostfriesische Wattenmeer, welches durch eine Kette von sieben Barriereinseln von der offenen, südlichen Nordsee getrennt ist.

Ein anerkanntes, prozessbasiertes Modellsystem wird für die Simulation relevanter hydro- und morphodynamischer Prozesse verwendet und ermöglicht die Abschätzung morphologischer Entwicklungen über kurze und mittelfristige Zeiträume, d.h. von der Dauer einer Tide bis hin zu zwei Jahren. Die untersuchten räumlichen Skalen reichen von der Morphologie einer Plate bis hin zum gesamten Untersuchungsgebiet, welches den Vorstrandbereich der Inseln, die Seegatten und die Inselrückseitenwatten umfasst. Die grundlegenden Ergebnisse der Untersuchungen wurden in drei Manuskripten zusammengestellt:

1. Die Wirkung der Hydrodynamik auf die Morphologie und Sedimentologie im Bereich von Seegatten und Ebbstromdeltas wird beispielhaft am gemischt-energetischen Seegatt Otzumer Balje zwischen den Ostfriesischen Barriereinseln Spiekeroog und Langeoog untersucht. Szenarienanalysen zeigen die Wirkung von verschiedenen meteorologischen und hydrodynamischen Randbedingungen auf sedimentologische und morphologische

Verteilungsmuster; dabei werden extreme Sturmbedingungen, die durch hoch-energetischen Seegang dominiert sind, mit mittelfristigen, tidedominierten Bedingungen verglichen. Ein Modellansatz unter Verwendung von fünf gestaffelten Korngrößenfraktionen ermöglicht die Beurteilung der Wirkung verschiedener hydrodynamischer Einflussfaktoren auf die Korngrößenverteilungsmuster der Oberflächensedimente und die residualen Sedimenttransportwege (Manuskript I).

2. Die großskalige, küstenparallele Sedimentdrift setzt eine Überbrückung des Sedimenttransports über die Seegatten zwischen Barriereinseln voraus. Die morphologische Entwicklung und die Sedimenttransportwege unter der Wirkung von Echtzeitrandbedingungen der Tide, des Windes und des Seegangs werden für zwei Seegatten der Ostfriesischen Inseln über einen repräsentativen Zeitraum von zwei Jahren simuliert. Die das Seegatt überbrückenden, residualen Sedimenttransportwege werden hinsichtlich drei unterschiedlicher Korngrößenfraktionen differenziert. Anerkannte, schematische Sedimenttransportwege zwischen Barriereinseln stützen sich meist auf Luftbildanalysen oder sedimentologischen Untersuchungen und werden hier angesichts der vorliegenden detaillierten Modellergebnisse diskutiert (Manuskript II).

3. Die residuale Zirkulation von Wassermassen zwischen den Rückseitenwatten der Ostfriesischen Barriereinseln und der offenen See wird vorrangig durch die nichtlineare Interaktion der Wirkung des Gezeitenstroms und meteorologischer Einflussfaktoren gesteuert. Als Folge des asymmetrischen Wasseraustausches während einer Gezeitenperiode treten zwischen den Tidebecken und der offenen Nordsee sowie unter benachbarten Tidebecken Ausgleichsströme durch Seegatten bzw. über Wattwasserscheiden auf. Die durchgeführten hydrodynamischen Modellsimulationen erlauben eine erstmalige Abschätzung dieser residualen Durchflüsse. Sie werden hinsichtlich der Wirkung unterschiedlicher Modellrandbedingungen, z.B. des Windes, verschiedener Sohlrauhigkeiten und eines Meeresspiegelanstiegs, evaluiert. Es wird gezeigt, dass ein bedeutsamer residualer Zustrom über beide laterale Seiten des Ostfriesischen Wattenmeeres stattfindet und somit relevante Auswirkungen auf die Akkumulation von Feinsedimenten, Wassererneuerungsraten und Nährstoffzyklen haben dürfte (Manuskript III).

Die prozessbasierte, numerische Modellierung ist als grundlegende Untersuchungsmethode dieser Studie anzusehen. Im Allgemeinen können Modellunsicherheiten nicht ausgeschlossen werden, wenn natürliche Prozesse durch mathematische Vereinfachungen und Reduktionsmethoden schematisiert werden. Um jedoch die Anwendbarkeit eines Modells in einem bestimmten

Gebietsbereich zu rechtfertigen, müssen Modellergebnisse anhand von Naturmessungen verifiziert werden (z.B. Wasserstände, Seegangshöhen, Sedimentzusammensetzung oder morphologische Veränderungen). Der relative Vergleich der durchgeführten Szenarienanalysen erlaubt die Annahme, dass sich Modellunsicherheiten und Fehler teilweise aufheben und das Vertrauen in den Modellansatz somit weiter erhöhen. Es konnte gezeigt werden, dass die vollständige Kopplung von Modellen zur Beschreibung der Hydrodynamik und des Seegangs sowie die Berücksichtigung des Sedimenttransports mehrerer Kornfraktionen eine Schematisierung der relevanten Prozesse und der Sedimentdynamik selbst in komplexen Seegatten erlauben. Die Analyse und Interpretation der Modellergebnisse wird jedoch immer anspruchsvoller desto mehr Prozesse betrachtet werden, was eine wohlbedachte Differenzierung der Modellrandbedingungen und Einflussgrößen erfordert, um schließlich die maßgeblichen Wirkungsprozesse zu isolieren und zu unterscheiden.

Chapter 1: Introduction

1.1. Motivation

The world's coastal zones are focal points of competing human interests in the view of the exploitation of natural resources, economic concerns for navigation and tourism, seaward growth of infrastructure, ecosystem protection, recreational values and the safety of lives and goods through coastal protection (Douvere, 2008; Herrling et al., 2011). Integrated coastal zone management (ICZM) on national and international levels is indispensable in order to mediate among the stakeholders of different sectors and levels of governance. This exceptionally holds for a variety of coastal habitats of the Wadden Sea in the southern North Sea stretching along the coasts of the Netherlands, Germany and Denmark (Fig. 1). The Wadden Sea with its world's largest system of intertidal sand and mud flats was designated a UNESCO World Heritage Site in 2009 because of its uniqueness and outstanding geomorphological and ecological values. On the other hand, it is subject to some of highly frequented navigational routes and the ongoing construction of offshore wind farms, cables and pipelines (BSH, 2014). This diversity of interests exemplarily illustrates some of the constraints being faced in conserving the Wadden Sea and treated by a number of different legal frameworks to regulate development in a sustainable manner. A challenge in the implementation of these frameworks, e.g. the Marine Strategy Framework Directive (MSRL), is to attain the necessary scientific knowledge of the features that define the actual status of the coastal environment (Herrling and Elsebach, 2008). Science thus has to provide the methodology upon which management strategies may build the legal tools for reaching 'Good Environmental Status' (Winter et al., 2014).

Accelerated sea level rise and possible intensified storm activity as consequences of projected climate change will affect coastlines worldwide, at which the Wadden Sea with its shallow coastal waters and continuously adapting morphology is particularly vulnerable. This becomes evident as this environment is relatively young and only evolved during the post-glacial transgression, around 7000 years ago (Behre, 2007; Ludwig et al., 1981). Inundations in the wake of medieval storm surges resulted in further changes of the coastline and the generation of nearshore basins. The Wadden Sea is a depositional system that tends to import sediments to the back-barrier basins; however, this natural transgressive response to sea level rise has been inhibited by human interventions since the last millennium by building dykes and land reclamation measures along the entire mainland coast (Flemming and Davis, 1994). This impact implies a change in the cross-shore energy gradient with a depletion of fine-sediments favoring the accumulation and building of sand-flats where cohesive

sediments were originally more dominant (Flemming and Nyandwi, 1994). Ongoing research faces the uncertainty of the future development of the Wadden Sea particularly in view of the basins to sufficiently import sediments in order to compensate the deficit created by the persisting and possibly accelerating sea level rise (Burchard et al., 2008; Flöser et al., 2011).

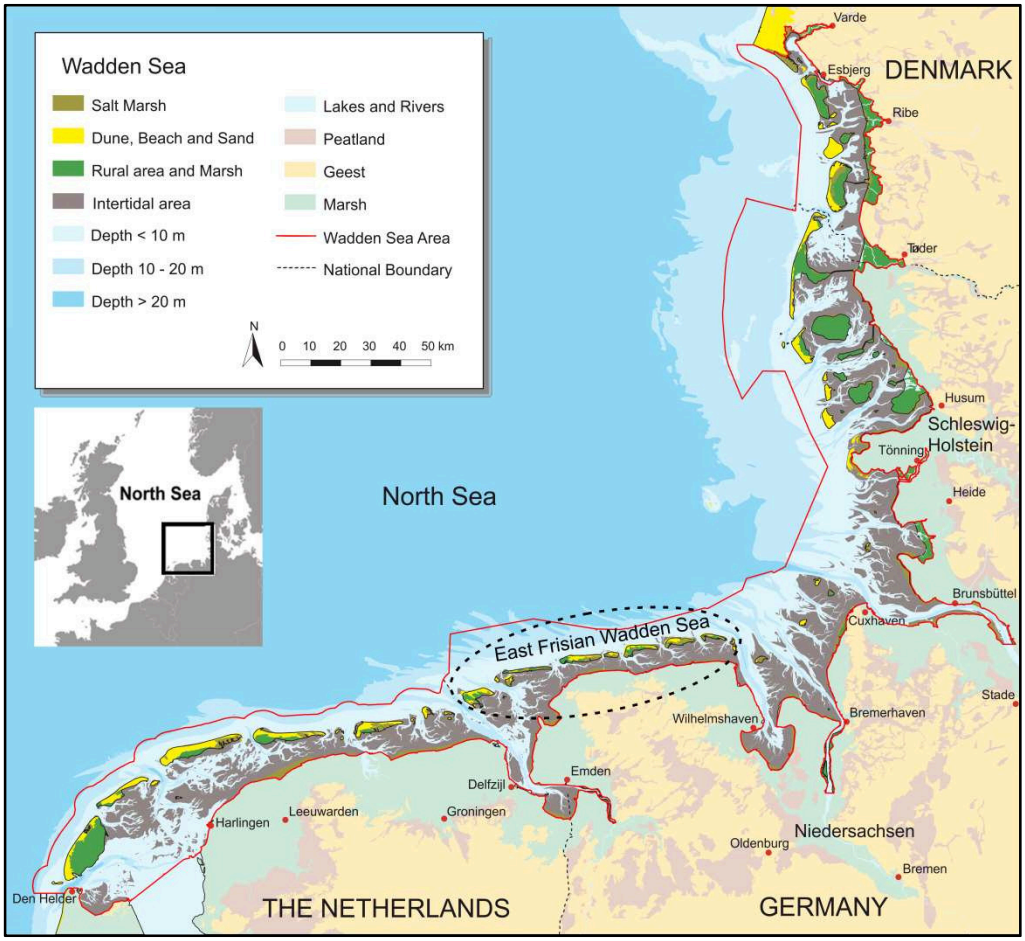

Figure 1: The studied multiple-inlet system East Frisian Wadden Sea covers seven populated barrier islands and is part of the Wadden Sea stretching along the southern coastline of the North Sea (original map by Common Wadden Sea Secretariat, 2008).

The morphological evolution of the Wadden Sea fringed by a chain of barrier islands is driven by a complex interaction of forcing conditions, i.e. the tide, wind and waves, controlling the morphodynamics of different interconnected units that characterize a multiple-inlet system: the shoreface, the island beaches and dunes, the tidal inlets, the back-barrier basins with their channel networks, tidal flats and salt marshes (De Swart and Zimmerman, 2009). The Wadden Sea geomorphology is highly dynamic with morphological changes on a variety of spatio-temporal scales. Morphological features range from small scale bedforms as ripples on sandy shoals or small dunes in

tidal channels up to much larger sand ridges on the upper shoreface reaching several kilometers into the sea (Blondeaux, 2012). Observations show the temporal development of these features from time scales of single waves to seasonal changes. The morphodynamics are intensified, however, when periodic storm events impact the entire system by extreme energy input by surge and waves. A very high morphological activity prevails at tidal inlets which connect the back-barrier basins to the coastal sea exchanging large volumes of water (tidal prism of typically 10^8 m³) four times a day (Winter, 2011). On an inlet channel transversal axis, they bridge between neighboring barrier islands by bypassing the littoral sediment drift. Tidal inlets thus act like the pivotal point of the system where tidal and wave energy focus and interact more than anywhere else (Bruun, 1978; Hayes, 1979). At the same time, ebb-tidal deltas are huge reservoirs that store and release large amounts of sand depending on the sediment demand through budget exchanges between morphological units in the system (FitzGerald, 1988; Walton and Adams, 1976). The establishment of the dynamic morphological equilibrium states is mainly driven by the competing effect of tides and waves.

Tide- and wave-dominated coastal environments are governed by both suspended and bed load sediment transport processes (Van Rijn, 1993), acting on diverse temporal and spatial scales, where the coexistence of different sediment grain-size fractions complicates in-situ observations as well as the interpretation of the dynamic feedback among the different features and units of the system (Oertel, 1988). The spatial dimensions and pathways of time-integrated sediment fluxes are still poorly understood. Recent advances towards a phenomenological understanding of sediment dynamics at tidal inlets was made by a joined evaluation of high-resolution model results and detailed field surveys (Barnard et al., 2013).

The broad spectrum of relevant spatial and temporal scales and the limited feasibility of field measurements in the Wadden Sea call for dedicated methods for a process-based understanding. State-of-the-art numerical models are here the preferred tool to identify erosional and depositional processes which act in response to the divergence of the sediment transport pathways (e.g., Dissanayake et al., 2009). Numerical models that enable the two-way-coupling of wave radiation and tidally- and wind-induced flow are necessary to simulate the non-linear interaction of the drivers and the morphology of the Wadden Sea (Elias et al., 2006a). Recent advances in sediment transport modelling of different grain-size fractions allow evaluating the sedimentological response to the imposed hydrodynamics (van der Wegen et al., 2011a). These models may be seen as a framework of a state-of-the-art system understanding, which is continuously improved by implementing new formulations of the relevant physical mechanisms into the modelling system by the scientific community. However, in order to justify the applicability of the model to a specific domain, the simulation must be validated against observations (e.g., Winter, 2007).

Given a suitable model realization (configuration) for the domain of investigation, the system's morphological response to distinct drivers which is normally obscured by the non-linear interaction inside the natural system may be deciphered by dedicated numerical model experiments (Elias and Hansen, 2013; Herrling and Winter, 2014). This is also referred to as the top-down approach which manifests in a step-by-step exclusion of certain underlying physical processes in order to identify (isolate) the system's response to the governing physical mechanisms. The application of process-based models thus implies that reality is reduced in the way that no relevant processes are lost, but the computational effort is still acceptable. Advances in computational power allow the schematization of the governing processes in an always increasing spatial accuracy while covering the interrelating morphological units of the system as a whole (Wang et al., 2012a). These models thus close the gaps with respect to locally restricted observations or monitoring methods by allowing inter- and extrapolation of the relevant parameters and processes describing the system in time and space.

1.2. Objectives and research questions

The objective of this study is to investigate relevant hydrodynamic drivers that determine the morphological and sedimentological response at barrier island coasts and multiple-inlet systems on different spatial and temporal scales; a representative study area is found at the East Frisian Wadden Sea. The modelling system Delft3D (Deltares, 2011; Lesser et al., 2004) is used to set-up numerical models covering coastal environments of different dimensions. Experimental and hindcast simulations allow evaluating sediment transport processes and morphological changes for distinct hydrodynamic conditions. The corresponding surface sediment grain-size distributions are derived by a multiple-grain-size approach (van der Wegen et al., 2011a). Available field observations of water levels, current velocities, wave parameters, morphology and sedimentology are employed to calibrate model settings and validate the output of the simulations. The configuration of the model domains and the imposed boundary conditions are adapted to the particular research question aiming a process-based understanding of the governing mechanisms.

This study addresses five research questions:

1. **What is the residual morphological and sedimentological response to distinct hydrodynamic drivers?**

   Morphodynamics at mixed-energy tidal inlets are driven by the combined action of waves and tides. These interacting hydrodynamic forces largely determine the morphological and sedimentological response of the tidal inlet channels and the ebb-tidal delta shoals. It is not

clear how particular hydrodynamic drivers contribute to the observed response at mixed-energy tidal inlets.

2. **What are the effects of storm events and fair-weather conditions on morphology and sedimentology?**

   During high energy storm events, wave energy dissipation on depth-limiting ebb-tidal delta shoals in combination with enhanced alongshore currents are considered as the main drivers for short-term morphological changes at tidal inlets. The resulting morphological and sedimentological changes are yet poorly understood due to a lack of suitable field observations. The question arises as to what the effects of periodic, extreme storm events are – compared to fair-weather hydrodynamic conditions – on morphology and sedimentology at tidal inlets and at the barrier island foreshore.

3. **What are the sediment transport pathways for distinct hydrodynamic forcing conditions?**

   Different morphological units at mixed-energy tidal inlets reveal gradations of surface sediment grain-sizes. Are particular sediment transport pathways controlled by the availability of specific grain-size fractions or by the imposed forcing mechanisms? How do hydrodynamic drivers control the sediment transport pathways at mixed-energy tidal inlets?

4. **How is sediment bypassed at mixed-energy tidal inlets?**

   At the East Frisian coast, a net eastward directed littoral sediment drift is observed that used to cause a lateral migration of the barrier islands to the east. This has ceased due to the construction of coastal protection measures in the last century, e.g. sea walls and groins, at the island shores (FitzGerald et al., 1984a). At the tidal inlet scale, what are the net transport pathways bypassing the alongshore sediment drift from one barrier island to the next?

5. **What is the residual circulation in multiple-inlet systems and among interconnected basins in response to the non-linear interaction of tidal and meteorological forcing?**

   The non-linear interaction of the offshore tidal signal, wind-induced flow and the irregular bathymetry of channels and basins generates complex water fluxes and residual circulations at multiple-inlet systems. What are the physical mechanisms that govern the resulting flood/ebb-dominance of water fluxes at tidal inlets? How do neighboring tidal basins communicate via

the tidal divides? What is the effect of meteorological forcing or an imposed sea level rise on the residual circulation in multiple-inlet systems?

1.3. Thesis outline

This dissertation is organized in a cumulative format around three manuscripts. They are arranged in individual chapters addressing different scientific questions. After the introduction, chapter 2 and chapter 3 account for sediment dynamics at tidal inlets and the island foreshore where tides and waves are the governing drivers. Barrier island systems cover as well back-barrier tidal basins that are largely sheltered from energetic wave forcing by the islands. Sediment dynamics are thus predominantly driven by tidally- and wind-induced currents. Prior to the investigation of complex sediment transport processes associated with the entrainment, advection and settling of very fine sands and cohesive sediments, it is essential to evaluate the water fluxes circulating in the back-barrier multiple-inlet system. This is addressed in chapter 4. Chapter 5 concludes the thesis with a synthesis of the main findings and an outlook on further research.

Paper I: 'Morphological and sedimentological response of a mixed-energy barrier island tidal inlet to storm and fair-weather conditions'

The Otzumer Balje between the barrier islands Spiekeroog and Langeoog is selected as a typical mixed-energy tidal inlet to exemplarily study the morphological and sedimentological response to wave- or tide-dominated forcing conditions. This is achieved by simulating a high-energy storm event in the North Sea that represents a period of wave dominance and a mid-term period of fair-weather conditions with waves smaller than average representing tide-dominant conditions. A multi-fractional approach allows the simulation of surface sediment grain-size distributions to the corresponding morphological evolution. Net sediment pathways are discussed for distinct drivers at low- and high-energetic conditions.

Paper II: 'Evaluation of sediment bypassing schemes at barrier island tidal inlets'

Theories of natural sediment bypassing at barrier island tidal inlets go back to early studies mostly based on aerial photographs and sedimentological surveys. This investigation reflects on the controversial assumptions on sediment bypassing by means of process-based modeling. A spatial and temporal high-resolution morphodynamical simulation of two years driven by representative real-time boundary conditions of tides, wind and waves is validated against morphological changes between two measured bathymetrical states. The underlying sediment transport pathways of distinct grain-size

fractions and the bypassing of the alongshore sediment drift are exemplarily studied at two tidal inlets of the East Frisian barrier island system.

Paper III: 'Tidally- and wind-driven residual circulation at the multiple-inlet system East Frisian Wadden Sea'

The residual circulation at barrier island systems with multiple-inlets is studied by a hydrodynamic model. The net water fluxes through tidal inlets and across tidal divides between interconnected basins are driven by the non-linear interaction of the tidal and meteorological forcing. The hydrodynamic response of the multiple-inlet system to various boundary conditions, i.e. variable meteorological forcing, imposed sea level rise or different bed friction values, is investigated. The physical mechanisms that control the generation of net circulation cells are discussed with reference to analytical model studies based on idealized system geometries.

Chapter 2: Paper I

Morphological and sedimentological response of a mixed-energy barrier island tidal inlet to storm and fair-weather conditions

G. Herrling and C. Winter

MARUM – Center for Marine Environmental Sciences, University of Bremen, Germany

Earth Surface Dynamics, 2, 1–20, 2014 (published)

Abstract

The environment of ebb-tidal deltas between barrier island systems is characterized by a complex morphology with ebb- and flood-dominated channels, shoals and swash bars connecting the ebb-tidal delta platform to the adjacent island. These morphological features reveal characteristic surface sediment grain-size distributions and are subject to a continuous adaptation to the prevailing hydrodynamic forces. The mixed-energy tidal inlet Otzumer Balje between the East Frisian barrier islands of Langeoog and Spiekeroog in the southern North Sea has been chosen here as a model study area for the identification of relevant hydrodynamic drivers of morphology and sedimentology. We compare the effect of high-energy, wave-dominated storm conditions to mid-term, tide-dominated fair-weather conditions on tidal inlet morphology and sedimentology with a process-based numerical model. A multi-fractional approach with five grain-size fractions between 150 and 450 μm allows for the simulation of corresponding surface sediment grain-size distributions. Net sediment fluxes for distinct conditions are identified: during storm conditions, bed load sediment transport is generally onshore directed on the shallower ebb-tidal delta shoals, whereas fine-grained suspended sediment bypasses the tidal inlet by wave-driven currents. During fair weather the sediment transport mainly focuses on the inlet throat and the marginal flood channels. We show how the observed sediment grain-size distribution and the morphological response at mixed-energy tidal inlets are the result of both wave-dominated less frequent storm conditions and mid-term, tide-dominant fair-weather conditions.

2.1. Introduction

Tidal inlets at barrier island systems connect the open sea with the back-barrier tidal basin. Typically, they feature an ebb-tidal delta seawards and a flood-tidal delta landwards of a deep inlet throat that is bordered by shallow sandy shoals and marginal flood channels (Hayes, 1979). Both tidal flow constriction through the narrow inlet and wave energy dissipation on depth-limited ebb-tidal delta shoals account for local enhanced sediment transport and rapid morphological evolution.

Morphodynamics at mixed-energy tidal inlets are driven by the combined action of waves and tides and the relative contribution of these interacting forces largely determines the morphological and sedimentological response. Komar (1996), De Swart and Zimmermann (2009), Davis and FitzGerald (2009) and FitzGerald et al. (2012) give recent and comprehensive reviews on morphodynamic processes at a large variety of tidal inlet systems. The early work of Hayes (1975, 1979) and a recent study applying process-based models (Nahon et al., 2012) classified mixed-energy inlet regimes in a range between tide-dominated and wave-dominated and suggested corresponding inlet geometries that are in equilibrium with the long-term energetic input from waves and/or tides. Sha and Van den Berg (1993) developed a descriptive model to explain ebb-tidal delta symmetry, i.e., the orientation of the seaward inlet channel with respect to shallow ebb-delta shoals, as a response to the relative direction of waves to the interplay of tidal currents alongshore and within the inlet. Very few studies at mixed-energy tidal inlets have investigated the complex interaction of tide- and wave-driven processes and distinguished the contribution of each agent to residual sediment fluxes and morphological changes (e.g., Bertin et al., 2009; Elias and Hansen, 2013; Elias et al., 2006a; Sha, 1989). Even fewer studies have managed to relate observed distributions of surface sediment grain-sizes at tidal inlet systems to distinct physical drivers (e.g., Sha, 1990; van Lancker et al., 2004).

Recent studies have shown the applicability of process-based numerical models for sedimentological studies, for example, to simulate surface sediment grain-size distributions in combination with morphological changes (Kwoll and Winter, 2011; Van der Wegen et al., 2011a, b). This suggests the application of multi-grain-size models to decipher the morphological and sedimentological effect of different hydrodynamic drivers, i.e., different model boundary conditions.

In this study we aim to investigate the effect of tide- and wave dominance on residual sediment pathways at a mixed-energy barrier island tidal inlet Otzumer Balje in the southern North Sea. It serves as an example of a mixed-energy, slightly tide-dominant inlet regime with similar characteristics as described, for example, by Hayes (1979). This is achieved by simulating a storm event that represents a period of wave dominance and fair-weather conditions with waves smaller than average representing tide-dominated conditions. Real-time data of tides, wind and waves are applied as

forcing conditions for each model scenario, and are assumed to be sufficiently representative to study the morphological and sedimentological responses to low- and high-energetic conditions. The following characteristics of tidal inlet systems are investigated:

1. It is commonly understood that ebb-tidal delta erosion during episodic storm events counteracts the continuous replenishment of the ebb-tidal delta during tide-dominated fair-weather conditions (De Swart and Zimmerman, 2009). We aim to show how this dynamic equilibrium behavior of either wave- or tide-dominated forcing conditions determines the sedimentology and morphology at a typical mixed-energy tidal inlet and the adjacent foreshore. After a synthetic separation of tide- and wave-dominated forcing conditions, we will point out relevant morphodynamics and sediment pathways that are due to the interaction of the driving forces leading to, for example, elongated channel fill deposits at the margin of the tidal inlet throat.
2. Son et al. (2010) postulated a dominant circular sediment pathway at the eastern ebb-tidal delta platform of the tidal inlet Otzumer Balje investigated here. Sediments are thought to be recycled between the ebb-tidal delta and the inlet throat without any evidence of sediment bypass to the downdrift beach. For the Dutch Ameland tidal inlet, authors have mentioned recirculation cells at the downdrift shoals of the ebb-tidal delta supporting reversed net sediment transports towards the inlet throat, but claim only minor significance with respect to the overall sediment dynamics (Cheung et al., 2007; Elias et al., 2006a; Sha, 1989). We evaluate the relevance of this recirculation cell at mixed-energy tidal inlets and identify the hydrodynamic drivers and interrelated mechanisms that induce these net circular sediment fluxes.

2.2. Study area

The tidal inlet Otzumer Balje is located between the East Frisian barrier islands Langeoog and Spiekeroog in the southern North Sea (Fig. 2). The back-barrier tidal basin represents a drainage channel system typical for the Wadden Sea. According to the classification of Hayes (1975, 1979), the study area is mesotidal with a mixed-energy to slightly tide-dominated regime. The tide is semidiurnal with a mean range of 2.8 m at Spiekeroog. The gorge in the inlet throat reaches maximum depths of approximately 24 m below German datum (around mean sea level) and a width of approximately 1 km. The residual flow in the inlet throat is ebb-dominant with maximum current velocities for neap to spring tides ranging from 0.5 to 1.0 and 0.8 to 1.6 m/s for flood and ebb tide, respectively (Bartholomä et al., 2009).

Mean wind directions are from the westerly sector with mean velocities of about 7 m/s observed at the offshore platform FINO1 at approx. 45 km off the East Frisian barrier islands. Here, mean significant wave heights of 1.4 m and mean peak periods of 6.9 sec have been measured (data from May 2004 to June 2006, Federal Ministry for Environment, Nature Conservation and Nuclear Safety (BMU) and the Project Management Jülich (PTJ)). Extreme storms from the northwesterly sector can generate surge water levels of up to 2.5 to 3.3 m above mean high water at the coast. During the extreme storm event on 9 November 2007, known as 'Tilo', significant wave heights of 10 m, maximum wave heights of 17 m and peak periods of up to 15 sec were measured offshore at water depths of 30 m at the research platform FINO1 (Outzen et al., 2008). The combination of a tidal wave that travels from west to east and the dominant westerly wind and wave directions generates an alongshore eastward-directed net sediment drift. FitzGerald et al. (1984a) estimated the net transport rate to be about 270,000 m^3/year of sand.

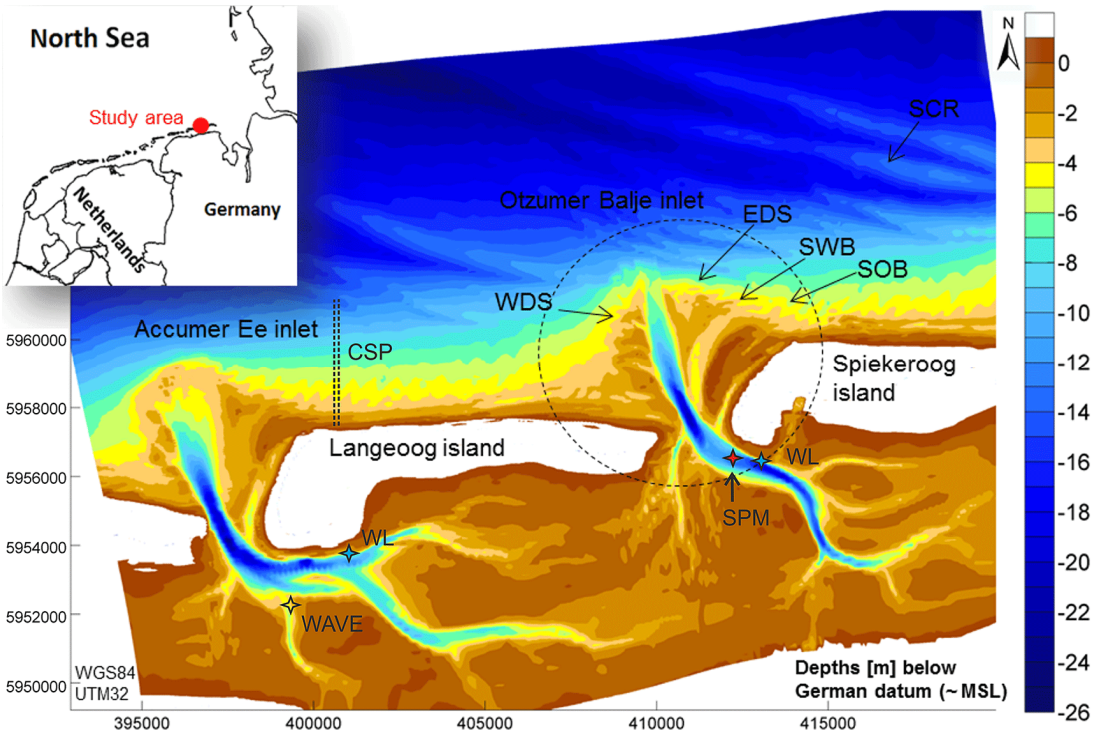

Figure 2. East Frisian barrier island system in the southern North Sea with the study area Otzumer Balje inlet between the islands Langeoog and Spiekeroog and nearshore morphological features such as the western/eastern ebb-tidal delta shoals (WDS/EDS), swash bars (SWB), shore-oblique sand bars (SOB) and shoreface-connected ridges (SCR). Measurement positions are indicated by wave (WAVE), water level (WL), suspended matter (SPM) and bathymetry at cross-shore profiles (CSP).

The inlet consists of a variety of morphological features such as ebb- and flood-tidal deltas, inlet throat and marginal flood channels bordered by shoals and swash bars. The latter are sand bars with dimensions on the order of a few hundred meters superimposed onto the ebb-tidal delta that migrate onshore and coalesce to larger intertidal bar systems in the vicinity of the shore (FitzGerald, 1982); it should be mentioned at this point that the nomenclature 'swash bars' is commonly used but is rather misleading as the physical processes involved are miscellaneous and not primarily related to swash. At the ebb-tidal delta of the Otzumer Balje inlet, their orientation is more shore-parallel compared to the shore-oblique sand bars that emerge downdrift of the ebb-tidal delta. The bed of the tidal inlet reveals different bed forms, from ripples to dunes. In the inlet throat, Noormets et al. (2006) measured three-dimensional sand dunes with mean lengths of 7.5 m and mean heights of 0.35 m. Medium to coarse, poorly sorted sands are found in the inlet channel; the ebb-tidal delta body mainly consists of fine sand but is superimposed by swash bars of medium-sized sand (Son et al., 2010).

2.3. Methodology

2.3.1. Modeling system

The modeling system Delft3D (Deltares, 2011) has been applied to set up and run high-resolution process-based morphodynamic models. The mathematical model solves the three-dimensional shallow-water equations and continuity equation on a staggered model grid by means of an implicit finite-difference scheme. The spectral wave model SWAN (Booij et al., 1999; Ris et al., 1999) is run in a stationary mode to simulate the wave propagation and deformation from the open sea to the shoreline. Wave measurements available at intervals of 30 min are applied as offshore boundary conditions. This coincides with the interval of the sequential two-way coupling between SWAN and the hydrodynamic module (Delft3D-FLOW) that allows the exchange of relevant parameters on curvilinear model grids via a communication file. Wave parameters and the forcing terms associated with the wave radiation stresses computed by SWAN are read by the FLOW module. Once the assigned runtime of 30 min has been reached by FLOW, bottom elevation, water level and depth-integrated current fields are used as input to the computation in SWAN. The model will loop through these sequential module applications until the simulation is accomplished. The interaction of wave forces (radiation stresses), tidal currents and the changing bed- and water levels is thus realized by a fully coupled wave-current simulation.

Wave forces being computed in SWAN by radiation stress gradients are implemented as a shear stress in the flow module at the water surface layer. The ongoing debate about the vertical distribution of wave-induced radiation stresses that generally split up into a surface component, a

bottom component and a body force and their implementation within 3D-momentum equations (discussed in, for example, Ardhuin and Roland, 2013; Ardhuin et al., 2008; Bennis et al., 2011) reflects on and indicates that important wave-induced processes interacting with the flow circulation may still be inadequately implemented in Delft3D. These model limitations are, however, accepted in the present study assuming minor effects on the sedimentology and morphology at the tidal inlet.

Important wave effects are incorporated in the 3D-simulations as wave-induced mass flux adjusted for the vertically nonuniform Stokes drift, additional turbulence and vertical mixing processes and streaming as an additional wave-induced shear stress in the wave boundary layer (Walstra et al., 2000). The effects of wave asymmetry on the suspended sediment transports are included based on the nonlinear wave approximation modified by Van Rijn et al. (2004) after the method of Isobe and Horikawa (1982). Mean and oscillatory bed shear stresses interact nonlinearly. Through the use of the parameterization of Soulsby et al. (1993), the wave-current interaction model of Fredsøe (1984) is applied to account for the wave-induced enhancement of the bed shear stress that affects the stirring of sediments and increases the overall bed friction.

The sediment transport formulation applied here differentiates bed- and suspended load mechanisms (Van Rijn et al., 2004). Suspended load is treated above a reference height, and bed load below (Van Rijn, 1993). For simulations including waves, the magnitude and direction of the bed load transport are calculated using an approximation method developed by Van Rijn (2003). The method computes the bed load transport accounting for the flow velocity in the bottom computational layer and the near-bed peak orbital velocity in the direction of wave propagation. Suspended sediment is entrained in the water column by imposing a reference concentration (Van Rijn, 2000) at the reference height. An advection-diffusion equation (Van Rijn et al., 2004) is solved for the current-related suspended transport. The settling velocity of sand is computed following the method of Van Rijn (1993), where different suspended grain-size diameters are accounted for by empirical formulations. The vertical sediment mixing coefficient follows directly from the vertical fluid mixing coefficient calculated by the $k-\epsilon$ turbulence closure model (Rodi, 1984).

The model is used to identify sediment transport patterns between consecutive morphological states and to differentiate between instantaneous and residual suspended load and bed load directions and quantities. For details on the equations and processes implemented in the modeling system Delft3D, the reader is referred to Lesser et al. (2004), Van Rijn et al. (2004) or the manual of Delft3D (Deltares, 2011).

2.3.2. Morphological acceleration factor

A morphological scale factor is applied to account for the acceleration of bed level changes during updates at each hydrodynamic time step (Roelvink, 2006). Through the use of this method, which aims to economize computational run-time, hydrodynamic timescales are adapted to much longer timescales of morphological evolution. Within this study, a morphological acceleration factor (MORFAC) of 20 is applied during a simulation of 17 tidal cycles between neap and spring tide (7. to 15. June 2007) in order to account for morphological changes that occur during approximately 5 months of fair-weather conditions. For the 5-day storm simulation (6. to 10. Nov. 2007), no morphological acceleration is applied (MORFAC = 1).

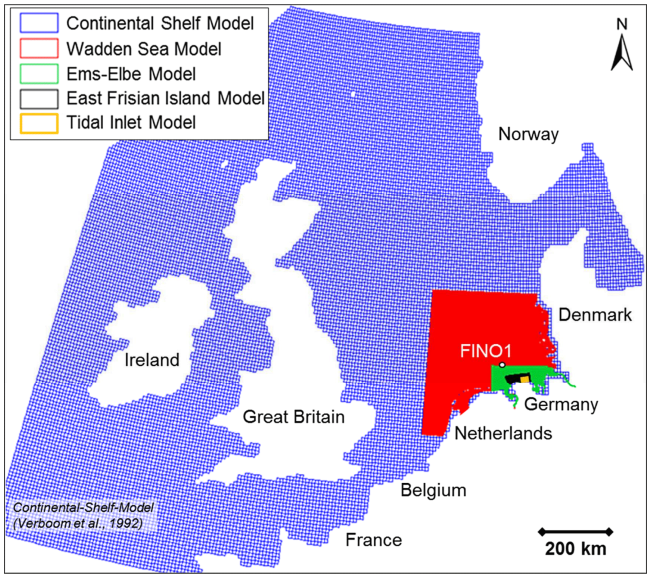

Figure 3. Cascade of five nested model grids and the position of wave measurements at FINO1 being applied as offshore boundary condition; wind- and atmospheric pressure fields computed by the German Weather Service cover all model grids.

2.3.3. Model nesting and boundary conditions

A hierarchical cascade of five model grids from the European continental shelf to the East Frisian barrier islands with decreasing spatial dimensions and increasing grid resolutions has been set up to derive water levels and wave climate at the study area (Fig. 3). Storm surge simulations in particular require large model domains as coastal surge is generated by wind drag effects and atmospherical pressure gradients acting over long distances on the open sea. The largest model with grid cell resolutions of 8000 m covers the continental shelf in the North Atlantic Ocean to the North Sea. Eight harmonic tidal constituents are applied to generate the astronomic tide at the sea boundaries

of the continental shelf model (Verboom et al., 1992). It embeds the Wadden Sea model with average grid sizes of 1200 m covering the entire North Sea from the Dutch coast in the south to Denmark in the north. The Wadden Sea model, in turn, generates water level time series at the seaward boundary of the smaller Ems-Elbe model with grid resolutions of approx. 200 m. The latter is additionally forced at the seaward boundary by wave data observed at the research platform FINO1 located 45 km offshore in water depths of 30 m. The next smaller model covers the East Frisian barrier islands from Juist to Wangerooge with model grid resolutions of 60–120 m and supplies wave- and water level boundary conditions to the most detailed tidal inlet model covering only Langeoog and Spiekeroog. At the end of the model cascade, this three-dimensional model with 10 sigma layers over the vertical is dedicated to simulate the sediment dynamics at the tidal inlet Otzumer Balje and adjacent beaches (Fig. 2). It consists of 140,000 active grid cells with average grid resolutions of 60 m and up to 20 m in the breaker zones, assumed to be sufficiently resolved for proper generation of wave-induced alongshore currents during storm conditions. During fair-weather conditions, wave-lengths are significantly shorter and the selected cross-shore grid resolution may not be ideally represented at the upper part of the beach, yet certain limitations are accepted in favor of reduced computational times.

2.3.4. Model bathymetry

Model bathymetries, i.e., depth schematizations for each particular model, have been assembled by interpolating measured data of sea bottom elevations onto curvilinear model grids. Near coastal sub- and intertidal areas are covered by data of the years 2006, 2005 and 2001 based on conventional sounding methods (Federal Maritime and Hydrographic Agency, BSH). Elevations of inter- and supratidal barrier island beaches are partly covered by beach profiles of the year 2007 or high-resolution airborne lidar scans that are spatially limited and available for the years 2008, 2007 and 2005 (data with permission of the Coastal Research Station of Lower Saxony Water Management, Coastal Defense and Nature Conservation Agency – FSK-NLWKN).

2.3.5. Meteorological forcing

Storms in the central part of the North Sea are associated with low-pressure systems. During the investigated extreme storm event, ‘Tilo’, between 5. and 10. Nov. 2007, with peak surge levels on 9. Nov. 2007, maximum wind velocities of 33 m/s and mean wind directions of north-northwest were recorded offshore (Outzen et al., 2008). Wind stress and horizontal atmospheric pressure gradients acted over a long fetch from the Arctic Sea across the entire North Sea inducing extreme surge setup superimposed by high astronomical tide. The storm surge simulations are forced by meteorological model data of the German Weather Service (DWD). Wind and atmospheric pressure fields are

available at 1 h intervals and spatial resolutions of 7 and 2.8 km for the models COSMO-EU and COSMO-DE, respectively.

The simulation representing fair-weather hydrodynamic conditions is forced by time series of wind data measured at the research platform FINO1 (provided by BMU, PTJ). Real-time data between 7. and 15. June 2007 are imposed to the wave and hydrodynamic simulations to account for a meteorological forcing with nonstationary wind velocities and directions. The mentioned period was selected based on visual comparison of generated wind roses due to the selected data set and a 2-year data set. Thus the selected data do not fulfill long-term statistical correctness, but the overall distribution of wind directions and intensity are similar to the long-term trend. Wind directions of the selected data series are from the westerly sector with a short intermittent period of easterly winds. The selected data are assumed to be sufficiently representative to account for typical low-energy wind- and wave conditions.

2.3.6. Multiple-grain-size model

2.3.6.1. Bed layer model for multiple sediment fractions

A dynamic bed layer model is applied that permits the redistribution of multiple sand fractions in relation to imposed bed shear stresses. It thus enables the computation of spatial distributions of surface sediment grain-size fractions and to evaluate arithmetic mean grain sizes in response to different hydrodynamic conditions. Each sand fraction depletes or increases in the bed cell according to erosion or deposition processes in the sediment transport formulation. A coefficient according to each mass percent is applied in the transport equation to account for the availability of the mobilized sand fraction at a given bed cell. Thus, sediment transport occurs if the critical shear stress is exceeded for a certain grain-size fraction, whereas its load is additionally controlled by the relative availability of each sand fraction. The uppermost layer of the bed layer model, the so-called active layer, has a constant thickness and records the grain-size composition of the underlayers beneath. The underlayers account for the bed level change, while their thicknesses increase or decrease depending on the prevailing erosion or deposition of a certain grain-size fraction. In the present study, the selected active layer thickness is 0.25 m. At the start of the simulation, the total thickness of the underlayers is 10 m in order to guarantee enough sediment supply in case of locally strong erosion. Simulations presented in this study consider continuous bed level updating. This is clarified against the background that Delft3D allows simulations without bed level updating but redistribution of sediment fractions only. For details on the setup and functioning of the bed layer model, the reader is referred to Van der Wegen et al. (2011a).

In the present study, because of computational expenses, model simulations were restricted to a limited number of noncohesive sand fractions (five), with grain sizes of 150, 200, 250, 350 and 450 µm. As the focus is on the sediment dynamics at the tidal inlet, a characteristic gradation of rather coarse sediment fractions between 150 and 450 µm was selected. Areas exposed to a low-energy wave impact such as the back-barrier tidal flats or the lower shoreface where significantly finer grain sizes occur in nature are, according to the grain-size configuration selected here, not subject to significant morphological changes and thus grain-size sorting processes. Here, the initial mean surface sediment grain-size does not change significantly during the simulations. This limitation is tolerated because back-barrier sediment dynamics and exchange processes between the back-barrier basin and the foreshore are not the focus of this study. Back-barrier tidal flats contain high amounts of fine sand and cohesive sediments and would require a different model setup and grain-size configuration.

2.3.6.2. Initial sediment grain-size distribution

Observations of surface sediments are restricted to the tidal inlet Otzumer Balje; samples of the ebb-tidal delta lobe are not available. The spatial inconsistency of measurements precludes the use of grain-size observations as initial conditions of simulations. The model is thus applied to allow for the redistribution of multiple sand fractions with the objective of generating a schematization of the observed surface sediments that can then be used to initiate more realistic simulations. According to this, two different model initializations are considered: on the one hand, the synthetic case of an initialization with uniform grain-size distribution; on the other hand, the more realistic 'analysis simulations' taking into account a sediment distribution of nonuniform grain sizes that was generated by preceding model runs.

Synthetic simulations are initiated with uniform sediment type distribution. Five sediment fractions (150, 200, 250, 350 and 450 µm) are available at 20 mass percent each and thus represent an initial mean grain size of 280 µm. First, two synthetic simulations are run and forced by approximately 5 months of fair-weather conditions and 5 days of storm conditions to exemplify the sedimentological response to tide- and wave-dominant hydrodynamic conditions for simplified sedimentological settings. For fair-weather conditions, elevated shear stresses due to tide-induced currents in the inlet throat and marginal channels cause mean sediment grain-sizes at the channel bottoms to increase, while fine sands are entrained, transported in the ebb direction and deposited at the ebb-tidal delta lobe (Fig. 4a). During storm conditions, however, sediment coarsening occurs due to wave-induced stirring and increased shear stresses at the ebb-tidal delta and adjacent shoals, whereas sediments at the tidal channels reveal only minor changes in mean grain size (Fig. 4b). Fine sediments being entrained by northwesterly waves on the elevated shoals are transported in the onshore direction and accumulate as elongated deposits along tidal channel margins. These simulations reveal synthetic sediment

distributions since sediments in nature are nonuniformly distributed and sediment grain-size availability may be a crucial factor in the development of sediment fluxes; however, they allow for highlighting of the idealized response of surface sediments to distinct hydrodynamic forcing conditions.

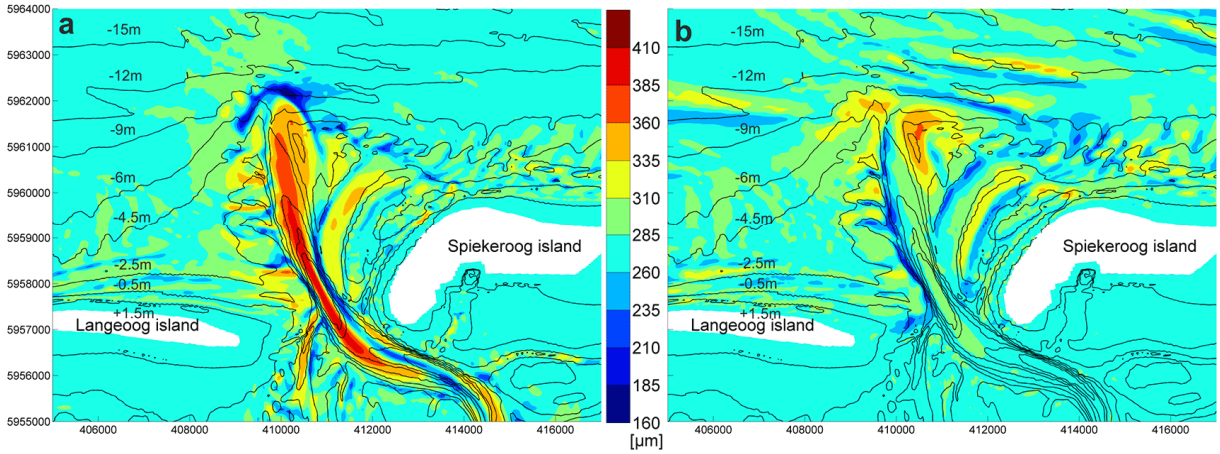

Figure 4. Distribution of arithmetic mean surface sediment grain-sizes as a response to fair-weather (a) and storm (b) conditions; synthetic simulations were initiated with five uniformly distributed sand fractions between 150 and 450 µm.

As a second step, a more realistic sediment distribution is generated that is in response to a combination of fair-weather and storm conditions: a simulation of 5 months being forced by fair-weather boundary conditions is followed by a storm simulation of 5 days and another period of 5 months of fair-weather conditions. Sediment mass fractions at the end of each model run are turned over to the subsequent simulation. At the end of the sequence of simulations, the predicted sediment distribution schematizes the sedimentological response to a mixed-energy tidal inlet regime (Fig. 5). This sediment distribution is used for model validation purposes based on a qualitative comparison of predicted and observed grain-size distributions (Sect. 2.4.3). Furthermore, it is applied as an initial condition for simulations that aim to analyze morphodynamics and sedimentology in response to fair-weather and storm conditions (Sect. 2.5), because it allows for a more realistic schematization of surface sediments with consistency all over the model domain and one avoids having to rely on spatially limited sediment grain-size measurements.

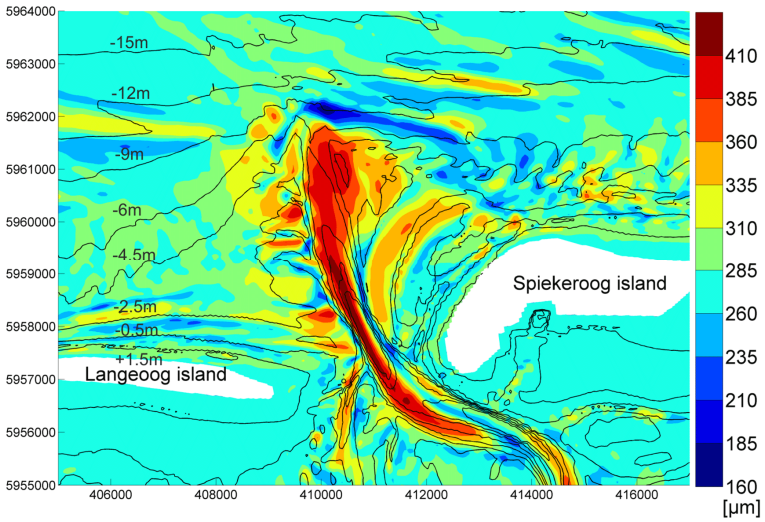

Figure 5. Arithmetic mean surface sediment grain-size due to the distribution of five sand fractions between 150 and 450 µm generated by a series of three simulations with alternating hydrodynamic forcing due to 5 months of fair-weather conditions, an extreme storm event and again 5 months of fair-weather conditions.

2.4. Model validation

The model system Delft3D has been widely tested in morphodynamic modeling studies for various environments (e.g., Dissanayake et al., 2009; Lesser et al., 2004; Van der Wegen and Roelvink, 2012), yet it has been verified in comparably few morphological studies on nonidealized tidal inlets that take into account a real-world bathymetry (e.g., Elias and Hansen, 2013; Elias and van der Spek, 2006b; Elias et al., 2012). The validation of simulated morphodynamics by field observations is generally difficult as in situ data are scarce and only available for very limited areas, if at all. This particularly applies to bathymetrical data measured just before and after a storm surge event. Data on storm-induced bed evolution are necessary for model calibration and verification purposes. Available observations and published data of the studied tidal inlet and adjacent barrier islands beaches are summarized and compared to modeled hydrodynamics, sediment dynamics and surface sediment grain-size distributions in order to determine the validity of the modeling approach below. Modeled data are from the two most detailed model domains of the cascade of nested model grids (Fig. 3).

2.4.1. Hydrodynamics

Time series of simulated water levels are compared to observations at available tidal gauges within the study area (data provided by the Federal Agency of Water and Navigation, WSV). Figure 6 shows modeled versus observed water level time series for the storm surge event at Spiekeroog tidal

gauge. High water levels are generally well reproduced by the model, whereas low water levels show discrepancies. The phase lag between modeled and measured water level time series is in the range of 10–20 min. The root-mean-square errors (RMSE) for the water level amplitudes for the fair-weather and storm simulations are 12 and 19 cm at Spiekeroog and 14 and 22 cm at Langeoog.

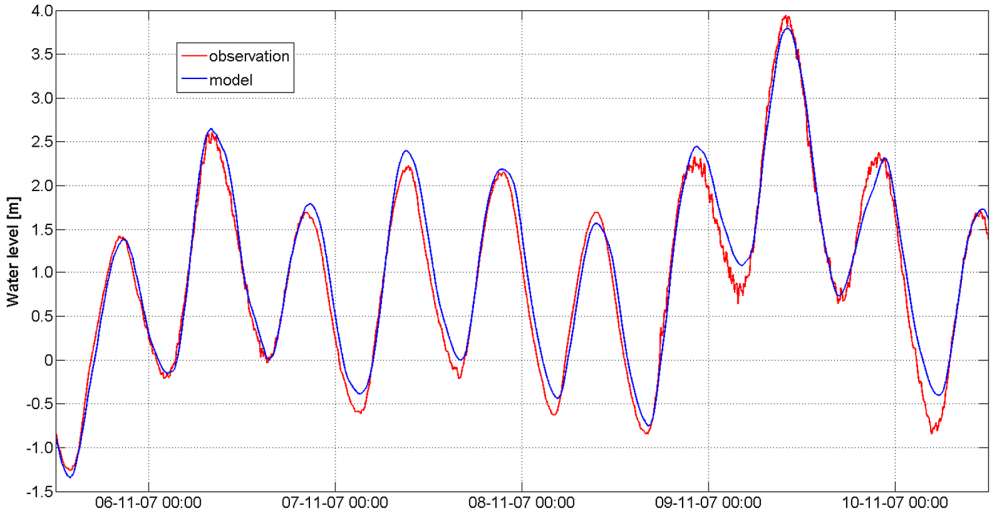

Figure 6. Comparison of modeled and observed water level time series at the water level gauge Spiekeroog for the storm event 'Tilo' with peak surge levels on 9. Nov. 2007.

Wave data measured during the storm event at the surf zone of the island of Norderney are available from a project report of the FSK-NLWKN (Kaiser et al., 2008). The island of Norderney is located 25 km to the west of the studied tidal inlet. The downward-looking ultrasound device mounted on a pole produced corrupted data once the distance between the water surface and the sensor was too small, due to unexpectedly high surge levels. Approximately 1 h before, on 9. Nov. 2007 at 07:00 UTC, a time-averaged significant wave height of 3.5 m is qualitatively compared to predictions of the storm simulation of the next larger model grid ('East Frisian Island Model', Fig. 3). The measured wave height is underestimated by 17 % in the simulation and thus confirms fair reliability of the predicted wave energy in the surf zone.

Time series of water levels and wave parameters were measured during the storm event at an observational pole located in the inner part of the Accumer Ee inlet separating the islands of Baltrum and Langeoog. The pole was operated between the years 2000 and 2007 by Helmholtz-Zentrum Geesthacht. Its configuration and functioning is described in Onken et al. (2007). The pole's location was not directly at the studied tidal inlet, but was still within the most detailed model domain (Fig. 2). The observation point is located at a hydrodynamic complex and morphologically dynamic location at the junction of the main tidal channel and a larger tributary. Here, bathymetrical information is only

available for spring 2005 and has been incorporated in the model bathymetry, two years ahead of the chosen validation period of November 2007. Local differences between the real and the model bathymetry may influence the local wave regime, making a quantitative model validation based on the existing observations ambiguous. Observed wave parameters were calculated from water level elevations recorded at a frequency of 2 Hz taken from a floater guided along a rod with a magnetic readout. Spikes and stuck values were cleaned from the data. The effect of this data cleaning is shown in Lane et al. (2000) and the usage of floater-derived wave parameters for model validation in the North Frisian Sylt-Rømø Bight demonstrated in Schneggenburger et al. (2000).

Phases and amplitudes of the observed water levels and wave parameters are fairly well reproduced by the model in view of the complexity of the wave-current interactions at the measuring site (Fig. 7). For significant wave height (Hs), model data exhibit a bias of 0.24 m. Statistical analysis of model predictions with respect to the observations allows for evaluation of the RMSE of 0.19 m for the water level, 0.26 m for Hs, 0.69 sec for the peak wave period (Tp) and 0.34 sec for the mean wave period (Tm). Discrepancies tend to be slightly larger during ebb and low water compared to flood. One explanation is that the measuring pole was exposed to the focused ebb currents in the tributary tidal channel that were opposite to wave propagation. The overestimated wave height during ebb may be a consequence of insufficient wave dissipation due to whitecapping incorporated by the saturation-based whitecapping formulation of Van der Westhuysen (2007). The enhanced dissipation of waves on negative current gradients after a recently published formulation (Van der Westhuysen, 2012) was successfully applied in Dodet et al. (2013). In the present study, however, uncertainty as to the bathymetry at the measuring site does not allow for the calibration of the model by the application of different whitecapping formulations.

It should be noted that no model calibration was performed by spatially varying bed roughness adaptation. Instead, the bed roughness was set to a uniform, constant value over the model domain (Manning parameter 0.024). Particularly against this background, this validation attests adequate model skill for the purpose of this study.

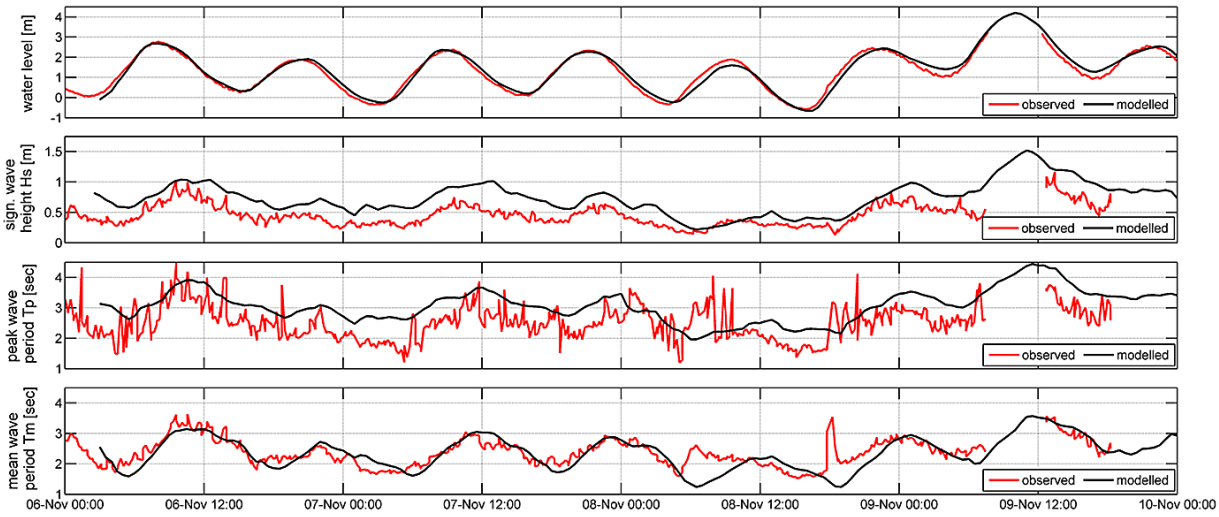

Figure 7. Observed and modeled water levels, significant wave heights (Hs), peak wave periods (Tp) and mean wave periods (Tm) at the back barrier of Langeoog during 'Tilo' in November 2007 (observations provided by Helmholtz-Zentrum Geesthacht).

2.4.2. Sediment dynamics and morphology

Time series measurements of suspended matter (SPM) concentrations observed at the tidal inlet Otzumer Balje during the storm surge peak tide on 9. Nov. 2007 show hourly mean (maximum) values on the order of 35 (65) mg/l and 55 (95) mg/l for maximum flood- and ebb-tide currents, respectively, at 0.5 m below mean low water level (Badewien et al., 2009). The three finest sediment fractions incorporated in the model simulation (150, 200 and 250 µm) reveal hourly mean (maximum) SPM concentrations of 45 (70) mg/l during maximum flood-tide currents at 2 m below German datum at the location of the measuring pole. During flood tide, SPM concentrations at the inlet are due to nearshore wave-induced sand resuspensions. The model reproduces suspended sediment dynamics fairly well for these conditions: hourly mean and maximum concentrations are overestimated by approximately 29 and 8 %, respectively. During ebb tide, however, predicted maximum SPM concentrations of 2 mg/l are strongly underestimated with respect to measurements (95 mg/l). This can possibly be explained by the fact that fine sand (< 150 µm) and cohesive sediments that are typically flushed out of the back-barrier tidal flats during increased storm surge ebb-flows (Bartholomä et al., 2009; Cuneo and Flemming, 2000) are simply not incorporated in this model set-up. However, discrepancies here are not relevant for this study, because the model is not applied to predict residual sediment rates between the foreshore and back-barrier basin.

Observations of morphological changes as a response to the storm event of November 2007 are available for two cross-shore profiles at the foreshore of Langeoog, both extending from the

coastal dune up to a distance of 3900 m from the beach into water depths of 14 m below German datum. Data of profiles 37 and 38 measured at Langeoog on 15 October and on 12 and 22 November 2007 by the Coastal Research Station were processed with permission from NLWKN (Kaiser et al., 2008). A direct comparison of observed and modeled morphological changes is not possible because bathymetrical data of spring 2006 being used to set up the model bathymetry do not coincide with the cross-shore profiles that were measured in October and November 2007. Morphological changes along these profiles are thus qualitatively compared to predicted patterns of erosion and sedimentation of the storm simulation (Appendix A).

Morphological changes evaluated from observations are on the order of 0.5 m to 1.0 m at the surf zone within the first 500 m of the profiles (Figs. A1 and A2). This order of magnitude is reproduced by the model; in particular, the erosion of the upper beach and the filling of the trough of the first berm are generally captured by the model (Fig. A3). Between 500 and 2000 m from the beach, the downdrift migration of two shore-oblique sand bars through the transversal profiles generates alternations in erosion and deposition of approximately 0.5 m, which reveals good agreement with model predictions. At 2000–3500 m from the shoreline, mostly deposition on the order of 0.1 to 0.3 m is observed. The landward trough of the shoreface-connected ridge at the end of the profiles accumulates sand, whereas the adjacent slopes tend to suffer from erosion. Predicted sand depositions of 0.05 to 0.1 m in between depth isolines −6 and −9 m are underestimated by the model.

This qualitative analysis shows fair similarities between model predictions and observations in terms of magnitude and alteration from net sedimentation to net erosion at the described morphological compartments.

2.4.3. Sedimentology

Mapping of surface sedimentology of the whole domain of interest is not available. However, Son et al. (2010) compiled surface sediment grain-size distributions in the Otzumer Balje tidal inlet from a grid of Shipek sediment grab samples at distances of approximately 280 m for the year 2005. Their data are reinterpolated here to allow for comparison with modeled data. Modeled mean surface sediment grain-sizes are due to redistributions of five sand fractions between 150 and 450 μm; and are generated by a series of three model runs with alternating hydrodynamic forcings due to fair-weather conditions, storm conditions and then fair-weather conditions once more (Sect. 2.3.6.2, Figs. 5 and 8a).

The initial bathymetry of the detailed tidal inlet model is based on bathymetrical data of the years 2006 and 2007and thus different from the inlet morphology of the sediment sampling campaign of 2005, here indicated by isolines based on available bathymetrical data of the years 2004 and 2005 (Fig. 8). The different morphological background explains the westerly bend of the channel through

the ebb-tidal delta for the sampling state compared to a more straightened orientation in the model bathymetry.

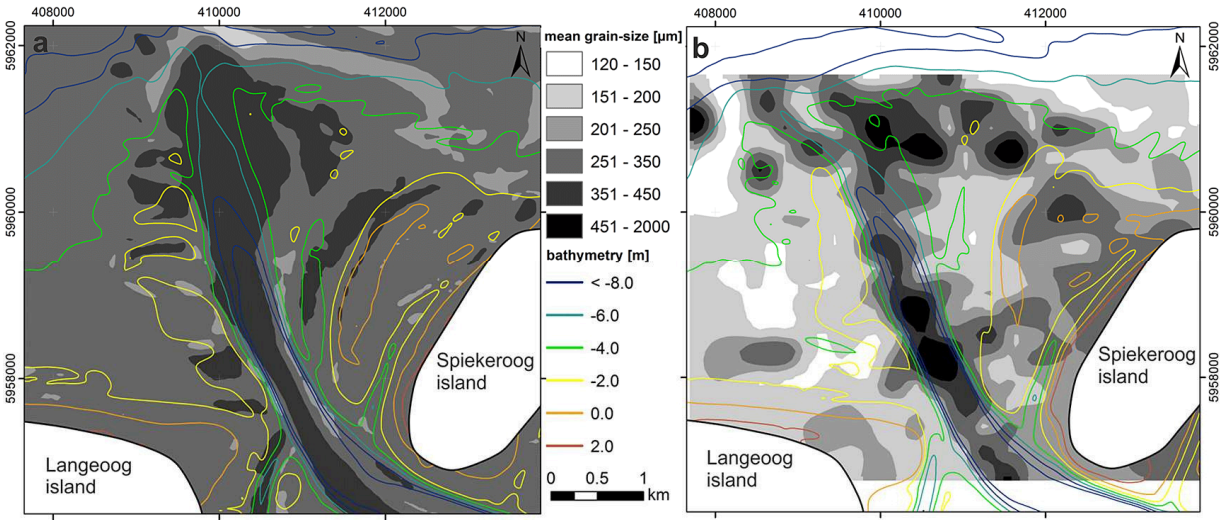

Figure 8. Modeled (a) and measured (b) arithmetic mean surface sediment grain-size distributions at Otzumer Balje inlet between Langeoog and Spiekeroog; depth isolines based on bathymetrical data measured in 2006/2007 (a) and 2004/2005 (b).

Modeled and measured arithmetic mean surface sediment grain-size distributions show distinct similarities (Fig. 8). Surface sediments are coarsest at the inlet channel, the ebb-tidal delta and the eastern ebb-tidal delta shoal where swash bars migrate onshore. The central part of the ebb-tidal delta with medium to coarse sands is divided by a characteristic south–north-oriented pattern of finer mean grain sizes shown by both modeled and measured distributions. At the foreshore, modeled mean grain sizes are generally coarser with respect to measurements. This is explained by the selection of the initial mean surface sediment grain-size of 280 µm composed of five uniformly distributed fractions that tend to be too coarse for specific areas, e.g., the foreshore or the back-barrier tidal flats, particularly as the performance of the model to predict surface sediment grain-sizes decreases as morphological changes are small and thus sorting of sand fractions cannot take place.

At the western ebb-delta shoals, on the other hand, distinct grain-size patterns of medium sand that are predicted by the model cannot be validated by field data as the distance between sample positions (approx. 280 m) is too large for these spatial patterns in surface sediment grain-sizes to properly be resolved.

2.5. Results

We compare the effect of an extreme storm surge event in the North Sea to a medium-term period (approx. 5 months) of representative fair-weather conditions on morphodynamics and sedimentology at the tidal inlet Otzumer Balje between the barrier islands Langeoog and Spiekeroog based on two model simulations.

Both simulations reveal sediment pathways for five distinct sediment fractions of 150, 200, 250, 350 and 450 µm. Residual total load (suspended and bed load) sediment transport of small sand fractions, i.e., 150 and 200 µm, shows pathways comparable to the residual suspended load sediment transport of all five fractions. On the other hand, residual total load transports of coarser sand fractions, i.e., 350 and 450 µm, resemble the pathways of the overall residual sediment transport due to bed load quantities. This is not unexpected and means that pathways of individual grain-size fractions do not give significant additional information compared to a presentation that only differentiates between pathways of bed load and suspended load transport. Figures of residual sediment transport pathways integrated over all five sand fractions are thus presented hereafter as total load, bed load or suspended load quantities.

It may be noted here that the morphological acceleration factor, i.e., MORFAC = 20 (Sect. 2.3.2), being applied during fair-weather simulations only accounts for an accelerated development of the morphology and the sediment grain-size distribution; however, it does not apply in the computation of sediment transport loads. The residual sediment transport load [$m^3/s/m$] is thus the time-averaged transport load over a runtime of 17 tidal cycles during fair-weather conditions and of 9 tidal cycles during the storm event.

2.5.1. Tide-dominated fair-weather conditions

Residual total sediment transport fluxes during fair-weather conditions are largest in the vicinity of the tidal inlet, particularly in the inlet throat and the eastern marginal flood channel (Fig. 9a). The residual total load sediment fluxes are differentiated into residual bed load transports (Fig. 10a) and residual suspended load transports (Fig. 10b). Residual suspended load quantities are approximately 4 times larger than the residual bed load quantities, but their residual directions are similar. North of the deepest location in the inlet throat, residual transport is ebb-dominant and directed towards the ebb-tidal delta, whereas southwards it follows the inlet channel towards the flood delta and the back-barrier basin.

At the easterly end of Langeoog, alongshore net sediment drift supplies bed- and suspended load towards the inlet throat of the tidal inlet. At the western ebb-tidal delta shoal, a residual sediment

import to the inlet throat takes place over the shallow shoals, whereas predominantly suspended sediment load is exported via ebb channels located in between these shoals.

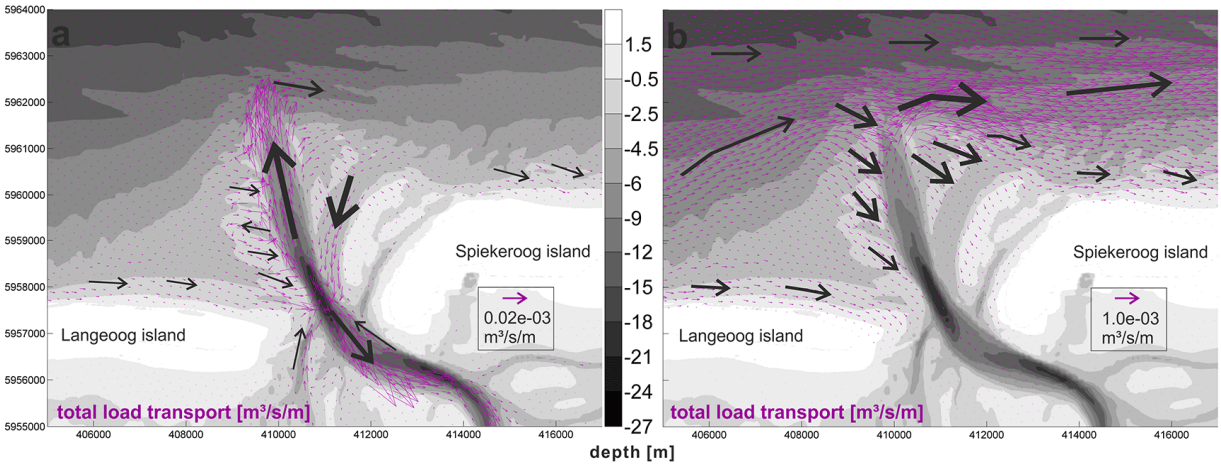

Figure 9. Residual total load transport for fair-weather conditions (a) and storm conditions (b); schematic main residual pathways indicated by black arrows.

At the northern part of the eastern ebb-tidal delta shoal, minor residual bed- and suspended load quantities are transported in a sharp bend from the center of the ebb-tidal delta to the eastern ebb-tidal delta shoal in a south-southeasterly direction. With increasing water depths landwards of the shoal, the sand is directed into a deeper, transverse tidal channel. Through this flood-dominant, marginal tidal channel significant residual suspended and bed load quantities are transported in a south-southwesterly direction back to the tidal inlet throat.

At the inlet widening towards the back-barrier tidal basin, the inlet throat is flood-dominant. Residual fluxes of predominantly suspended sediment point along the main inlet channel towards the flood-tidal delta and adjacent tidal flats. At the northern margin of the main channel and alongside the western head of Spiekeroog, minor residual bed- and suspended load fluxes are opposite and thus ebb-directed via a bordering transport pathway. Between the easterly end of Langeoog and the flood delta, a marginal tidal channel is also ebb-dominated and leads residual suspended and bed load fluxes out of the basin.

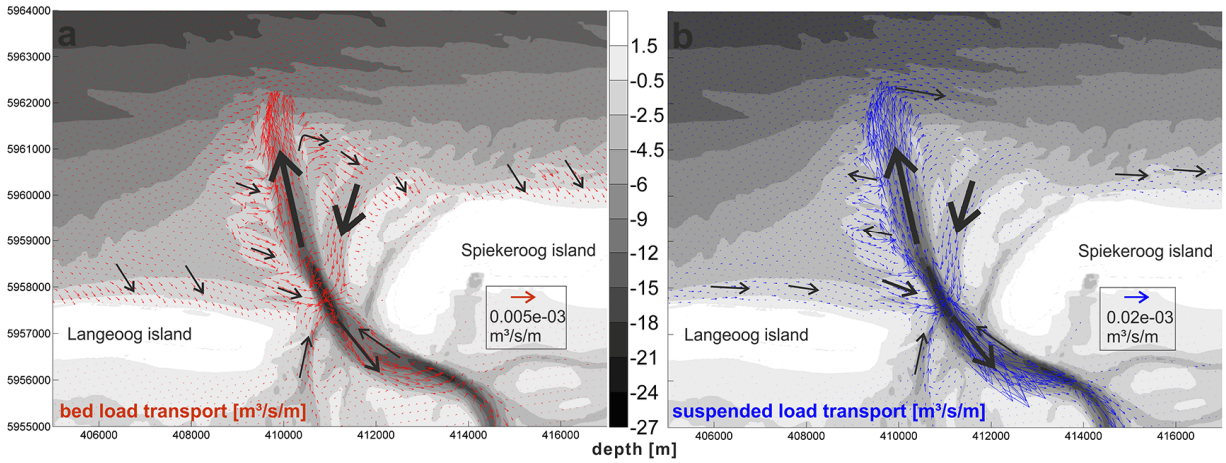

Figure 10. Residual bed load (a) and residual suspended load (b) transport for fair-weather conditions; schematic main residual pathways indicated by black arrows. Relative vector scaling indicates suspended load to be approx. 4 times larger than bed load transport.

The mid-term fair-weather simulation reveals morphological and sedimentological changes at the tidal inlet and adjacent channels, at shore-parallel bars in the surf zone and shore-oblique sand bars (Figs. 12a and 13a). Sediment dynamics at the foreshore are insignificant and net morphological changes are below 0.05 m (Fig. 12a). Sediments being eroded in the inlet throat and tributary channels are transported and deposited at the ebb-tidal delta and adjacent shoals. The most northern part of the ebb-tidal delta increases and protrudes offshore with net depositions exceeding 1.0 m at the ebb-delta lobe during the simulated period of 5 months.

The sediment distribution shows a relative coarsening of the mean surface sediment grain-size on the order of 30–50 µm at the western ebb-tidal delta shoals and at the tidal channels, whereas the ebb-tidal delta lobe is fed by the entrained finer sand fractions and decreases the mean grain size by approx. 30–40 µm (Fig. 13a). Sedimentological changes are in relation to the initial, nonuniform sediment distribution (Fig. 5); thus the redistribution of surface sediments is small because the sedimentological response to fair-weather hydrodynamic conditions is largely included in the initial condition already. The absolute mean sediment grain-size distribution due to synthetic simulations (Fig. 4a), however, shows that the depositional area at the ebb-tidal delta experiences a grading of sediment grain-sizes. The finest sand is deposited at the outermost ebb-tidal delta lobe where ebb-directed current velocities decrease due to increasing water depths.

Shore-oblique sand bars migrate eastwards in the same direction as the overall littoral sediment drift (Fig. 12a). Similar to fluvial low-energy bed forms, erosion takes place on the stoss side and sedimentation on the lee side. Once again, synthetic simulations reveal a gradient in mean surface sediment grain-sizes with medium (fine to medium) sands at the upper stoss side and the crest (lee side

and trough) (Fig. 4a); this indicates that tide-dominated alongshore current velocities during fair-weather conditions are strong enough to develop typical sediment gradients over morphological features.

2.5.2. Wave-dominated high-energy storm conditions

During the storm event, residual eastward-directed total sediment fluxes are predicted to be largest at the barrier island foreshore, particularly directly off the ebb-tidal delta, whereas residual sediment load is very small in the tidal inlet throat (Fig. 9b). Across the tidal inlet, the residual total sediment transport direction is flood-dominant, but only a marginal amount of sand tends to be imported to the back-barrier basin. The residual total load transport is differentiated into residual bed- and suspended load transport vectors (Fig. 11a and 11b).

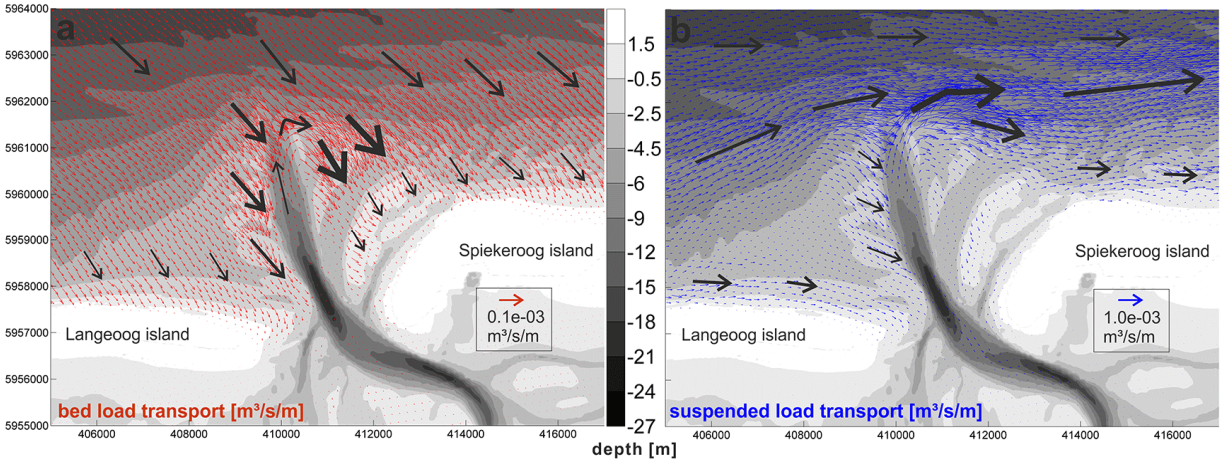

Figure 11. Residual bed load (a) and residual suspended load (b) transport for high-energy storm conditions; schematic main residual pathways indicated by black arrows. Relative vector scaling indicates suspended load to be approx. 10 times larger than bed load transport.

Disregarding the residual transport directions, the relative scaling of the vectors indicates that the net suspended load quantity is overall approximately one order of magnitude higher than the net bed load quantity. The residual bed load transport is south-southeastward-directed, particularly at the eastern ebb-tidal delta shoal where it drives the migration of swash bars. The residual bed load transport direction agrees with the mean direction of wave propagation. Residual suspended sediment transport load is largest close to the ebb-tidal delta and in the extended surf zone from the islands' beaches to the transition of upper to lower shoreface. Here, residual directions are downdrift-oriented due to wave-induced alongshore currents that advect the entrained sand to the east.

During the storm event, significant morphological and sedimentological changes occur over large areas of the barrier island foreshore and upper shoreface, but particularly in the northern part of the ebb-tidal delta (Figs. 12b and 13b). High-energetic waves refract and break on the depth-limited ebb-tidal delta shoals, stirring large quantities of sediment. In the vicinity of the ebb-tidal delta, morphological changes along distinct linear patterns are predicted to be 1 m or more during this storm event (Fig. 12b). Fine sand fractions of 150, 200 and 250 µm are transported as suspended load by the combined flow of tide-, wind- and wave-induced currents downdrift to the east. Mostly medium-sized sands with sand fractions of 250, 350 and 450 µm remain, and as a result they increase the mean surface sediment grain-size by up to 100 µm at the most seaward part of the ebb-tidal delta shoal (Fig. 13b).

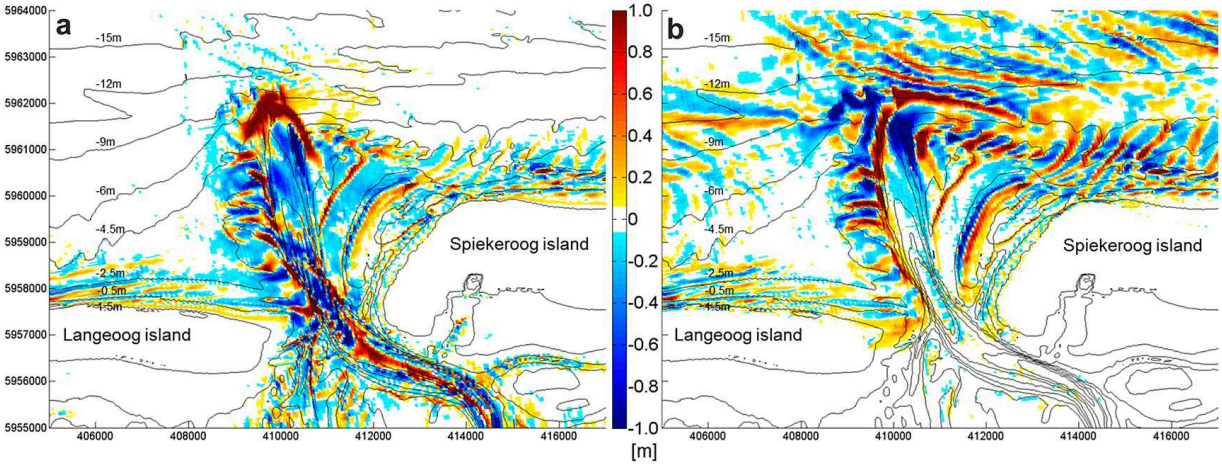

Figure 12. Morphological changes, i.e., sedimentation (red) and erosion (blue) as a response to fair-weather (a) and storm (b) conditions; analysis simulations were initiated with nonuniformly distributed sediment fractions (Fig. 5).

The morphology and sedimentology of the inlet throat and marginal flood channels are less affected, as the driving wave energy is dissipated at the shallow ebb-tidal delta shoals. In addition, bottom shear stress decreases as the tidal flow slows down through the relatively increased cross-sectional area of the inlet because of elevated surge levels.

Grain sizes increase insignificantly at the inlet gorge, whereas fine sands accumulate at the western margin of the inlet throat (Fig. 13b). Here, transport over the western ebb-tidal delta shoal directs finer sand south-southeastwards to the western margin of the inlet throat where settling starts, with increasing water depths and thus decreasing shear stresses causing a lateral shift of the inlet throat to the east (Fig. 12b).

At the eastern ebb-tidal delta shoal, alternating erosion and deposition patterns indicate a south-southeastward migration of large swash bars that are oriented almost parallel to the shore and thus deviate from shore-oblique sand bars (Fig. 12b). At the northeastern edge of the ebb-tidal delta shoal, shore-oblique sand bars connecting the eastern ebb-tidal delta with the downdrift surf zone migrate eastwards during storm conditions. The sediment distribution due to the synthetic simulation being initiated with uniformly distributed sediment fractions predicts coarser grain sizes at the bed form crests with respect to the troughs of the shore-oblique sand bars (Fig. 4b). Analysis simulations of the storm event being initiated by a nonuniform sediment distribution (Fig. 5) reveal this gradient to be further enhanced (Fig. 13b). At the lower shoreface, fine sand fractions are winnowed and eroded in the troughs between and at the landward slopes of shoreface-connected sand ridges being located in water depths of 15–20 m below German datum (Fig. 13b). Fine sand tends to accumulate on the crests and the seaward slopes of the shoreface-connected ridges. Thus the shoreface-connected ridges experience a positive morphological feed-back and a downdrift migration (Fig. 12b).

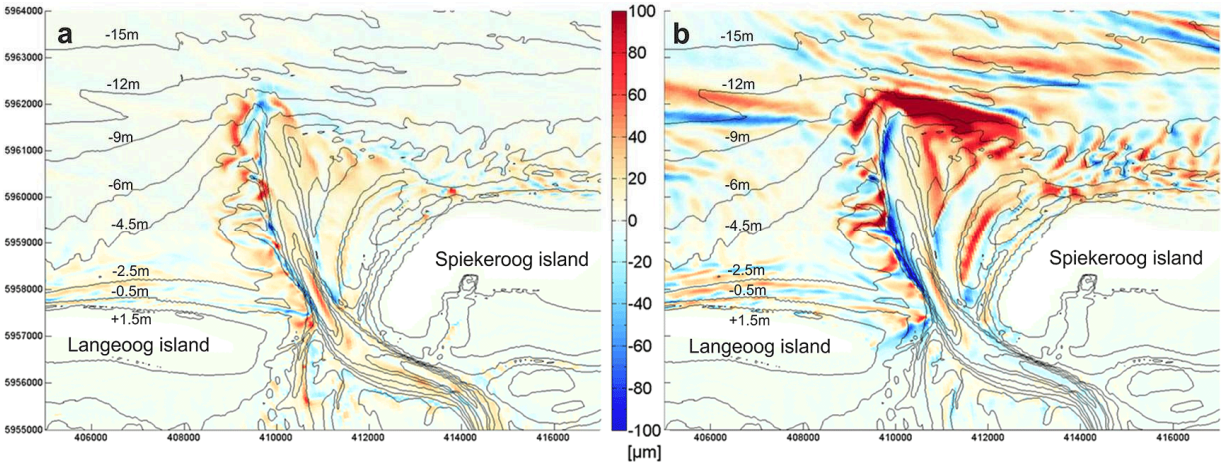

Figure 13. Sedimentological changes, i.e., relative increase (red) and decrease (blue) of mean surface sediment grain-size as a response to fair-weather (a) and storm (b) conditions; analysis simulations were initiated with nonuniformly distributed sediment fractions (Fig. 5).

2.6. Discussion

2.6.1. Mixed-energy tidal inlet morphology and sedimentology in response to tide- and wave-dominated conditions

The main drivers determining the morphodynamic development of a mixed-energy tidal inlet system are commonly assumed to be waves that induce sediment stirring, transport and dispersal at the ebb-tidal delta and tidal currents in the inlet (e.g., FitzGerald et al., 2012; De Swart and Zimmerman,

2009). Mixed-energy barrier island tidal inlets are morphologically highly dynamic environments where both drivers continuously interact. Numerical model scenario experiments allow for the separation of processes and boundary conditions for greater understanding of the system. However, a potential model approach that reduces the forcing to either tides or waves alone would be misleading as the natural interaction at mixed-energy tidal inlets would be ignored. Instead, tide- and wave-dominated forcing conditions are represented here by realistic fair-weather and storm scenarios, respectively, which allow the evaluation of the morphological and sedimentological responses to distinct hydrodynamic drivers by preserving the mixed-energy regime of the system at the same time.

For typical mixed-energy tidal inlets, it is commonly assumed that ebb-tidal delta erosion during episodic storm events counteracts the continuous replenishment of the ebb-tidal delta lobe during tide-dominated fair-weather conditions (FitzGerald et al., 2012; Hayes, 1979). This study reproduces and thus confirms this hypothesis: model simulations of mid-term fair-weather conditions reveal that the morphological activity mainly focuses on the inlet throat. East-ward littoral drift along the foreshore beaches supplies fine sands to the inlet throat. In the deep inlet channel, bed shear stress due to tidal currents is strong enough to remove fine sands. As residual sediment fluxes in the seaward part of the inlet throat are ebb-directed, the entrained fine sands mainly feed the ebb-tidal delta terminal lobe. During storm conditions, wave refraction and shoaling over steep bottom gradients focus wave energy towards the ebb-tidal delta lobe and its shallow shoals where energy dissipates due to wave breaking. Here, the fine sand deposited during fair-weather periods is easily mobilized and transported eastwards by the ambient flow, dominated by alongshore velocity components induced by high-energy waves. These waves, approaching at an angle with respect to the shore, generate alongshore momentum flux that is greatest in the zone of breaking waves (Longuet-Higgins and Stewart, 1964). Furthermore, the model predicts transportation of coarse sand fractions as bed load in the landward direction and by migration of large swash bars superimposed onto the ebb-tidal delta shoals. As mentioned previously, the term ‘swash bars’ is misleading as these sand bars are not primarily exposed to swash, and particularly not during storm surge conditions. Bertin et al. (2009) note a physical explanation based on a shore-directed component of forces due to wave breaking (i.e., radiation stress gradients) over the delta shoal that is not compensated for by pressure gradient terms in the momentum balance equation as the associated wave-induced water level setup is spread into the tidal inlet and the back-barrier basin; it is also referred to as the ‘bulldozer effect’, i.e., the shoaling and prograding of the ebb-tidal delta (Hageman, 1969).

Sediment grain-size-sorting mechanisms and thus the spatial distribution of surface sediments are related to bed shear stress controlled by wave- and tide-induced flow: residual distributions of surface sediment grain-sizes make it clear that both storm conditions with high-energy waves and fair-

weather conditions where tidal currents dominate contribute to the sedimentology of barrier island tidal inlets and fore-shore. At the tidal inlet, for instance, we can generalize that winnowing of fine sand at the inlet throat and marginal channels is attributed to tidal forcing, whereas high-energy waves are the driver for sorting mechanisms at shallow shoals of the ebb-tidal delta (Fig. 4). Simulations have shown that only the combined scenario forcing, i.e., alternating fair-weather and storm simulations, results in a surface sediment grain-size distribution that is in fair agreement with sedimentological field observations at Otzumer Balje inlet (Fig. 8; Son et al., 2010). This suggests that the combination of both hydrodynamic forcing conditions is needed to determine the inlet sedimentology. Furthermore, in light of the analogy of modeled and observed sedimentological patterns, this confirms the model setup applied here to reliably simulate sediment dynamics in general and the evaluation of morphological and sedimentological features in response to representative boundary conditions in particular. The applied model resolution and necessarily reduced multi-fractional approach proves the ability to reproduce gradients in grain sizes on the spatial scale of morphological features equal and larger than swash bars and shore-oblique sand bars. Although smaller morphological features and bed forms such as ripples and dunes are not resolved in the model bathymetry, the modeling approach demonstrated here allows for the identification of distinct pathways of particular sediment grain-size fractions in response to wave-current interactions.

In the following, an example is given where simulated fluxes of particular sediment grain-sizes combined with detailed information on three-dimensional hydrodynamics allow for the identification of larger scale sorting mechanisms at the ebb-tidal delta lobe and the upper shoreface.

Surface sediment grain-size composition reveals simulated mass fractions of up to 65 and 35 % for sand fractions of 150 and 200 µm, respectively, which accumulate at the ebb-tidal delta terminal lobe during tide-dominated fair-weather conditions. Here, predicted mean grain sizes are 170 µm and thus in fair agreement with observations of 120 to 150 µm at Otzumer Balje (Son et al., 2010) and 120 to 180 µm at ‘Harle’ (Hanisch, 1981), the tidal inlet to the east of Spiekeroog. The two finest sand fractions of 150 and 200 µm are obviously stirred by wave action at the outer margin of the ebb-tidal delta but also bypass the inlet along the upper shoreface due to the storm-driven alongshore drift to the east. The finest fraction of 150 µm primarily settles at areas of reduced energy off the downdrift island of Spiekeroog within a shore-parallel band between the surf zone and the sloping faces of the shoreface-connected ridges. Here, after the storm simulation, 20–30 % of the surface sediment is made up of this finest grain-size fraction of 150 µm. Antia (1995) observed an almost shore-parallel elongated pattern of accumulated fine sands with mass fractions between 10 and 30 % for settling velocities of 1–1.5 cm/s, which translates to grain sizes of 115–150 µm after Gibbs et al. (1971). Antia (1995) also describes this pattern as being extended between two bands of medium sands, one at the

surf zone and the other along the shoreface-connected ridges. The storm simulation reveals the physical process that explains this established deposit of fine sediments at the upper shoreface: wave-induced currents counteract the opposing westerly directed along-shore ebb-tidal currents in the expanded surf zone. The ebb-tidal flow is restricted within this zone of wave-dominated alongshore currents and shifted to deeper waters outside the surf zone. This results in a band of reduced bottom shear at the interfacial boundary area of eastwards-directed wave-induced flow and westward-directed ebb-tidal flow. In this area, settling of fine-grained sand is possible. Inside the surf zone, alongshore wave-induced bottom currents are diverted slightly offshore at a shore-oblique angle due to the opposing ebb currents. In nature, enhanced offshore-directed cu rents due to undertow or downwelling (e.g., Niedoroda et al., 1984) may supply additional fine sand to the zone of reduced bottom shear. The latter process is most likely under-estimated by the model. The onshore-directed wave streaming (Walstra et al., 2000) opposes and reduces the offshore-directed bottom shear stresses induced by undertow that is driven by wind surge and wave setup.

Besides these deposits of fine sand at the terminal lobe of the ebb-tidal delta and the shore-parallel band at the upper shoreface, additional characteristic spatial patterns are identified that stand out due to pronounced depositional processes within the surface sediment layer. Particularly for storm conditions, the simulation reveals elongated channel fill deposits of fine-grained sand at the northern fringe of the marginal eastern flood channel, which is even more pronounced at the westerly, sloping side of the inlet throat (Figs. 12b and 13b). The latter has been classified as channel margin linear bars (Hayes, 1979). Hubbard et al. (1979) called this a ‘zone of equilibrium’, where landward wave-induced flow over the marginal shoal platform is opposed and dominated by the ebb-directed tidal jet in the inlet throat. As described earlier, we identified several similar zones of fine-grained deposits that evidently all have in common that tidal flow is partly or fully retarded and balanced by the opposing wave-induced momentum flux or vice versa. This results in a local reduction of bottom shear along the lateral interface of counteracting current fields and supports accumulation of fine-grained sediments. Wind- and wave-induced setup increases the water depth and the cross-sectional area within the inlet, supporting further reduction of bottom shear stresses.

All other patterns at the tidal inlet and the foreshore region can be explained by erosional processes where fine sands are winnowed from surface sediments and thus medium to coarse sediment grain-sizes remain, e.g., the bottom of the tidal channels during tide-dominated fair-weather conditions and the ebb-tidal delta shoals during wave-dominated storm conditions.

2.6.2. Sediment recirculation patterns at the eastern ebb-tidal delta shoal

A simulation of tidal inlet morphology, sedimentology and sediment pathways calls for the identification of the communication and coupling of mesoscale hydro- and sediment dynamics between morphological units such as the ebb-tidal delta shoals, the inlet channels and the adjacent barrier coast.

Dissanayake et al. (2009) simulated the interaction between inlet tidal currents and alongshore tidal currents for an idealized tidal inlet by applying a process-based model. The residual flow pattern showed that a rotational current field is only developed to the east of the ebb-tidal delta. The physical description relates to the fact that strong directional velocity fields are developed to the west of the inlet when the alongshore current is eastward (westward) and the inlet current is landward (seaward), whereas the rotational current field supports the ebb-tidal delta growth in the east. These findings agree with the conceptual hypotheses of Sha (1989) and Sha and Van den Berg (1993). In a numerical model study for an idealized and a natural tidal inlet, Hench and Luettich (2003) give an additional explanation of how momentum balances contribute to circulation processes by tidal forcing alone. The inlet jet induces a 'dynamical wall effect' with momentum imbalances due to tidal phase lags resulting in transient, cross-inlet elevation differences and thus secondary circulation for different stages of the tide. With respect to the symmetrical geometry of their idealized inlet, the authors were able to show that the morphology of the natural inlet, i.e., particularly marginal tidal channels, plays an additional role in focusing the identified fluxes. In contrast to these tide-controlled circulation cells, FitzGerald et al. (1976) and Smith and FitzGerald (1994) describe 'sediment gyres' downdrift of the inlet due to wave refraction and swash over the ebb-tidal delta shoal platform that drive swash bars in a net landward direction, whereas wave-induced setup shoreward of the swash bars augments the inlet-directed currents in the marginal flood channel. Smith and FitzGerald (1994) conclude from sediment budgets due to assessed transport rates and morphological evolution analysis at the Essex River ebb-tidal delta system that the circulated sediment flux within the sediment gyres is estimated to be even larger than the amount that bypasses the inlet. Finley (1978) further adds that refraction of moderate waves around the inlet ebb-tidal jet is a process that contributes to ebb-tidal delta growth. The shoals are an efficient trap of reversed littoral sediment drift that would otherwise be carried alongshore.

These examples from the literature show the importance of recirculation cells for tidal inlet morphology and its budget in particular. Sediment dynamics involved are explained by physical processes that are controlled by either tides or waves. However, at mixed-energy tidal inlets, it is questionable which of the drivers contribute to the net circulation.

At the Otzumer Balje inlet, residual sediment fluxes reveal a pronounced recirculation cell at the eastern ebb-tidal delta shoal. The circular pathway of particular grain-size fractions is obviously of importance for the overall sediment dynamics. During storm conditions, individual swash bar migration and wave-induced bed load transport of medium sand point in the landward direction over the eastern ebb-delta shoal platform. During fair-weather conditions, however, residual transport is concentrated in the transverse, flood-dominated tidal channel to the south of the eastern shoal platform and leads towards the southwest into the inlet throat. Once in the inlet throat, ebb-directed residual transport directs fine and medium sand to the ebb-tidal delta, where the cycle restarts. This suggests that solely the combination of wave-dominant storm and tide-dominant fair-weather conditions leads to net sediment fluxes describing a circular pathway to the east of the tidal inlet redirecting predominantly medium sand to the inlet throat.

The simulated sediment pathways confirm the conceptual model of Son et al. (2010), who assumed a recirculation cell over the eastern ebb-tidal delta shoal of Otzumer Balje tidal inlet in which sediment is recycled towards the inlet throat. Their hypothesis was primarily derived from the orientation of sedimentary structures found in box- and vibrocores. Sediment beds showed parallel lamination, which, according to the authors, originated from storm events that are better preserved in the long term than cross-laminated features generated during moderate conditions and that indicate dominant sediment pathways of medium-grained sand in a shoreward direction over the eastern ebb-delta shoal.

Separation into wave- and tide-dominated conditions allows for the differentiation of residual sediment fluxes that contribute to the recirculation cell. First, closed sediment circulation cells are not recognized for storm conditions. Here, wave-induced bed load transport is onshore-directed over the shoal platform, but no direct reversal to the inlet throat is evident. During fair-weather conditions, a complete circulation cell is weakly identifiable with prominent residual sediment transport through the ebb-dominated inlet throat and the flood-dominated eastern marginal channel but only minor residual transport in the shoreward direction over the eastern shoal platform. Hence, we conclude that – at least for the tidal inlet studied here – significant recirculation of sand to the inlet is only possible from a combination of both fair-weather and storm conditions.

In this context, we would like to address the aforementioned sediment bypass at the Otzumer Balje inlet. Son et al. (2010) suggest that there is no evidence for fine sand by-passing the tidal inlet. If at all, bypassing would take place along the subtidal margin of the terminal lobe and be independent of processes acting on the ebb-tidal delta. However, no evidence was given to support this hypothesis, as no data were collected from regions seaward of the ebb-tidal delta. Our simulations reveal sediment bypass to the downdrift beach and foreshore for both moderate and extreme conditions, in

disagreement with the hypothesis of Son et al. (2010). The magnitudes of the bypass, seaward extent and the dominant grain size are primarily controlled by wave energy, i.e., wave-induced alongshore currents, and are consequently increased for storm compared to fair-weather conditions.

The question of whether the net volume of sand that is recirculated to the inlet throat is dominant over the bypassed quantity must be answered by future studies, as the simulated scenarios are representative of either tide- or wave-dominated conditions but nonrepresentative of the long-term regime of this mixed-energy tidal inlet. Ongoing research aims to elucidate the sediment budget at the tidal inlet.

2.7. Conclusions

This study identifies residual sediment fluxes of particular grain-size fractions and related morphological and sedimentological responses of a mixed-energy tidal inlet system. We use a process-based numerical modeling system to differentiate the effects of either tide- or wave-dominant forcing. During storm conditions, the ebb-tidal delta loses sand through wave impact. For fair-weather conditions, the ebb-tidal delta is replenished by ebb-directed residual sediment transports. The model simulations satisfactorily reproduce this well-known dynamic behavior. Sediment grain-size sorting mechanisms are also affected by the interacting tide- and wave-driven flow. We have shown that only a combined scenario forcing, i.e., alternating fair-weather and storm simulations, can result in a surface sediment grain-size distribution that is in agreement with measured grain-size distributions (Son et al., 2010). Medium-sized sand is found at either tidal inlet channels exposed to tidal-flow-induced bottom shear or at the ebb-tidal delta shoals where winnowing of fine sand is a result of wave stirring. Furthermore, it is shown that surface sediments at the barrier island foreshore and the inlet system in this setting can be explained by erosional, and not depositional, processes. Morphological patterns that are prone to depositional processes and accumulation of fine sand are identified to occur in zones of reduced bottom shear as a result of opposing tidal currents and waves.

The model study confirms the significance of the recirculation of sand at this tidal inlet. Mainly medium-sized sands are redirected to the inlet throat via a semicircular pattern across the eastern ebb-tidal delta and through the easterly marginal flood tidal channel. The combination of residual sediment fluxes of both scenarios, wave-dominated storm and tide- dominated fair-weather, is able to achieve this net sediment recirculation. The model shows additional sediment bypass, mainly by suspended sediment load, to the downdrift foreshore and beach, in disagreement with earlier findings of Son et al. (2010). The magnitude of the bypass, its seaward extent and the dominant grain-

size fraction are primarily controlled by wave energy, i.e., wave-induced alongshore currents, and are consequently more significant for storm compared to fair-weather conditions.

The overall shape of the tidal inlet of study in the German Wadden Sea appears to be similar to typical textbook tidal inlets described, for example, by Hayes (1979). Its geometry is characterized by a single ebb-dominated tidal inlet channel through the ebb-tidal delta with a slightly asymmetric outline of the shoals to the downdrift. This allows for the assumption that the processes and sediment pathway schemes discussed here are also applicable for many other mixed-energy tidal inlets within barrier island systems. This study thus reveals residual sediment transport pathways for tide- and wave-dominated conditions. It improves our understanding of complex sediment dynamics at mixed-energy tidal inlets as it identifies and qualitatively evaluates how the morphology and sedimentology respond to the contribution of distinct drivers that in nature are obscured by continuous interaction.

Appendix A

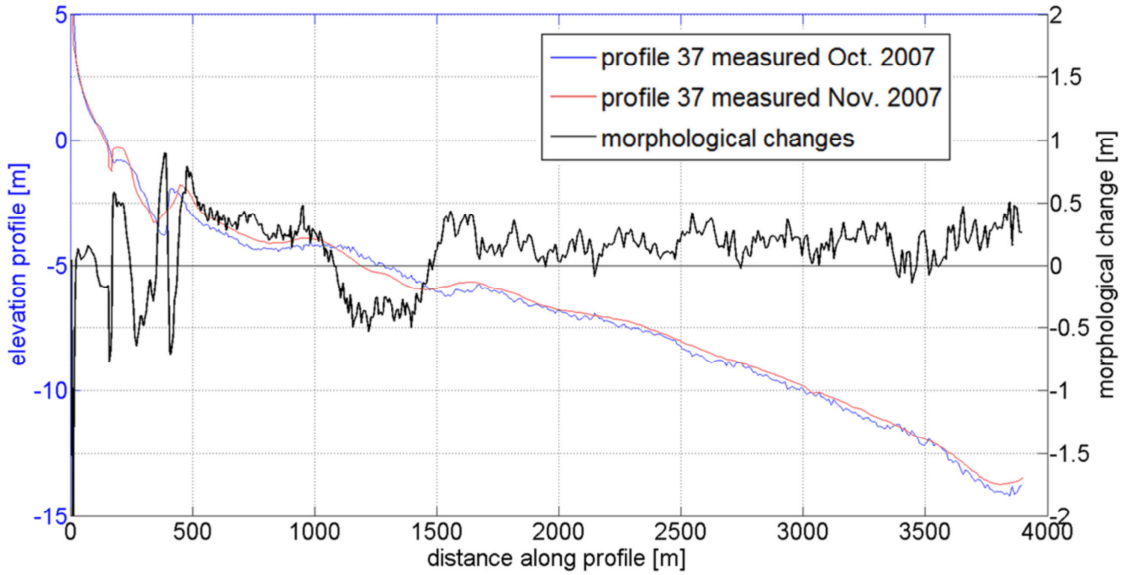

Figure A1. Elevation of cross-shore profiles at Langeoog fore-shore measured in October and November 2007 and morphological changes as the response to the storm event 'Tilo' (data of profile 37 with permission of the Coastal Research Station of Lower Saxony Water Management, Coastal Defense and Nature Conservation Agency, FSK-NLWKN).

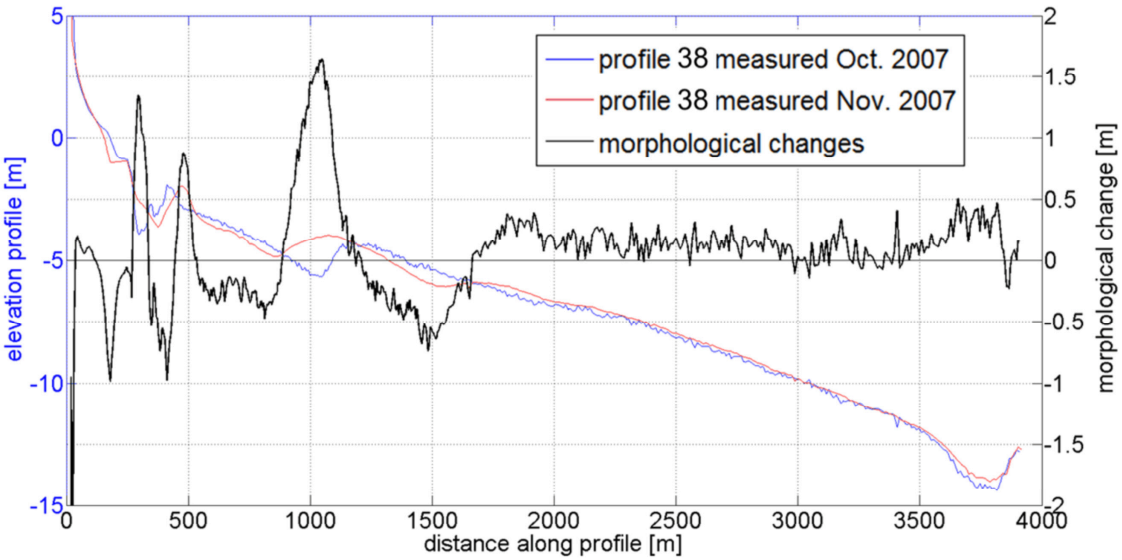

Figure A2. Elevation of cross-shore profiles at Langeoog fore-shore measured in October and November 2007 and morphological changes as the response to the storm event 'Tilo' (data of profile 38 with permission of the Coastal Research Station of Lower Saxony Water Management, Coastal Defense and Nature Conservation Agency, FSK-NLWKN).

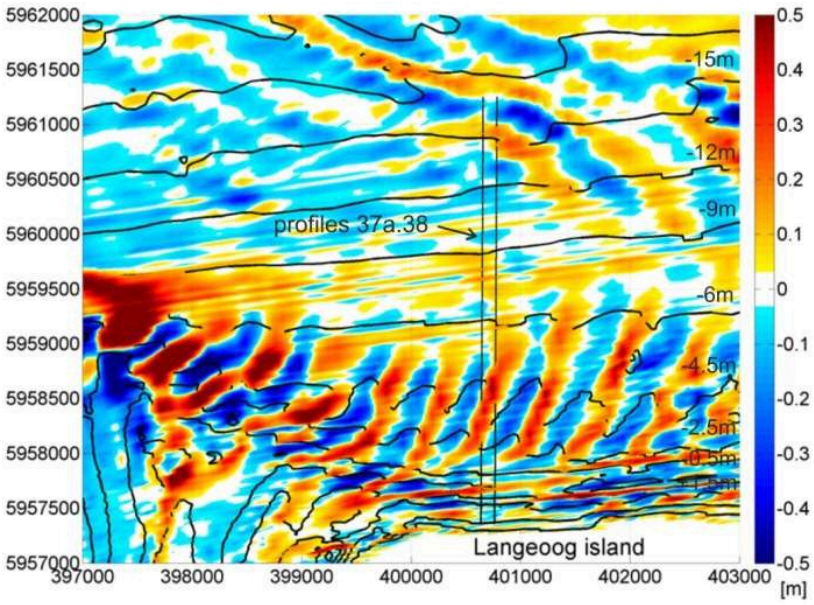

Figure A3. Morphological changes, i.e., sedimentation (red) and erosion (blue) patterns, predicted by the storm simulation at the foreshore of Langeoog with position of cross-shore profiles 37 and 38; the initial model bathymetry is based on observational data of 2006 and thus inconsistent with pre-storm cross-shore profiles of October 2007 that are shown in Figs. A1 and A2.

Acknowledgements

This study is associated with and funded by the research project WIMO (www.wimo-nordsee.de) and is financed in equal parts by two ministries in Lower Saxony: the Ministry of Environment, Energy and Climate Protection, and the Ministry of Science and Culture.

We gratefully acknowledge the authorities and research institutes, namely the Federal Maritime and Hydrographic Agency (BSH) and the Coastal Research Station of Lower Saxony Water Management, Coastal Defense and Nature Conservation Agency (FSK-NLWKN) for furnishing bathymetrical data; the Federal Ministry for Environment, Nature Conservation and Nuclear Safety (BMU) and Project Management Jülich (PTJ) for providing measured data of waves and wind related to the research platform FINO1; the German Weather Service (DWD) for making meteoro-logical model data available via the PAMORE database; and Senckenberg at Sea Wilhelmshaven (SaM) for furnishing in situ data of surface sediment grain-size. We acknowledge the Helmholtz-Zentrum Geesthacht Zentrum für Material- und Küstenforschung GmbH, notably Rolf Riethmüller and Götz Flöser, for providing wave data recorded at the back barrier of Langeoog within the framework of the Coastal Observing System for Northern and Arctic Seas (COSYNA) and for text passages in Sect. 4.1 describing their data. Many thanks go to OpenEarth.nl (DELTARES), which is at the European forefront in disseminating high-quality data, tools and models, particularly for making the Dutch Continental Shelf Model available (Verboom et al., 1992).

The authors would like to thank Mick Van der Wegen, the anonymous reviewer and the editor, Giovanni Coco, for their valuable comments and suggestions, which helped to improve the quality of this paper.

Chapter 3: Paper II

Evaluation of sediment bypassing schemes at barrier island tidal inlets

G. Herrling and C. Winter

MARUM – Center for Marine Environmental Sciences, University of Bremen, Germany

Some aspects of this study have been published as an extended abstract in the conference proceedings 'Physics of Estuarine and Coastal Seas' (PECS, Brazil, 2014); the extended paper will be submitted to the Journal of Coastal Engineering.

Abstract

The large scale littoral sediment drift involves alongshore sediment transport at barrier islands and tidal inlets. Sediment bypassing at mixed-energy tidal inlets is controlled by combined wave action and tidal currents. Commonly, alongshore sediment bypassing at tidal inlets is assumed to occur by migration of transverse swash bars along the ebb-tidal delta periphery or by delta breaching and bar welding in direction to the downdrift beach. In contrast to these schemes a recent publication showed field data evidence for a circular sediment pattern at the ebb-tidal delta between the East-Frisian barrier islands Langeoog and Spiekeroog at the southern North Sea coast; in which sediment is transported in a recirculation cell at the eastern ebb-tidal delta shoal being reversed to the tidal inlet throat. Here, we discuss the controversial assumptions on tidal inlet bypassing by process-based numerical modeling of sediment dynamics at barrier island systems. A spatial and temporal high-resolution morphodynamic simulation of 26 months driven by real-time boundary conditions of tides, wind and waves is validated against morphological changes between two measured states of May 2004 and June 2006. Residual sediment fluxes of distinct grain-size fractions and morphological changes allow for the evaluation of complex tidal inlet processes that are driven by the non-linear wave-current-interaction. Pathways of sediment bypassing are identified and the ratio of recirculated to bypassed sediment volumes is assessed. The model reveals how different bypassing schemes depend on particular sediment grain-size fractions.

3.1. Introduction

Tidal inlets at barrier islands interrupt the natural continuity of large scale littoral sediment drift and therefore play a significant role in sediment budgets and exchange processes, both, between the foreshore and the back-barrier basin and between the islands' shorelines and the ebb-tidal delta. Early studies of O'Brien (1931, 1966), Escoffier (1940) and Bruun (1978) improved the understanding of morphological equilibrium and stability criteria at tidal inlets; however, tidal inlet behavior is complex and the theoretical relationships do not allow for the evaluation of detailed sediment transport pathways at tidal inlets, in particular of sediment bypassing. Bruun and Gerritsen (1959) generalized natural sediment bypassing into two principal mechanisms: bar bypassing and flow bypassing. Bar bypassing occurs by migration of large bars across the ebb-tidal delta, whereas flow bypassing is via the tidal inlet throat where strong ebb-directed currents spill the sediment seawards over the ebb-tidal delta. The type of bypassing mechanism is controlled by the littoral drift to tidal inlet flow ratio: high ratio (> 200 to 300) suggests bar bypassing, low ratio (< 10 to 20) flow bypassing. Other less general theories of natural sediment bypassing at barrier island tidal inlets go back to early studies mostly based on aerial photographs and sedimentological or bathymetrical surveys and can be summarized from literature by way of simplification into three principal mechanisms (Fig. 14): (A) Surf-zone alongshore sediment drift delivers sand to the inlet throat where ebb-dominant channel flow directs the sand to the ebb-tidal delta where it is entrained by wave- and tide-driven alongshore currents and bypassed either continuously (Bruun and Gerritsen, 1959; De Swart and Zimmerman, 2009) or by the formation and landward migration of large bars (FitzGerald, 1982; FitzGerald et al., 1984a). The latter form at the ebb-tidal delta downdrift shoal by merging of smaller swash bars to one bar complex or by a sequence of processes referred to as channel breaching. They migrate and ultimately attach to the shoreline which is referred to as 'bar welding' and is known to happen in cycles of several years. (B) A recent study (Son et al., 2010) postulated a recirculation of sand at the downdrift shoal which directs sand back to the inlet throat and thus to the ebb-tidal delta claiming sediment bypassing not to be evident. If at all, sand is bypassed at the upper shoreface independently of ebb-tidal delta dynamics. (C) At more wave-dominant and/or large tidal inlets wave-driven sediment transport occurs continuously along the periphery of the ebb-tidal delta from the updrift to the downdrift beach via a series of migrating transverse sand bars (originally by Gaye and Walther, 1935; cited in Hanisch, 1981).

This study aims a process-based understanding of bypassing mechanisms exemplified at two tidal inlets of the East Frisian barrier island system. After Hayes (1975, 1979), they are classified as mixed-energy slightly tide-dominated tidal inlets. The combined forcing of waves and tidal currents driving the sediment dynamics at the tidal inlet systems suggests the application of a process-based

morphodynamic model that accounts for wave-current interactions. An earlier study (Herrling and Winter, 2014), deciphered the morphological response of a mixed-energy tidal inlet to wave-dominant (short-term storm) and tide-dominant (short- to mid-term fair-weather) hydrodynamic conditions. But in the present investigation, average sediment dynamics are evaluated in response to representative mixed-energy conditions of a mid-term period of 26 months.

The objectives of this study are twofold: A spatial and temporal high-resolution morphodynamical simulation of 26 months is set-up and forced by real-time boundary conditions of tides, waves and wind. The hindcasted morphological evolution is validated against morphological changes between two bathymetrical observations in May 2004 and June 2006. Given a suitable model realization, a multi-fractional modeling approach then allows identifying pathways of sediment transport of distinct grain-size fractions at two tidal inlets. The detailed analysis of time-integrated sediment pathways is then used to evaluate existing bypassing schemes.

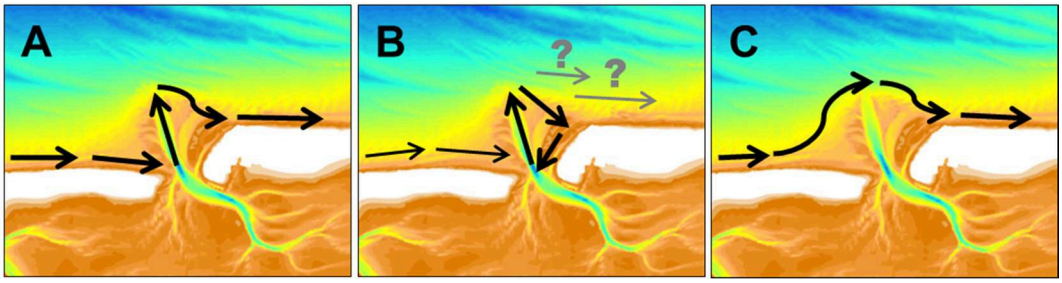

Figure 14. Common tidal inlet bypassing schemes at barrier island tidal inlets: (A) ebb-dominant flow in the inlet throat and shoreward shoal migration at the eastern ebb-tidal delta, (B) dominant semicircular sediment circulation over the eastern ebb-tidal delta redirecting sand to the inlet throat, (C) bypassing by transverse bar migration via an arcuate pathway at the ebb-tidal delta periphery.

3.2. Study area

The study area covers the East Frisian barrier islands fringing the German Wadden Sea in the southern North Sea (Fig. 15). This mesotidal, mixed-energy to slightly tide-dominant coast (Hayes, 1975, 1979) is exposed to predominant wave directions from the north-westerly sector. The tide is semidiurnal with increasing mean tidal ranges of 2.5 m at the island of Juist in the west to 3.0 m at Wangerooge in the east. Both, the dominance of the eastward directed flood currents over the opposing ebb currents and the oblique wave attack induce a net alongshore sediment drift to the east (Zeiler et al., 2000). FitzGerald (1984b) estimated the net annual sand transport to about 270,000 m³/year at the island foreshore. The investigated tidal inlet systems Accumer Ee and Otzumer Balje are both

characterized by a single inlet throat of depths of up to 25 meters spreading into a network of tidal channels towards the back-barrier basin. Bartholomä et al. (2009) measured maximal current velocities for neap- to spring-tides ranging from 0.5-1.0 m/s and 0.8-1.6 m/s for flood- and ebb-tide at the tidal inlet Otzumer Balje. Typical mean sediment grain-sizes are 120 to 180 µm at the upper shoreface, fine sand of 180 to 250 µm at the islands' foreshore beaches, medium to coarse sand of 350 µm and more in the tidal inlet gorges and the ebb-tidal delta shoals and very fine sand of 88 to 125 µm with local mud contents of more than 30% at the back-barrier intertidal flats (Antia et al., 1994; Flemming and Nyandwl, 1994; Son et al., 2010).

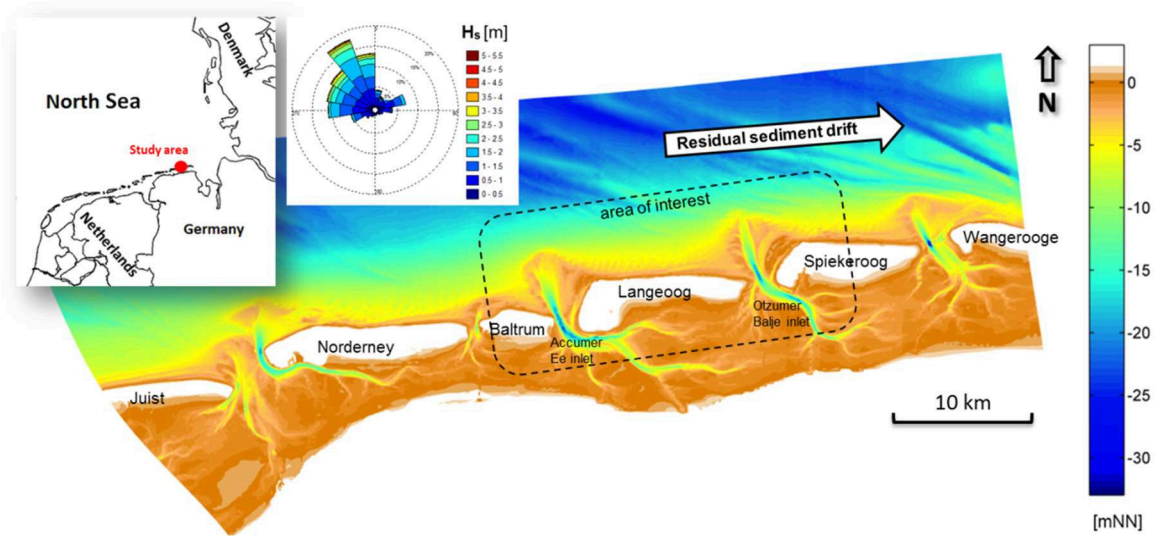

Figure 15. The study area covers the East Frisian barrier islands in the German Wadden Sea, southern North Sea; sediment bypassing is investigated at the tidal inlets Accumer Ee and Otzumer Balje.

3.3. Methodology

The modeling system Delft3D (Deltares, 2011) has been applied to set-up and run process-based hydrodynamic models of different extent and resolution in a two-dimensional, depth-integrated configuration. The numerical models solve the shallow water equations and continuity equation on a staggered model grid by use of an implicit finite-difference-scheme. A two-way-coupling between the hydrodynamic model and the spectral wave model SWAN (Booij et al., 1999; Ris et al., 1999) is implemented by incorporating the depth-integrated wave forces (radiation stresses) in the momentum equation of the hydrodynamic module. For a detailed description of the equations and implementation into Delft3D, it is referred to Lesser et al. (2004).

The morphodynamic simulation is driven by real-time boundary conditions of tides, wind and waves for 26 months from May 2004 to June 2006. This mid-term period is selected to be long enough to account for representative, average hydrodynamic conditions, but to be still acceptable in terms of computational effort. On the other hand, the time frame is specified by the availability of subsequent bathymetrical data having spatial overlap in order to assess morphological changes.

3.3.1. Model grids and wave-current coupling

Water level boundary conditions of the smaller East Frisian Island Model (EFIM) are generated by nesting into the larger Wadden Sea Model (WSM) covering the German Bight in the southern North Sea (Fig. 16). Eight tidal constituents generate the astronomic tide at the open sea boundaries of the WSM that constitutes average grid cell sizes of 1200 m (Chu et al., 2013). The EFIM covers the chain of East Frisian barrier islands from Juist to Wangerooge and extends offshore to water depths of about 30 meters. The cross-shore resolution of the curvilinear grid is approx. 200 m at the coastal sea and in the back-barrier basins but up to 20 m at the surf-zone due to a narrowing of horizontal grid lines towards the barrier islands. The alongshore resolution ranges between 100 to 150 m but is locally increased to 50 m at the area of interest between the islands Baltrum and Spiekeroog. The open model boundaries are selected in a sufficiently long distance to the area of interest.

The spectral wave model SWAN covering a significant larger area than the EFIM is run in a stationary mode to simulate the wave propagation and deformation from the open sea to the shoreline. The cross-shore resolution of the curvilinear grid is 400 m at the offshore boundary and steadily increases to 20 m at the surf-zone; alongshore resolutions are between 200 and 80 m with increasing resolutions towards the area of interest. Wave and wind data measured at the research platform FINO1 are applied at intervals of 60 min as boundary conditions.

This time interval coincides with the sequential two-way-coupling between SWAN and the hydrodynamic model (EFIM) that allows exchanging relevant parameters on curvilinear model grids via a communication file. Wave parameters and the forcing terms associated with the wave radiation stresses computed by SWAN are read by the hydrodynamic module. In turn, bottom changes, water level and depth-integrated current fields generated by the hydrodynamic module during the assigned run-time of 60 min are used as input to the computation in SWAN. The model loops through these sequential module applications until the simulation from May 2004 to June 2006 is accomplished. The interaction of wave forces (radiation stresses), tidal currents and the changing bed- and water levels is thus realized by a fully coupled wave-current simulation. Output of the wave model and hydro-/morphodynamic parameters are recorded at intervals of 60 and 20 min, respectively.

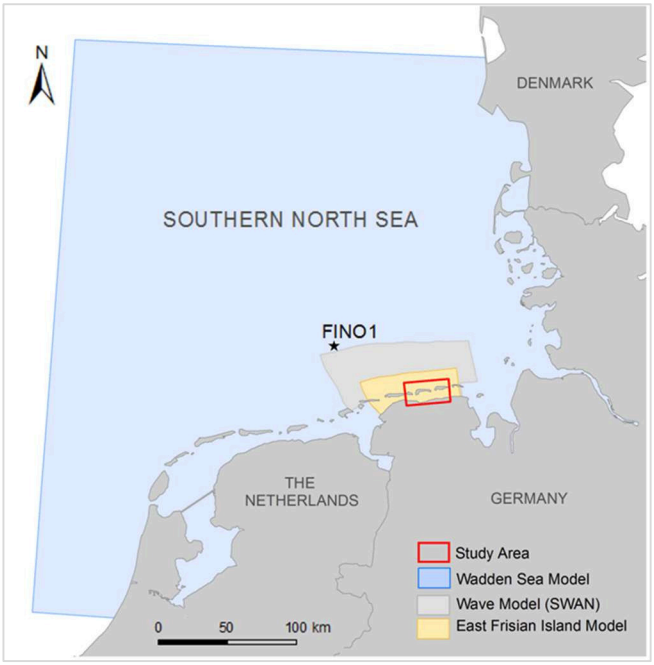

Figure 16. Extent of the hydrodynamic and wave models and position of the offshore platform FINO1 where wind and wave data are available as model boundary conditions.

3.3.2. Wind and wave forcing

The wind velocity and direction measured at the research platform FINO1 are used as meteorological boundary conditions of the hydrodynamic models (WSM and EFIM) and the wave model. The wind is imposed spatially uniform but non-stationary with an interval of 60 minutes. The fetch is limited to the seaward extent of the WSM and consequently the coastal surge is reduced for strong westerly or northerly wind conditions. On the other hand, magnitudes of southerly wind directions that are measured offshore may be overestimated at the coastal zone. These limitations are accepted as spatial information on wind and atmospheric pressure is not available to force the entire simulation.

The probability of occurrence per wind direction and velocity range assessed for the simulation period between May 2004 and June 2006 shows fair agreement with respect to wind observations of eight years between 2004 and 2011 (Fig. 17). The wind forcing imposed to the model yet shows slightly higher probabilities of occurrence for the north-westerly sector and smaller overall probabilities for the south-westerly sector compared to the long-time series.

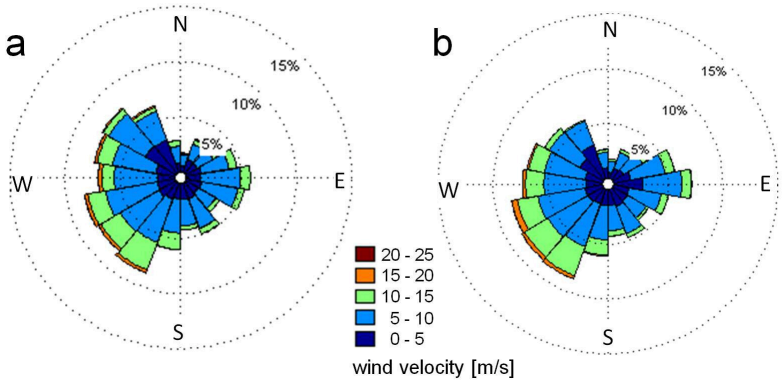

Figure 17. Probability of occurrence [%] per wind direction and velocity range based on hourly wind data measured 45 km offshore at the research platform FINO1 and converted to a height of 10 m above sea level for (a) the simulated 26 months from May 2004 to June 2006 and (b) for 8 years between 2004 and 2011 (based on data of BMU, PTJ).

Wave parameters as the significant wave height Hs [m], the peak wave period Tp [sec] and the wave direction [deg] are measured at the FINO1 offshore platform using two different measuring systems: a radar based wave monitoring system (WAMOS) and a wave rider buoy anchored in the vicinity of the platform. Data gaps in the time series from May 2004 to June 2006 are substituted by one or the other data set, yet two periods of respectively two weeks (27. June – 11. July 2004 and 12. – 26. Nov. 2004) are complemented by linear interpolation. The probability of occurrence in percent per wave direction is presented for Hs and Tp (Fig. 18).

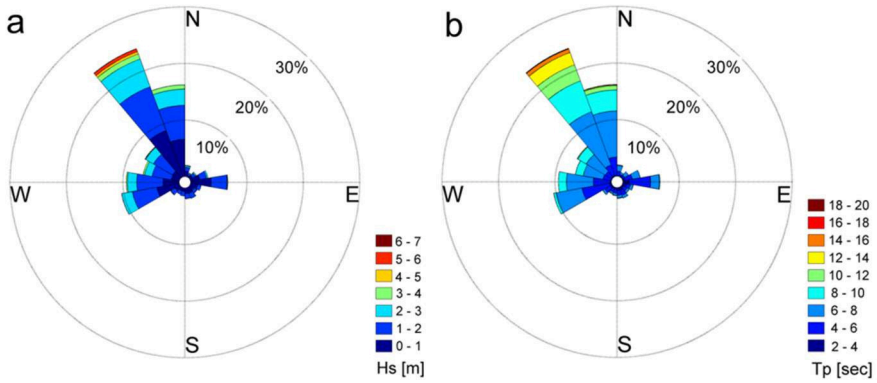

Figure 18. Probability of occurrence [%] per wave direction for ranges of (a) significant wave height Hs and (b) peak wave period Tp based on hourly wave data measured 45 km offshore at the research platform FINO1 from May 2004 to June 2006 (based on data of BMU, PTJ).

The dominant offshore wave direction is from north-north-west occurring at a probability of approx. 40 %. Data are imposed at the offshore boundaries of the wave model SWAN at intervals of 60 min.

Data of FINO1 is provided with permission of the Federal Ministry for Environment, Nature Conservation and Nuclear Safety (BMU) and Project Management Jülich (PTJ).

3.3.3. Model bathymetry

The digital elevation model has been assembled by interpolating measured bathymetric data onto the curvilinear model grids (Fig. 15, Fig. 19). The tidal inlet systems Accumer Ee, Otzumer Balje and the foreshore of the island Langeoog are covered by data of 2004 based on conventional echo sounding (Federal Maritime and Hydrographic Agency, BSH); other near coastal sub- and intertidal areas are subject to a coverage by data of the years 2006, 2005, 2004 and 2001. Elevations of inter- and supra-tidal barrier island beaches are partly covered by geodetic beach surveys of the years 2005 and 2004 or high-resolution airborne LIDAR scans that cover spatially limited parts of some of the barrier island beaches while a full coverage of an island is only available for dissimilar years between 2008 and 2005 (data with permission of the Coastal Research Station belonging to Lower Saxony Water Management, Coastal Defense and Nature Conservation Agency, NLWKN).

Simulated morphological changes at the tidal inlets are verified by bathymetrical data being provided by local authorities (Federal State Agency of Navigation and Hydrology, BSH). Monitored morphological changes, i.e. the difference between the bathymetrical state of May 2004 and June 2006, are used for the purpose of model calibration and validation (Fig. 19).

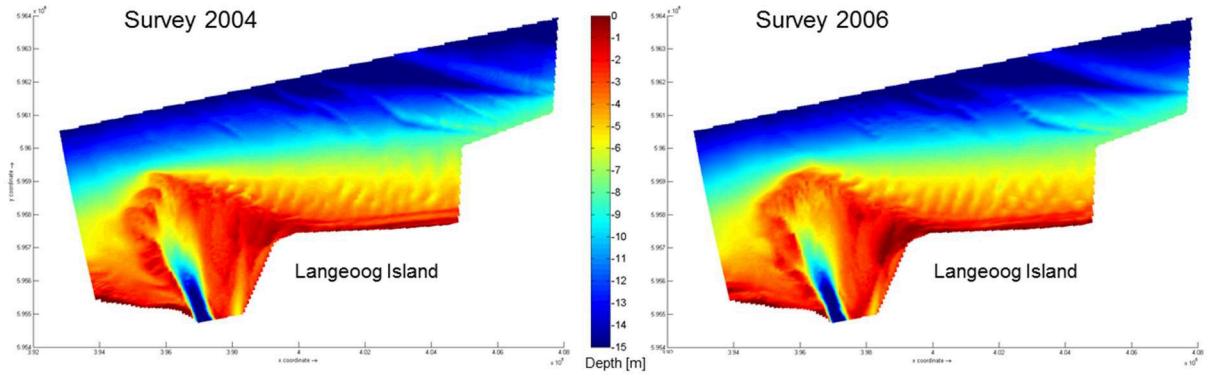

Figure 19. Depth soundings of the Accumer Ee tidal inlet system of the surveys in May 2004 and June 2006 (BSH) interpolated by way of triangulation onto the numerical grid.

3.3.4. Sediment grain-size distribution

A bed layer model (van der Wegen et al., 2011a) is applied to redistribute multiple sediment grain-size fractions in response to the hydrodynamic forcing. It allows the identification of residual sediment transport fluxes of distinct sand fractions. This approach is used to redistribute three sand

fractions with mean grain-sizes typical for the lower shoreface and the back-barrier basin (125 µm), the upper beaches and the main ebb-tidal delta body (250 µm) and the inlet channels (375 µm). The sediment composition is first estimated by sediment grain-sizes of 125, 250 and 375 µm constituting spatially uniform mass-fractions of 25, 50 and 25 %, respectively. In a next step, these sediment grain-size fractions are redistributed in response to hydrodynamic forcing conditions to allow for a more realistic sediment composition prior to running the intended morphodynamic simulations. Herrling and Winter (2014) showed how a sequence of three simulations driven by forcing of 5 months of fair-weather conditions, an extreme storm event and again a period of 5 months of fair-weather conditions generates a sediment grain-size distribution that is in fair agreement with observations. Following this methodology, an initial sediment grain-size distribution is generated in response to a combination of alternating mid-term tide-dominated and short-term wave-dominated conditions (Fig. 20).

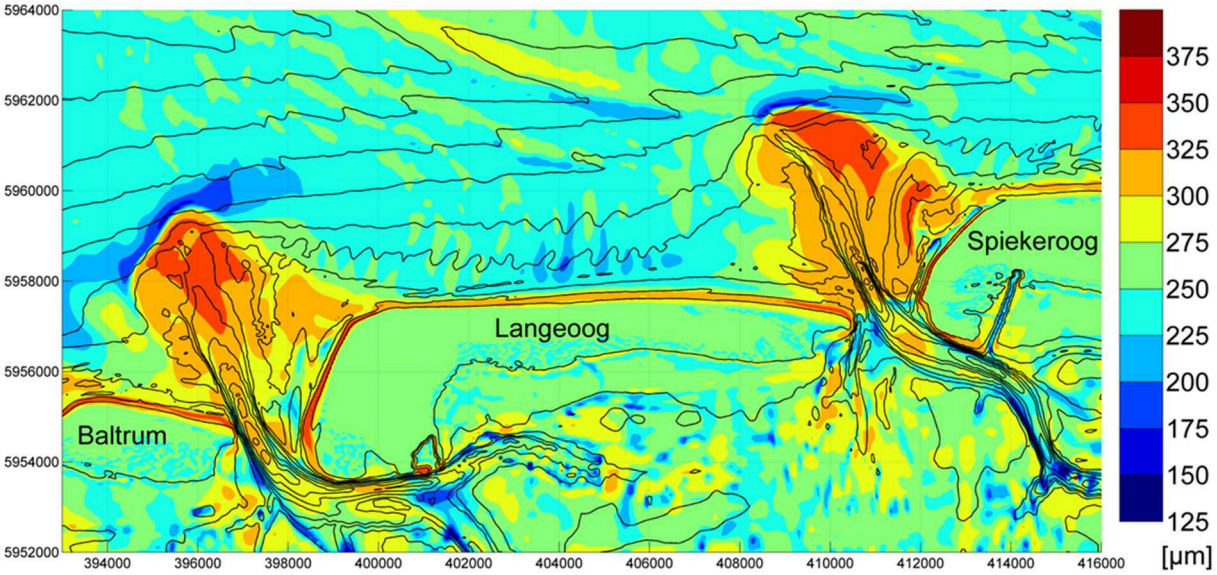

Figure 20. Simulated distribution of mean sediment grain-size composed of three sand fractions of 125, 250 and 375 µm is applied as initial condition for morphodynamic simulations. Depth isolines (black lines) schematize the initial morphology of May 2004.

3.4. Results

3.4.1. Water levels

Time series data of available water level gauges in the study area, i.e. Norderney, Langeoog, Spiekeroog are compared with model hindcasts. Observed and modeled water level time series show a fair agreement at the gauge location Langeoog during a neap-spring-neap cycle from 26. March to 9.

April 2006 (Fig. 21); absolute differences are slightly higher at the end of the presented time series which is attributed to increased wind-surge. For the simulated period of 26 months, the root-mean-square errors (RMSE) are assessed for observed and simulated water levels at the gauge locations Norderney Riffgat, Langeoog and Spiekeroog to 0.29, 0.21 and 0.29 meters, respectively. The elevated RMSE compared to earlier investigations at this area are explained by meteorological effects on water levels. In the actual study, wind is forced spatially uniform in the model domain, while in Herrling and Winter (2014) meteorological forcing was incorporated by spatially nonuniform wind- and atmospheric pressure fields of meteorological models of the German weather service. Spatial wind fields are yet not available for the period of 26 months simulated hereafter.

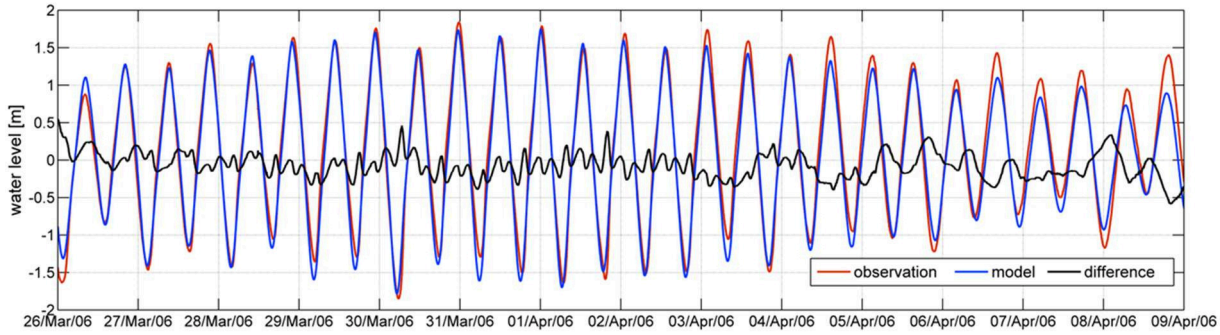

Figure 21. Observed and modelled water levels at the tidal gauge station Langeoog during a neap-spring-neap cycle from 26. March to 9. April 2006.

3.4.2. Current velocity

The alongshore sediment transport at the barrier island foreshore and particularly in the surf-zone is predominantly driven by the combined flow induced by wind and waves approaching the coast in a shore-oblique angle. Reliable data on sediment transport load that drifts alongshore and reaches a tidal inlet from updrift is not available. For this reason, secondary model parameters as the alongshore current velocity controlling the alongshore sediment drift are validated against observations (Fig. 22). Current magnitudes available from ADCP (Acoustic Doppler Current Profiler) transects were collected along cross-shore profiles at the island of Spiekeroog during a measuring campaign with the research vessel Senckenberg in Sept. 2012 (Coord: 417521, 5961018; 417515, 5966719; WGS84, UTM32N). These profiles are used to calibrate the bed roughness coefficient on the basis of detailed current velocities at the upper shoreface. A three-dimensional simulation with 11 sigma layers over the vertical was set-up using the same horizontal grid (EFIM) but an updated model bathymetry interpolated from available soundings of the years 2010 and 2011. The seaward model forcing by

tides, wind and waves was generated analogously to the depth-integrated model approach but for Sept. 2012. The bed roughness was calibrated aiming the best possible agreement of the currents at the shoreward part of the profile. Best agreement to the observations of 5. Sept. 2012 16:30 UTC was achieved by the setting of a spatially uniform bed roughness coefficient Chezy 68, which then is assumed to reach good model skill for the mid-term simulation of depth-integrated currents between March 2004 and June 2006, too.

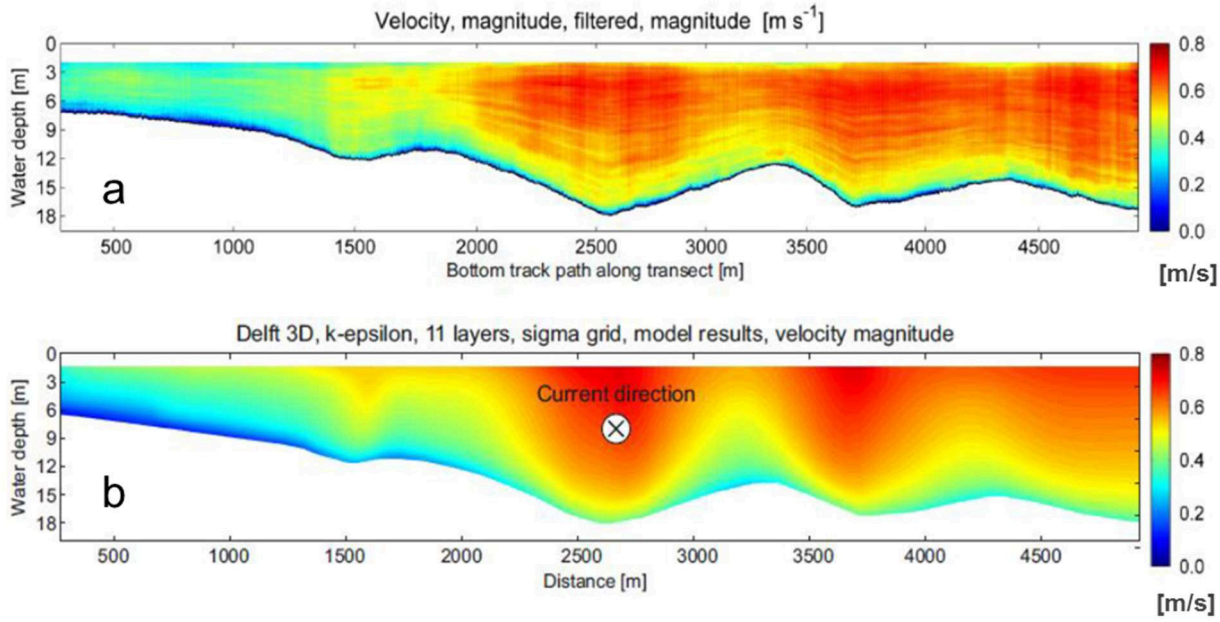

Figure 22. Comparison of (a) measured and (b) modelled alongshore flow due to the interaction of opposing westerly-directed ebb-currents (pointing into the figure) and easterly-directed alongshore-current induced by wind and waves from the north-westerly sector for a cross-shore profile at Spiekeroog.

3.4.3. Morphological changes

Data of two successive morphological states are available from depth soundings operated in May 2004 and June 2006; the spatial overlap of the measurements is yet restricted to the tidal inlets Accumer Ee, Otzumer Balje and the foreshore of Langeoog. Morphodynamics are hindcasted between 1. May 2004 and 30. June 2006 and time-integrated morphological changes are verified against bathymetrical observations. Simulated patterns of net erosion and net sedimentation show fair agreement with patterns determined from measurements of the same period of time (Fig. 23). The shift of the inlet throat to the east and ebb-tidal delta growth are reproduced, although the model overestimates the transport load along the inlet throat and thus accretion at the ebb-tidal delta. Large

bars at the downdrift side of the tidal inlets migrate shoreward. The eastward migration of near shore-oblique sand bars as well as the cross-shore evolution of beach berms is captured by the model while beach accretion is overestimated.

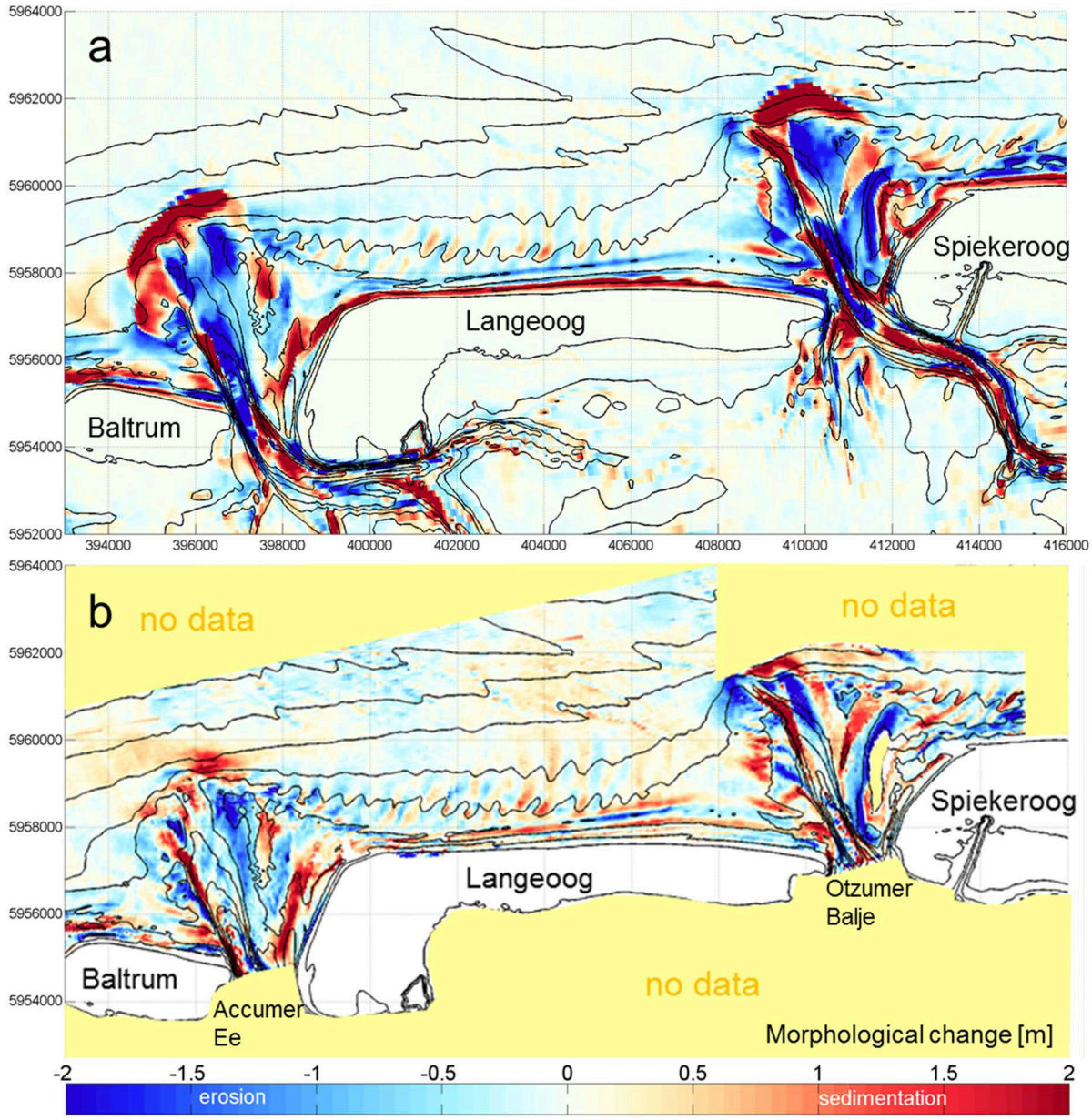

Figure 23. Morphological changes simulated during 26 months (a) are verified against patterns of net erosion (blue) and net sedimentation (red) being evaluated from bathymetrical data measured in May 2004 and June 2006 (b). Depth isolines (black lines) schematize the initial morphology of May 2004.

The model allows for the interpolation between the observed states of 2004 and 2006 and reveals the outer channel oscillating from west to east over the ebb-tidal delta. It thus provides a tool to estimate the yearly net transport fluxes at several tidal inlets of the East Frisian barrier islands, particularly at Accumer Ee and Otzumer Balje.

3.4.4. Sediment transport pathways

The sediment transport load [$m^3/s/m$] and direction is recorded in intervals of 20 min for sand fractions of 125, 250 and 375 µm during the simulated period from May 2004 to June 2006. The data of sediment transport load is first time-integrated and then annualized. Vectors representing the annual transport load and direction per sediment grain-size fraction [m^3/year/m] are interpolated on a raster with equidistant cell lengths of 180 m to better the visualization (Fig. 24).

The similarity of sediment transport pathways between both investigated tidal inlets suggests a general, qualitative description that solely differentiates between distinct sediment grain-size fractions. Sediment bypassing is identified for all three sand fractions, although the bypassed amounts and the residual pathways are different:

Medium sand (375 µm) is barely transported from the updrift foreshore to the tidal inlet. At the center of the inlet throat, medium sand is predominantly transported in a net seaward direction to the ebb-tidal delta. Here, residual sediment fluxes sharply bend in a south-eastward direction to the eastern ebb-tidal delta shoal, where the medium sand is either directed to the most western shore of the island and/or southwards via the marginal flood channel or across the southern shoals back to the inlet throat.

Fine to medium sand (250 µm) is transported with the residual alongshore sediment drift at the island's foreshore and particularly in the surf-zone. Most of the sand reaches the tidal inlet via the lower beach and surf-zone of the updrift island. At the inlet throat, residual sediment transport is directed to the ebb-tidal delta, but just as much is carried by flood-directed flow inside the deep inlet channel to the back-barrier. The sediment that leaves the ebb-tidal delta is either directly bypassed to the downdrift island or via a semicircular pathway back to the inlet throat.

Very fine to fine sand (125 µm) constitutes the alongshore sediment drift at the islands foreshore and at the upper shoreface. The bigger part is thus directly bypassed along an arcuate pathway seaward of the ebb-tidal delta. An important amount though reaches the tidal inlet throat from the updrift shore. Here, it is either transported by net flood-directed currents far into the back-barrier basin or by net ebb-directed currents just north of the ebb-tidal delta lobe. In the latter case, it then

joins the amount of very fine to fine sand that followed the arcuate bypassing and is thus incessantly transported to the downdrift foreshore and upper shore-face.

Schematic residual pathways delineate the bypassing of different sediment grain-size fractions as exemplified for the tidal inlet Accumer Ee (Fig. 25). Fine to medium sand (250 µm) and medium sand (375 µm) is reversed to the inlet throat, whereas the quantity bypassed to the adjacent beach is composed of very fine to fine (125 µm) and fine to medium (250 µm) sand. This is in agreement with typical mean grain-sizes observed at the foreshore beaches and the inlet throat.

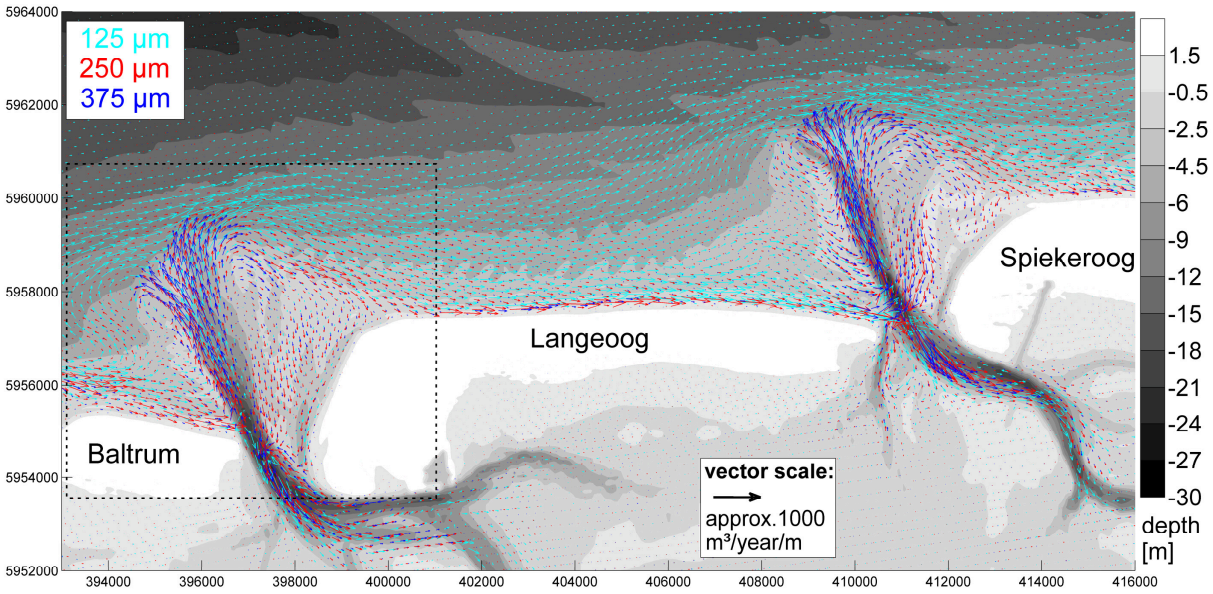

Figure 24. Vectors present the annual sediment transport [m³/year/m] for grain-size fractions of 125, 250 and 375 µm.

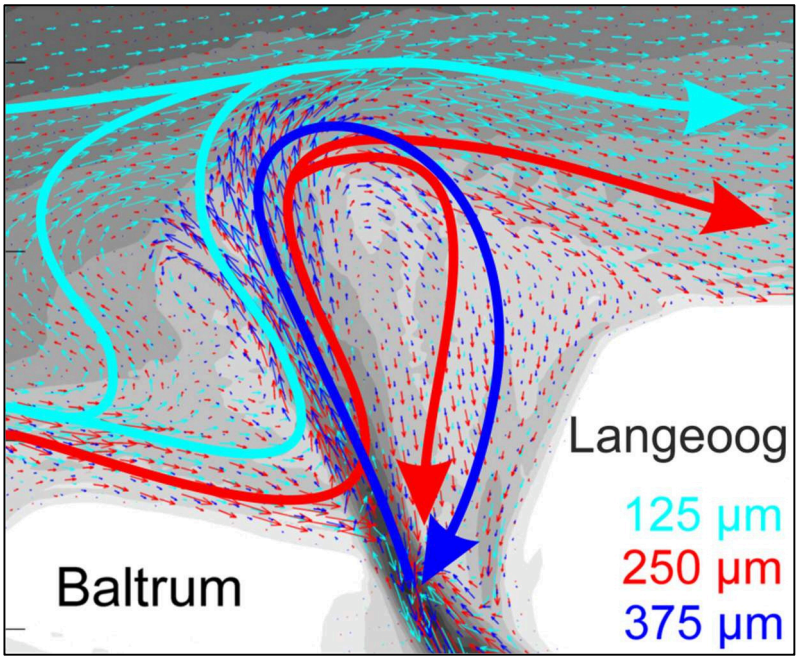

Figure 25. Schematic main residual pathways of tidal inlet bypassing for sediment grain-size fractions of 125, 250 and 375 µm highlighted at Accumer Ee.

The analysis of residual sediment fluxes allows estimating the exchange of sediment budgets between the morphological units of the tidal inlet system. The annual total sediment fluxes [m³/year/m] are assessed by integrating transports of all three sand fractions for the second year of simulation from July 2005 to June 2006 (Fig. 26). The relation of the annual sediment volume [m³/year] being bypassed versus the volume that is reversed to the inlet throat is estimated through predefined cross-sections (Fig. 26). The annual sediment volume that is bypassed downdrift of the ebb-tidal delta is assessed to 407,000 (536,000) [m³/year] and the sediment being recirculated is estimated to 205,000 (282,000) [m³/year] at the Accumer Ee (Otzumer Balje). Even though the sediment volumes may vary with the positioning of the predefined cross-sections, an approximate ratio of two can be estimated for the bypassed to the reversed annual sand volume at both investigated tidal inlets.

The general classification of tidal inlet bypassing after Bruun and Gerritsen (1959) relates the annual mean volume [m³/year] of bypassed sediment to the maximal tidal discharge [m³/s] through the inlet cross-section for spring-tide conditions and differentiates into bar-bypassing (ratio > 200 to 300) and flow-bypassing (ratio < 10 to 20). Simulated maximal spring-tide discharges are between 12,000 and 15,000 m³/s at both investigated tidal inlets. By considering the estimated annual volumes of bypassed sediment, ranges of littoral drift to tidal flow ratio are assessed to 27–34 at Accumer Ee and 36–45 at Otzumer Balje.

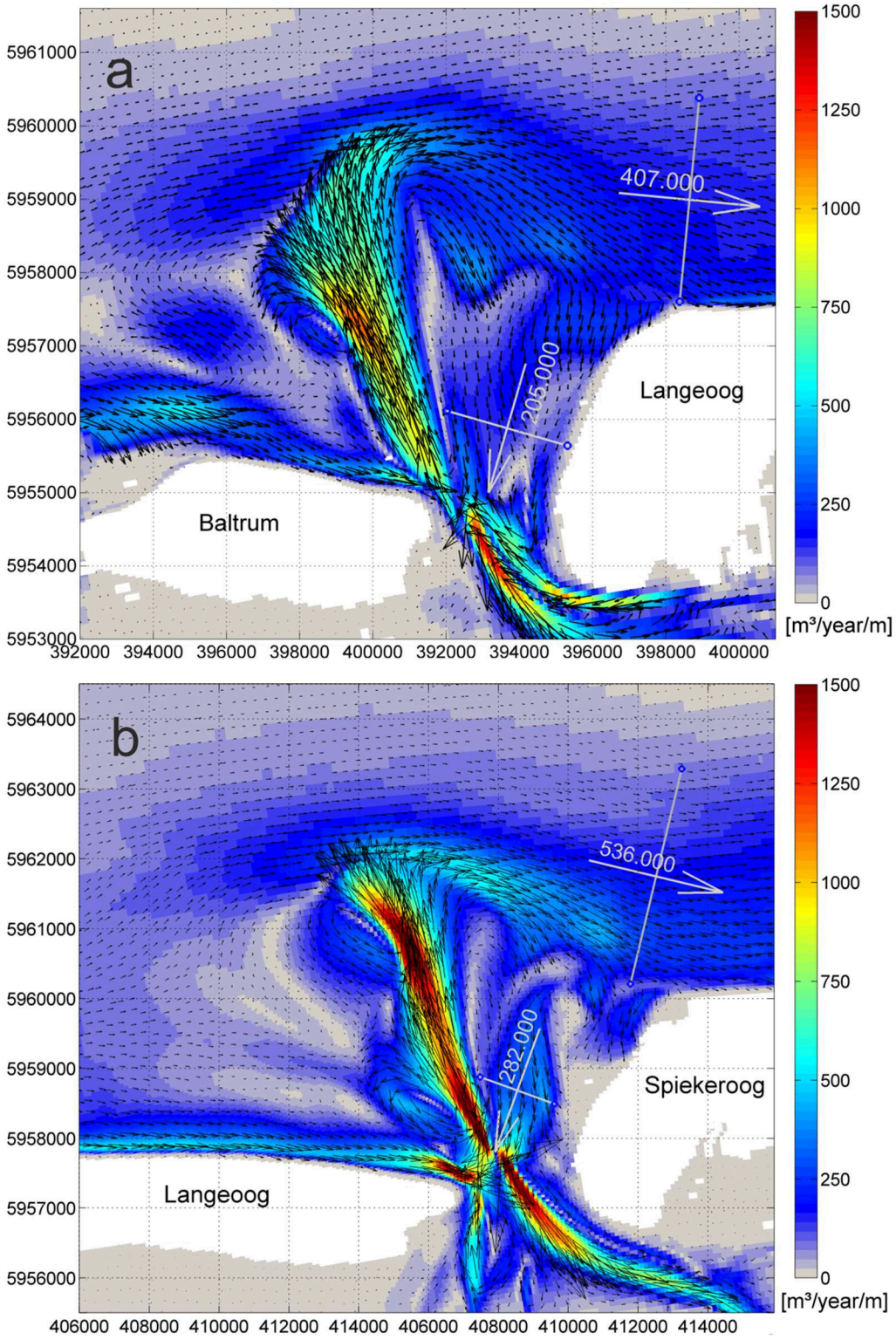

Figure 26. Annual total sand fluxes [m³/year/m] at the tidal inlets (a) Accumer Ee and (b) Otzumer Balje and at predefined cross-sections [m³/year] showing the relation of bypassed versus recirculated sediment.

3.5. Discussion

The early bypassing scheme after Gaye and Walther (1935; cited in Hanisch, 1981) suggested a transverse bar/shoal migration and sediment bypassing around the deltaic periphery from the updrift to the downdrift barrier island. Later authors established a similar bypassing theory in most cases based on patterns of morphological evolution interpreted from sedimentological and bathymetrical field data or from aerial photographs between subsequent morphological states (e.g., Homeier and Kramer, 1957, cited in Hanisch, 1981; Luck, 1975, cited in Hanisch, 1981; Nummedal and Penland, 1981). They mainly refer to the sediment bypassing at the western tidal inlet between Juist and Norderney where they claim the identification of migrating sand bars at the arcuate ebb-tidal delta shoal; also referred to as 'reef-bow'. For the investigated tidal inlets, however, the model confirms almost only very fine to fine sand (125 µm) to be bypassed along this arcuate pathway. Process analysis suggests this sand fraction to be transported as suspended load driven by wave-induced currents independent of any bar migrations. Herrling and Winter (2014) also showed for mixed-energy tidal inlets that fine sand is dominantly bypassed in suspension: the magnitude and seaward reach of the bypassed fluxes and the dominant grain-size are primarily controlled by wave-induced alongshore current and are consequently more significant for storm compared to fair-weather conditions. Our model investigation thus does not fully support this early bypass scheme along the ebb-tidal delta shoals at the west of the inlet. Field based findings by Hanisch (1981) are in accordance with our model results: The shoals at the updrift side of the ebb-tidal delta do neither migrate around the deltaic arc nor play an active role in sand bypassing from the updrift beach to the ebb-tidal delta lobe. Our model reveals the shoals at the western side of the inlet throat as highly mobile but without distinct transport directions. The channels in between the shoals act as alternating ebb- and flood-tidal channels transporting sand of different grain-sizes and quantity depending on the tidal stage and wave conditions. Under the influence of the north-westerly wind and wave regime, these shoals move rather shoreward and pile up along the western edge of the inlet throat, where they compete with the erosive force of the ebb-tidal currents. The elevation and shape of these shoals is thus controlled by tidal currents and wave-energy impact but are not part of a migrating set of transverse bars along the western arc of the ebb-tidal delta. Nummedal and Penland (1981) describe a similar zig-zag transport due to tidal currents in between the western shoals at the inlet between the barrier islands of Juist and Norderney but claim an additional residual downdrift-directed movement. This larger inlet is fanned-out by multiple inlet channels with shoals in between acting as individual ebb-tidal deltas. These are exposed almost perpendicular to the wave attack as mentioned by Nummedal and Penland (1981) which facilitates the wave-induced lateral transport. This might explain the difference with respect to the more narrow tidal inlets like 'Otzumer Balje', 'Accumer Ee' and 'Harle' inlet, the latter described

by Hanisch (1981), where the western ebb-tidal delta shoals do not play an active role in sand bypassing.

Bruun and Gerritsen (1959) classified into bar-bypassing (ratio > 200 to 300) and flow-bypassing (ratio < 10 to 20) for different littoral drift to tidal flow ratios. The assessed ratios of approx. 30 and 40 at the investigated tidal inlets Accumer Ee and Otzumer Balje, respectively, are in between both categories but tend towards flow-bypassing. The widely accepted flow-bypassing scheme at mixed-energy tidal inlets (Bruun and Gerritsen, 1959; Elias et al., 2006a; Swart and Zimmerman, 2009) supports the sediment transport pathway from the updrift beach and foreshore into the inlet throat and via ebb-directed currents to the ebb-tidal delta. This bypassing pathway is confirmed by our model for very fine to fine (125 μm) and fine to medium (250 μm) sand. Medium sand (375 μm), however, is barely bypassed from the updrift island's shore.

FitzGerald and FitzGerald et al. (1982; 1984; 2012) describe bypassing initiated either by small swash bars merging over the eastern ebb-tidal delta shoal to one bar complex or by an abandoned shoal from a mechanism referred to as ebb-tidal delta channel breaching. After the authors, both have in common that large bars migrate landwards and finally weld and attach to the downdrift beach bypassing sand volumes of up to 300,000 m³. The migration of large bars across the eastern ebb-tidal delta and welding to the downdrift beach is recognized as the most significant contribution to sand bypassing across mixed-energy tidal inlets. It is found that the initial process of bar migration over the downdrift ebb-tidal delta shoal is still in agreement to the bar migration described by Son et al. (2010). However, FitzGerald et al. (1984a) claim bar welding as the main contribution to sediment bypassing, while Son et al. (2010) postulate the sand being recirculated to the inlet throat once it reaches the marginal flood channel. Furthermore, FitzGerald et al. (1984) mention minor sediment quantities continuously bypassed over the eastern ebb-tidal delta to the downdrift beach, whereas Son et al. (2010) did not find any evidence for sediment bypassing at these shoals. Our model results indicate that both schemes are valid for the investigated tidal inlets but refer to net transport pathways of distinct grain-size fractions. Residual transport fluxes of the coarsest investigated sand fraction (375 μm); indeed, indicate the reversal towards the inlet throat. However, fine to medium sand is predicted to be directly bypassed to the downdrift foreshore, on the one hand, or to be trapped by large bar complexes that show a coastward migration, on the other. Although the model does not reproduce the initial formation of bars, the shoreward migration across the downdrift ebb-tidal delta shoal is indicated by alternating patterns from net erosion to net sedimentation. This is yet slightly more obvious at the tidal inlet Otzumer Balje than at Accumer Ee.

3.6. Conclusions

A process-based model is applied to simulate mid-term sediment dynamics in response to representative, average hydrodynamic conditions and evaluate different bypassing schemes at two mixed-energy tidal inlets of the East Frisian barrier island system. Hindcasted morphological changes are satisfactorily validated against bathymetrical observations of May 2004 and June 2006. Simulated patterns of net erosion and net sedimentation show fair agreement with patterns determined from measurements of the same period. The numerical model thus provides a tool to estimate the annual net transport fluxes at the tidal inlets Accumer Ee and Otzumer Balje.

The model allows for the differentiation of sediment transport of distinct grain-size fractions and corresponding bypassing pathways. It predicts very fine to fine sand (125 µm) to be bypassed at the tidal inlets largely after the bypassing scheme (C) and partly after scheme (A). Fine to medium sand (250 µm) bypasses the tidal inlets via residual transport pathways after scheme (A) but shows also a reversal of sand at the easterly ebb-tidal delta after scheme (B). Medium sand (375 µm) follows the residual fluxes described by scheme (B). The annual sand volume being integrated over all fractions and bypassed directly downdrift of the ebb-tidal delta is approx. twice as much as the sand volume reversed to the inlet throat; this is evaluated for both investigated tidal inlets.

The common theory (originally by Gaye and Walther, 1935; cited in Hanisch, 1981) that assumes continuous bypassing to occur by migration of transverse bars along the ebb-tidal delta periphery could only by confirmed for the very fine to find sand. Furthermore, the ebb-tidal delta shoals westwards of the tidal inlet throat do neither migrate around the deltaic arc nor play an active role in sand bypassing. Continuous flow-bypassing (Bruun and Gerritsen, 1961; De Swart and Zimmerman, 2009) via the inlet throat is yet confirmed for all three sand fractions. Residual pathways of fine to medium and predominantly medium sand show a recirculation (Son et al., 2010) across the eastern ebb-tidal delta shoal and via the marginal flood channel back to the inlet throat. Model results thus confirm common theories, but reveal the dependency of different bypassing schemes on distinct sediment grain-size fractions. The simulations thus emphasize the necessity of a multi-fractional model approach to evaluate sediment bypassing at areas that are as complex as mixed-energy tidal inlets.

Acknowledgements

This study is associated to and funded by the research project WIMO (www.wimo-nordsee.de) being financed in equal parts by two ministries in Lower Saxony, Germany, the Ministry of Environment, Energy and Climate Protection and the Ministry of Science and Culture.

We gratefully acknowledge the authorities and research institutes, namely the Federal Maritime and Hydrographic Agency (BSH) and the Coastal Research Station belonging to Lower Saxony Water Management, Coastal Defense and Nature Conservation Agency (FSK-NLWKN) for furnishing bathymetrical data, the federal agencies of hydrology (BfG) and water and navigation (WSV) for water level data and the Federal Ministry for Environment, Nature Conservation and Nuclear Safety (BMU) and the Project Management Jülich (PTJ) for providing wind and wave data measured at the offshore platform FINO1.

Marius Becker is acknowledged for processing the ADCP data of Fig. 22.

Chapter 4: Paper III

Tidally- and wind-driven residual circulation at the multiple-inlet system East Frisian Wadden Sea

G. Herrling and C. Winter

MARUM – Center for Marine Environmental Sciences, University of Bremen, Germany

Continental Shelf Research (submitted)

Abstract

The residual circulation in lagoon-type multiple-inlet systems is primarily driven by the non-linear interaction of the offshore tides, wind-induced currents and the morphology of communicating sub-basins. Residual discharges at tidal inlets and across tidal divides of a chain of back-barrier basins are calculated with a process-based hydrodynamic model in the East Frisian Wadden Sea, southern North Sea. Non-linear mechanisms of dominant water fluxes between the sub-basins and the coastal sea are deciphered with respect to tidal and meteorological drivers. The orientation of residual pathways of annually-integrated water fluxes is consistent and similar for variable model scenarios, i.e. meteorological forcing, an imposed sea level rise or different bed friction coefficients, which permits the identification of dominant residual circulation cells in the system. It is further shown that the multi-basin system imports a substantial surplus of water from the lateral margins of the East Frisian Wadden Sea having an impact on the mass budget of the interconnected basins that has been underestimated so far in hydrological, sedimentological and ecosystem studies. The implications for the accumulation of fine-grained sediments, flushing capacities (residence times) and nutrient cycles in the Wadden Sea area are discussed.

4.1. Introduction

Multiple-inlet systems are geomorphological features that are characterized by sub-basins connecting to the coastal sea by individual tidal inlets. In contrast to single inlet systems, the connectivity among sub-basins implicates an additional degree of freedom that increases the non-linearity of the hydrodynamics in the system and thus the complexity in evaluating morphodynamics

and related sedimentological and ecological processes. The morphological response of these multiple-inlet systems to a future climate change, e.g. an accelerated sea level rise, is in the focus of ongoing research and the knowledge is essential for the protection and management of the coastal zone (Wang et al., 2012b). Lagoon-type systems often fringed by barrier islands had evolved during a period of continuous sea-level rise and are found, for instance, at the south coast of Portugal (Ria Formosa lagoon), in Italy (Venice lagoon), at the North American east coast (e.g., Cape Hatteras, Massachusetts, Georgia, Florida) and in the Wadden Sea extending along the Dutch, German and Danish North Sea coast. At the Wadden Sea, sub-basins are separated by a topographic high commonly also termed watershed or tidal divide; the latter nomenclature is used hereafter. The location of the hydrodynamic tidal divide where fluxes converge from neighboring basins and fluxes tend to be minimal does not implicitly agree with the location of the morphological tidal divide, i.e. the topographic high. Tidal divides allow water exchange only at elevated sea surface, i.e. approx. from mid-tide. After Van der Kreeke et al. (2008), the morphological stability of interconnected tidal basins and their inlet cross-sections is strongly linked to the existence of topographic highs. On the other hand, tidal divides only persist when the ratio of the tidal amplitude tends to be important in relation to the back-barrier water depth.

The fluxes of water in and out of basins are driven by water level gradients among the sub-basins and between the coastal sea. Although the overall mass balance must be closed, the exchange through individual inlets and across tidal divides may be asymmetric: A net flow or residual discharge between the sub-basins and at the tidal inlets can be determined by temporal integration. For the East Frisian Wadden Sea (EFWS), Stanev et al. (2003) found that every basin reveals individual correlations between the inlet transport and net transport, which they explained by mass exchange from the neighboring basins. Sub-basins of multiple-inlet systems thus should be considered as water bodies and morphological units with considerable interactions.

The natural evolution of tidal basin systems is driven by the interaction of tidal, wind and wave forcing and the morphological development of different units in the system: the ebb-tidal delta, the tidal inlet throat and the channel networks and tidal flats in the basin (Herrling and Winter, 2014; De Swart and Zimmerman, 2009). On the other hand, human interferences to the morphological system, e.g. by reduction or closure of a part of the basin or the inlet cross-section, may alter residual flow patterns and cause new morphodynamic states (Elias and van der Spek, 2006b; Kragtwijk et al., 2004). The cross-sectional stability of tidal inlets and thus the equilibrium state of a multiple inlet system has been evaluated by linear analytical models (Van de Kreeke and Cotter, 1974; van de Kreeke, 1990a, 1990b; van de Kreeke et al., 2008; Ridderinkhof, 1988b; de Swart and Volp, 2012). These lumped-parameter models have been extended with an assumed stability criterion allowing for

stable equilibria. An empirical relationship was then imposed, e.g. the equilibrium velocity at the tidal inlet (Brouwer et al., 2012; van de Kreeke, 2004), which was derived from the prism-cross-sectional-area relationship (Escoffier, 1940). However, the non-linearity of the system is often neglected by assuming prismatic channels, linear bottom friction and water levels inside the basin fluctuating uniformly besides further simplifications made by the model formulation.

Liu and Aubrey (1993) and Salles et al. (2005) state that solely numerical models are a reliable tool to predict the interactive response of the residual flow to the non-linear forcing in a realistic multiple inlet system. Some authors strengthened their findings by a combination of analytical and numerical models (Herman, 2007; Liu and Aubrey, 1993; Ridderinkhof, 1988a, 1988b; Wang et al., 2013). The combination allowed for a more reliable result as the non-linearity of the system is well captured by numerical models but the more general conclusions can be drawn from idealized lumped-parameter models. In case of multiple-inlet systems, the analysis and interpretation of a combination of both modelling approaches is found to be most promising in order to reliably evaluate the residual circulation. Recently, complex process-based models have been applied to predict the residual discharges as a response to the interaction of density-driven flow with tidally- and wind-driven currents in between sub-basins of the Western Dutch Wadden Sea (Duran-Matute et al., 2014).

The objectives of the present study are twofold. The first is to estimate the quantity of the residual water volume circulating within interconnected back-barrier basins and to the coastal sea; the significance of residual flow over tidal divides has been underestimated so far. The second is to study the effect of wind-induced net currents with respect to the tidally-driven residual circulation. A sensitivity analysis aims to study the response of residual flow to changes of the bottom friction and sea surface elevation, both having an influence on the tidal propagation along the channels inside the basin. A related work is the study of Herman (2007) who investigated the residual circulation by use of an analytical and a numerical model. She studied the westerly part of the EFWS including three basins with the focus on the catchment area south of Norderney. In this study we extend the area of investigation to the whole EFWS including seven interconnected basins aiming to identify residual circulation cells for the case of a solely tidally-driven flow and with boundary conditions imposing an additional wind forcing. The physical mechanisms that generate the asymmetries of water fluxes within the system are discussed with respect to theoretical findings adopted from above-mentioned earlier studies.

4.2. Study area

The East Frisian Wadden Sea is composed of seven sub-basins that are fringed by a chain of eight barrier islands (Figure 27). According to the classification of Hayes (1975, 1979), the coast of the southern North Sea is mesotidal with a mixed-energy to slightly tide-dominated regime. The tide is semidiurnal with increasing mean ranges of 2.4 m at the island of Borkum in the west to 3.0 m at Wangerooge in the east. Despite water level gauges at five proximate locations, field data on flow hydrodynamic properties is scarce in this area. Only at Otzumer Balje, i.e. the tidal inlet of the back-barrier basin of Spiekeroog, the residual flow in the inlet throat has been measured to be ebb-dominant with maximal current velocities for neap- to spring-tides ranging from 0.5-1.0 m/s and 0.8-1.6 m/s for flood- and ebb-tide, respectively (Bartholomä et al., 2009). Average wind directions are from the westerly sector with mean velocities of about 7 m/s observed at the offshore platform FINO1 at approx. 45 km off the island of Borkum. Here, mean significant wave heights of 1.4 m and mean peak periods of 6.9 sec have been measured (data of May 2004 to June 2006, Federal Ministry for Environment, Nature Conservation and Nuclear Safety (BMU) and the Project Management Jülich (PTJ)).

The coastal morphology of the EFWS is driven by a longshore eastward-directed net sediment drift generated by the combination of an eastward propagating tidal wave and the dominant westerly wind and wave directions. FitzGerald et al. (1984a) estimated the net transport rate of foreshore sand to about 270,000 m^3/year which used to cause an eastward movement of the barrier islands. At the end of the 20th century this migration ceased which can be explained by the fixation of the westerly island heads by groins and seawalls in the mid-19th century (FitzGerald and Penland, 1987; Luck, 1976). Most of the back-barrier tidal basins feature an asymmetric drainage channel system with 70-80% of the tidal prism coming from the east (FitzGerald et al., 1984a). Sediments in the back-barrier depositional environment show a gradation in correspondence to the decreasing cross-shore energy gradient. Coarser fine sand (177 to 250 µm) dominates the margin of the islands, contents of more than 80 % of finer fine sand (125 to 177 µm) represent the tidal flats and 70% of very fine sand (88 to 125 µm) with local mud contents of locally more than 30% compose the sediments adjacent to the mainland dike (Flemming and Nyandwl, 1994). At the landward side of the Baltrum basin pronounced accumulation of fine to very fine sediments are observed.

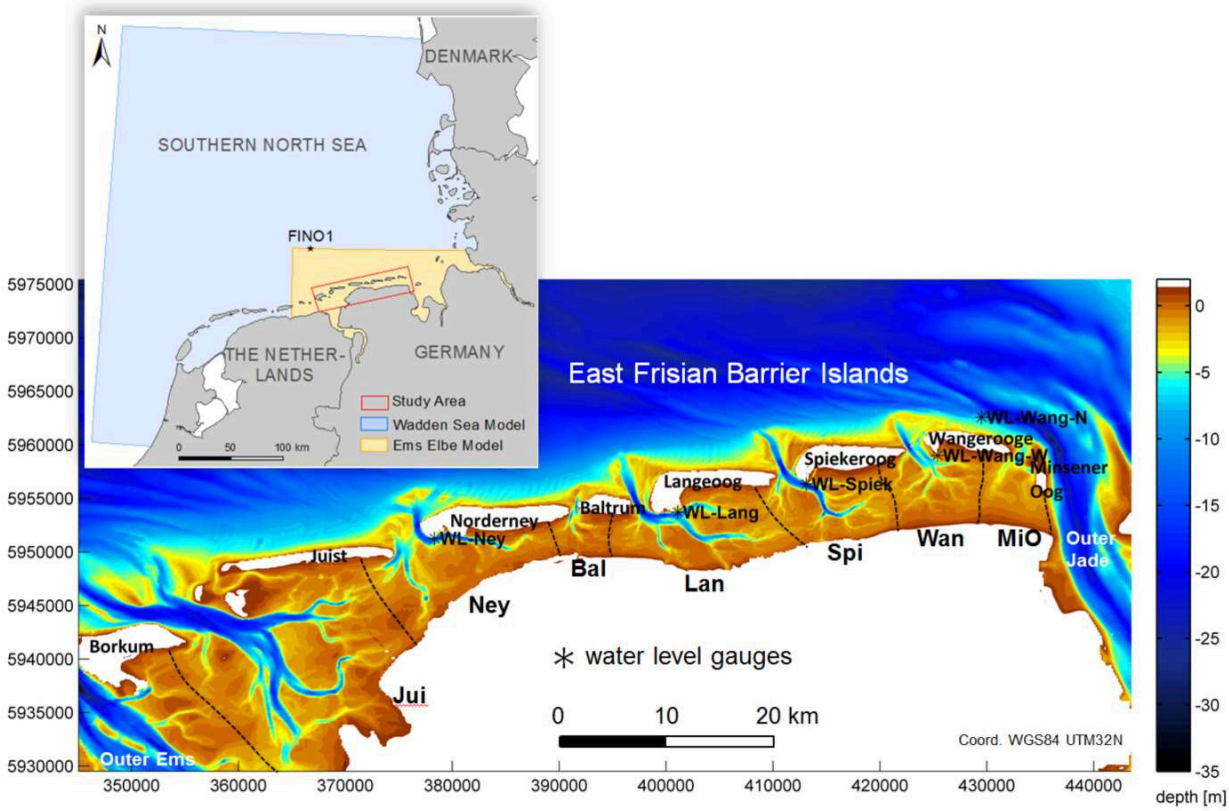

Figure 27. Overview of the model domains applied in the southern North Sea and the bathymetry of the East Frisian Wadden Sea; the approximate positions of tidal divides are schematized by dashed lines indicating the extent of particular sub-basins.

4.3. Methodology

The modeling system Delft3D (Deltares, 2011) has been applied to set-up and run process-based hydrodynamic models of different extent and resolution in a two-dimensional, depth-integrated configuration. The numerical models solve the shallow water equations and continuity equation on a staggered model grid by use of an implicit finite-difference-scheme (Deltares, 2011; Lesser et al., 2004).

4.3.1. Model grids and open boundary conditions

The Wadden-Sea-Model (WSM) with average grid sizes of 1200 m covers the southern North Sea from the Dutch coast in the south to Denmark in the north (Chu et al., 2013). Eight harmonic tidal constituents (M2, S2, N2, K2, K1, O1, P1 and Q1) generate the astronomic tide at the open sea boundaries. The smaller Ems-Elbe-Model (EEM) is nested into the WSM, using calculated water level time series at the seaward boundary (Fig. 27). The EEM covers the southern German Bight from the

Ems-Dollard estuary to the Elbe estuary and extends 45 km seawards almost until the island of Helgoland. The open model boundaries are selected in a sufficiently long distance to the area of interest. In particular at back-barrier basins that are prone to drying and flooding, intersecting open model boundaries need to be avoided in order to properly simulate residual mass fluxes with the adjacent water bodies. The curvilinear model grid consists of 1912 x 1063 grid cells with resolutions of 150 m offshore, 100 m at the back-barrier basins and about 70 m at the tidal inlets to sufficiently resolve the inlet geometry.

Freshwater runoffs are schematized by stationary, mean discharges of 81, 324 and 711 m^3/s from the estuaries Ems-Dollard, Weser and Elbe to the southern North Sea, respectively. Based on data of local authorities (Rupert et al., 2004), the average freshwater runoffs of four floodgates discharging to the basins of Langeoog, Spiekeroog and Wangerooge are in total 3.81 m^3/s for the years 1993 to 2003. These input rates are negligible with respect to the processes and water fluxes studied here and have thus been neglected in the simulations.

4.3.2. Wind forcing

Time series of the wind velocity and direction measured at the offshore research platform FINO1 are used as meteorological boundary conditions of the EEM. The wind is imposed spatially constant but non-stationary with an interval of 60 minutes. The wind stress is parameterized with a drag coefficient of Smith and Banke (1975). Wind forcing is only considered in the EEM thereby potentially reducing the fetch and consequently the coastal surge in case of strong northerly wind conditions. The magnitude of southerly wind directions measured at the open sea, however, may be overestimated. The effect of low pressure systems passing the North Sea is not taken into account. These limitations are accepted as no spatial information on wind and atmospheric pressure is available to force the year-long simulations.

The probability of occurrence per wind direction and velocity range calculated for the simulation period between May 2004 and April 2005 shows good agreement with respect to wind observations of eight years between 2004 and 2011 (Fig. 28). The wind forcing imposed to the model thus is assumed to be representative in order to calculate the annual average effect of the wind-drift on the circulation at the EFWS.

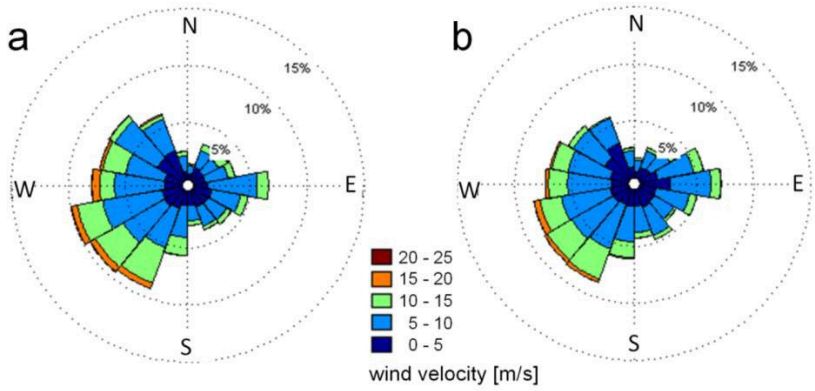

Figure 28. Probability of occurrence [%] per wind direction and velocity range based on hourly wind data measured 45 km offshore at the research platform FINO1 and converted to a height of 10 m above sea level for a) the simulated year from May 2004 to April 2005 and b) for 8 years between 2004 and 2011 (based on data of BMU, PTJ).

4.3.3. Model bathymetry

The digital elevation model has been assembled by interpolating measured bathymetric data onto the curvilinear model grids (Fig. 27). Near coastal sub- and intertidal areas are covered by data of the years 2006, 2005, 2004 and 2001 based on conventional echo sounding (Federal Maritime and Hydrographic Agency, BSH). Elevations of inter- and supra-tidal barrier island beaches are partly covered by geodetic beach surveys of the years 2005 and 2004 or high-resolution airborne LIDAR scans that cover spatially limited parts of some of the barrier island beaches while a full coverage of an island is only available for dissimilar years between 2008 and 2005 (data with permission of the Coastal Research Station belonging to Lower Saxony Water Management, Coastal Defense and Nature Conservation Agency, NLWKN).

4.3.4. Model quality

4.3.4.1. Validation of tidal amplitudes and phases

Time series data of available water level gauges in the study area, i.e. Norderney, Langeoog, Spiekeroog,Wangerooge West and Wangerooge North, are used to perform a harmonic analysis using the matlab-routine T_Tide by Pawlowicz et al. (2002). The measured signal is separated into tidal and non-tidal components; the latter are mainly induced by wind effects and atmospheric pressure. The 12 astronomical components with the largest amplitude are used for the comparison of tidal amplitude and phase between observed and modelled data at five gauge locations in the domain (Fig. 29).

Although the deviations from the observation are not negligible for the semi-diurnal components S2 and N2, it shows that the model with the settings here applied is able to reasonable reproduce the tidal propagation in the multiple inlet system. In particular, the principal lunar component M2 is of very good agreement to the observation for the tidal amplitudes and phases at the investigated tidal gauges (Table 1). The largest error in amplitude at Wangerooge West is 4 cm, the largest phase difference is 3 degrees (6.2 minutes) and occurs at Spiekeroog. The best agreement is found at the gauge location of Langeoog, where the difference to the measured M2 component is negligible.

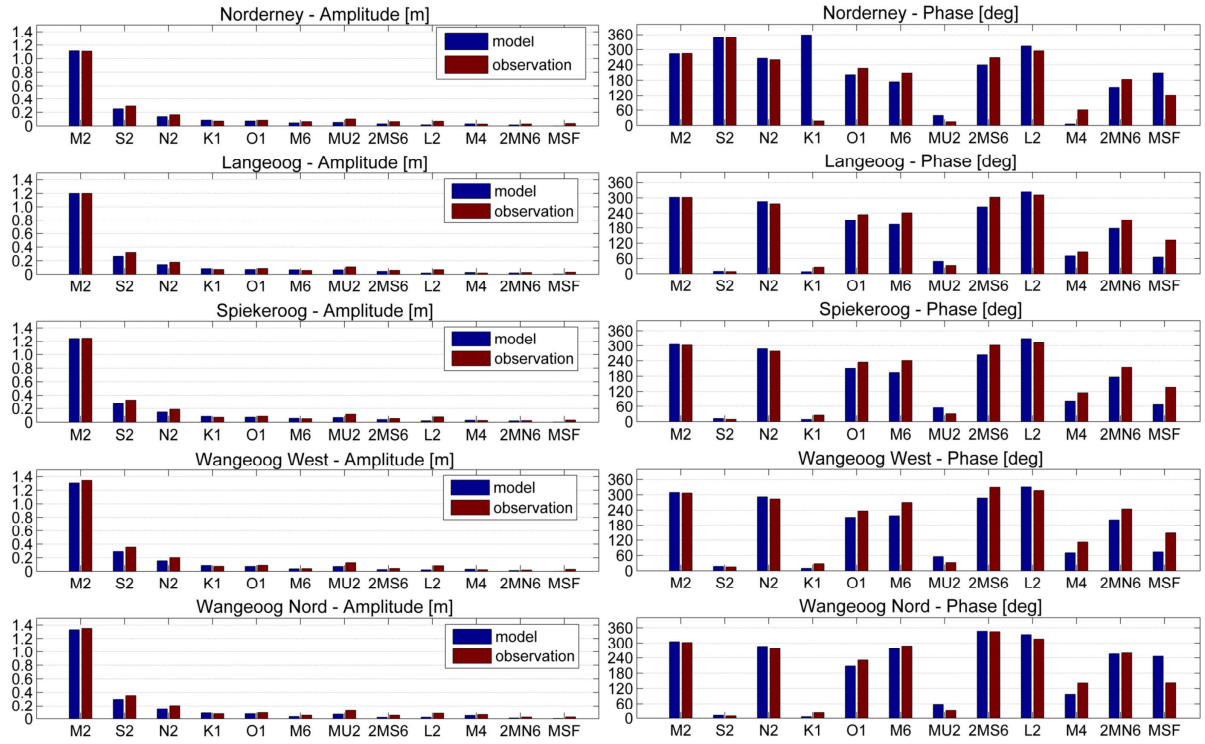

Figure 29. Harmonic analysis of observed and modelled water level time series comparing amplitudes [m] and phases [deg] with respect to 12 major astronomical constituents at the gauge positions Norderney, Langeoog, Spiekeroog, Wangerooge West and Wangerooge North (positions see Fig.27, gauge data provided by the federal agencies of hydrology (BfG) and water and navigation (WSV)).

The hydrodynamic model with similar settings had been successfully applied particularly for the simulation of storm surges in the same area of interest (Herrling and Winter, 2014). A spatially constant bed friction coefficient Manning of n=0.023 and a horizontal viscosity of 1 m/s² are used. These settings are referred to as the reference configuration. Excessive (over-) calibration of the model

by spatially tuning the bed friction was not done here and should generally be avoided. The aim of the study was to compare the model outputs qualitatively and relatively in order to improve our understanding of the dynamics of the system in response to the forcing imposed. A sensitivity analysis shows the response of the tidally-driven net circulation in the multi-inlet system to the increase and decrease of the bottom friction coefficient relative to the reference value (Sect. 4.4.3).

Table 1. Differences of modelled and observed tidal amplitudes [m] and phases [degree] of the principal lunar component M2 at five gauge positions in the study area (positions see Fig.27).

	M2 amplitude [m]			M2 phase [degree]		
Gauge station	Model	Observation	Difference	Model	Observation	Difference
Norderney Riffgatt	1.115	1.110	0.006	283.9	285.0	-1.1
Langeoog	1.200	1.200	0.000	302.2	302.1	0.1
Spiekeroog	1.244	1.248	-0.004	305.0	302.1	3.0
Wangerooge West	1.306	1.344	-0.038	309.1	306.9	2.2
Wangerooge Nord	1.330	1.351	-0.021	305.1	302.2	2.9

4.3.4.2. Mass conservation inside the system

The verification of the conservation of mass in the numerical models is a prerequisite condition for the target of the study. The conservation of mass within a basin is verified by integrating the import and export of year-averaged net discharges for the studied system and for each tidal basin individually. In the study area, the largest mass error occurs at the smallest basin MiO with 0.12 % and 0.19 % relative to the mean tidal prism Pm for the forcing scenarios with and without wind (Tab. 2). The error may be attributed to the positioning of the cross-sections that aim to record the discharge: the little island Minsener Oog is separated by a low lying area being prone to additional flooding and import of water that went past the cross-sections during elevated surge. Numerical errors, e.g. related to the schematization of the drying and flooding of tidal flats, may be liable to give rise to the negligible mass errors in the other basins, i.e. below 0.01 % of the respective tidal prism.

4.3.5. Residual discharges at tidal inlets and divides

The temporal integration of cross-sectional discharge, i.e. the product of the depth-integrated velocity and the time-varying cross-sectional area, allows determining the tidal prism and the residual discharge. The residual discharge integrated over a tidal cycle derives from the dominance of the flow in one direction and is evaluated in the time domain. The flow through tidal inlets is indicated as positive (negative) in ebb- (flood-) direction. Local extremes of the cumulative discharge are identified: i.e. maxima (minima) at low (high) water slack (Fig. 30a). The accumulated discharge

between a local maximum and a subsequent minimum determines the tidal prism during the flooding; inversely during the ebbing of the sub-basin. The residual tidal discharge Qr [m³/tide] is the volumetric difference between the tidal prisms during ebb (Pe) and flood (Pf) integrated over the period of one tidal cycle (Fig. 30b).

This methodology determining time series of the residual discharge at tidal inlets is not applicable to tidal divides in the same way. The time window during the tidal cycle when the water spills over the tidal divide depends on the topographic elevation of the tidal divide, the tidal range and the pressure gradient driving the circulation. Generally, the water spills over from approx. mid-tide level to high water and until mid-tide level; thus during the late flooding and the early ebbing. The instantaneous discharge, however, is highly variable with several peaks over a tidal cycle precluding the identification of the discharge minima and maxima in the time domain and thus the analysis of the flood and ebb prisms. This is particularly the case, as the location of the hydrodynamic tidal divide where throughflow is minimal does not necessarily fall at the position of the morphological tidal divide, i.e. the topographic high. However, the appropriate location of the tidal divide is not required to derive the residual discharge in between adjacent basins in this study. An arbitrary cross-section between the barrier island and the facing mainland coast is sufficient to record the cumulative discharge in the time domain – in contrast to the instantaneous discharge – which is then used to derive the residual discharge at the tidal divide. Around low water, there is no throughflow at the natural tidal divide as tidal flats falling entirely dry during an extended time period, whereas the moment of minimal discharge at the tidal inlet positioned nearby is short and distinct. According to that, we identify the low water discharge slack at the natural tidal divide based on the discharge slack at the tidal inlet. This allows defining the accurate length of the respective tidal cycle and to derive the residual discharge between two consecutive discharge minima. By use of this methodology it is possible to determine the residual discharge at the tidal divide representative during one tidal cycle without the requirement of recording the discharge at the exact positioning of the hydraulic tidal divide which is generally not evident. At tidal divides, eastward (westward) flow is positive (negative).

4.4. Results

4.4.1. Tidally-driven residual discharges

Residual tidal discharges Qr are calculated from simulated time series of cumulative discharges of one year between May 2004 and April 2005 (Tab. 2). Annual residual discharges Qr, QrW and QrE refer to the exchange with the North Sea through the tidal inlet and the water fluxes across the tidal divides in west and east, respectively.

For the simulation driven by tidal forcing only, the time series of accumulated discharges do either decrease or increase quasi-linearly at tidal inlets and tidal divides on time scales larger than a lunar day. At the inlet Otzumer Balje between the islands Langeoog and Spiekeroog, for instance, the time series of the accumulated discharge shows a positive linear trend indicating an overall, persistent net export of water out of the basin. The linearity is superimposed by a weak modulation due to the spring-neap cycle which in turn reveals an inter-annual variability (Fig. 30a). To eliminate the daily inequality of the signal, Qr is averaged over two consecutive tidal cycles, i.e. a lunar day, and is defined hereafter as the (lunar-) daily mean residual tidal discharge QrDay [m³/tide] (Fig. 30b). We normalize the residual discharge to the relative basin size by weighing the ratio [%] of Qr to the mean tidal prism Pm, i.e. the average of the ebb and flood tidal prisms identified for the same tidal cycle (Fig. 30c). Accordingly, the quotient of QrDay to the lunar-daily mean tidal prism (PmDay) is defined as the normalized lunar-daily residual discharge.

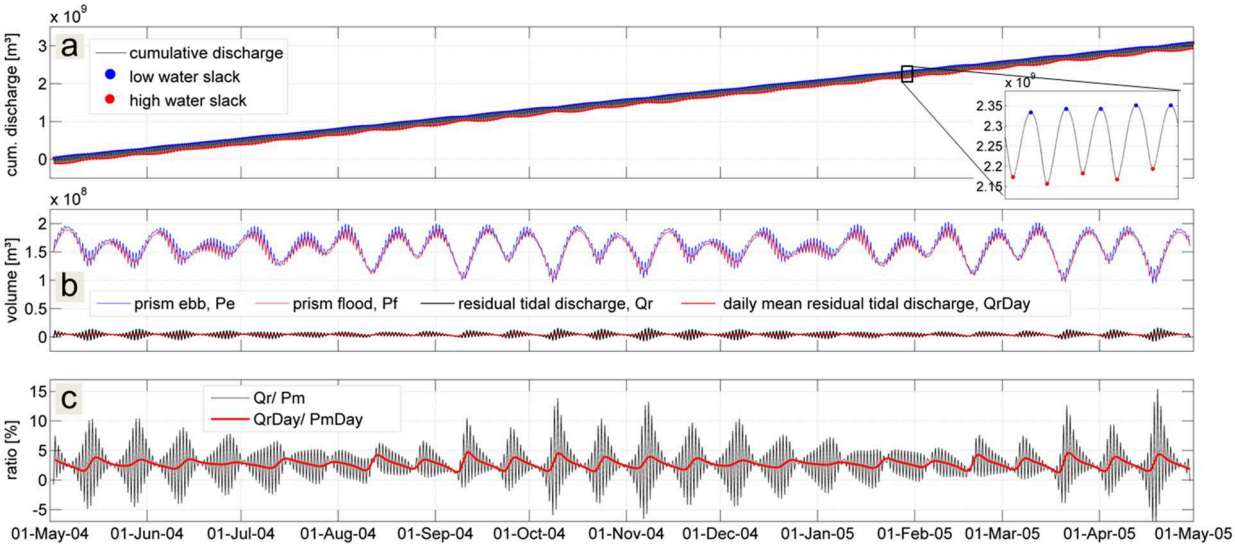

Figure 30. (a) accumulated, tidally-driven discharge through Spiekeroog basin tidal inlet (Otzumer Balje) from May 2004 to April 2005 with local extremes referring to low and high water discharge slack at the cross-section; (b) derived time series of ebb and flood prisms (Pe, Pf) with residual tidal discharge (Qr) and daily mean residual tidal discharge (QrDay), i.e. Qr averaged over two consecutive tidal cycles; (c) Qr normalized to the respective mean tidal prism Pm, i.e. ratio [%] of Qr/Pm and QrDay/ PmDay.

At the Otzumer Balje inlet, the quotient of Qr/Pm may change the sign during the lunar day thus fluctuates from net ebb-directed flow to net flood-directed flow for two consecutive tides. However, the ratio QrDay/PmDay is constantly positive, i.e. net ebb-directed flow, and results into less fluctuation compared to Qr/Pm. The intensity of the fluctuation of Qr, thus a measure of the lunar-

daily inequality, appears to be maximal at varying states of the simulated spring-neap cycles. The peak of the amplitude tends to shift with respect to the spring-tide in a half-year periodicity. The ratio QrDay/PmDay, however, reveals the maximum always shortly after neap tide.

The variability of the residual tidal discharge Qr and derived parameters is evaluated by the probability distribution of Qr; here, shown for the simulation considering tidal forcing only (Fig. 31). The basins of Norderney, Baltrum, Wangerooge and Minsener Oog show strictly positive Qr at the tidal inlets thus, after the definition used herein, export a residual water volume during each tidal cycle all year long. The basin of Spiekeroog has a positively defined annual-mean residual discharge, although 18 % of all tidal cycles show a net import to the basin. A contrary behavior of Qr is assessed for the basins of Juist and Langeoog. The annual-mean residual discharges are negative and thus reveal a dominant import of water to the back-barrier basins, yet during 30 % and 17 % of the tidal cycles this is inversed for the basins of Juist and Langeoog.

Table 2. Annual-mean (Mai 2004 to April 2005) values of basin specific parameters for the simulation with tidal forcing only (left) and combined tidal and wind forcing (right). Residual tidal discharges are defined as positive to the north at tidal inlets (ebb-directed) and positive to the east at tidal divides.

model forcing	tidal forcing only							tidal and wind forcing						
basin name	Jui	Ney	Bal	Lan	Spi	Wan	MiO	Jui	Ney	Bal	Lan	Spi	Wan	MiO
mean prism ebb, Pe [10^6 m³]	539.8	199.3	38.1	172.1	160.2	129.2	72.3	538.1	202.7	37.9	168.7	159.7	129.5	74.5
mean prism flood, Pf [10^6 m³]	506.5	166.7	31.4	177.8	155.9	118.0	67.7	510.1	163.9	31.0	179.3	155.7	117.3	66.6
mean prism, Pm [10^6 m³]	523.2	183.0	34.7	174.9	158.1	123.6	70.0	524.1	183.3	34.4	174.0	157.7	123.4	70.5
res. disch. tid. inlet, Qr [10^6 m³/tide]	-33.3	32.5	6.7	-5.7	4.3	11.2	4.6	-28.0	38.8	6.9	-10.7	3.9	12.2	7.9
res. disch. tid. divide West, QrW [10^6 m³/tide]	4.0	37.3	4.7	-2.0	3.7	-0.7	-11.9	18.2	46.1	7.4	0.5	11.1	7.2	-5.0
res. disch. tid. divide East, QrE [10^6 m³/tide]	37.3	4.7	-2.0	3.7	-0.7	-11.9	-16.6	46.1	7.4	0.5	11.1	7.2	-5.0	-13.0
basin mass error / Pm [%]	0.001	0.007	0.013	-0.001	0.005	0.005	0.120	-0.003	-0.004	0.001	0.001	0.008	0.011	0.192
Qr / Pm [%]	-6.4	17.8	19.4	-3.3	2.7	9.1	6.6	-5.3	21.2	20.0	-6.1	2.5	9.9	11.2
QrW / Pm [%]	0.8	20.4	13.6	-1.2	2.3	-0.6	-17.0	3.5	25.2	21.4	0.3	7.1	5.8	-7.1
QrE / Pm [%]	7.1	2.6	-5.8	2.1	-0.4	-9.6	-23.7	8.8	4.0	1.4	6.4	4.6	-4.0	-18.4
STD tidal inlet, Qr_STD [10^6 m³/tide]	22.5	10.7	1.5	5.6	4.9	3.0	1.9	29.8	22.8	2.2	14.4	5.2	4.9	8.7
STD tidal divide East, QrE_STD [10^6 m³/tide]	5.8	1.1	0.2	0.3	0.4	0.4	0.8	28.3	7.8	6.6	19.4	20.6	18.3	10.7

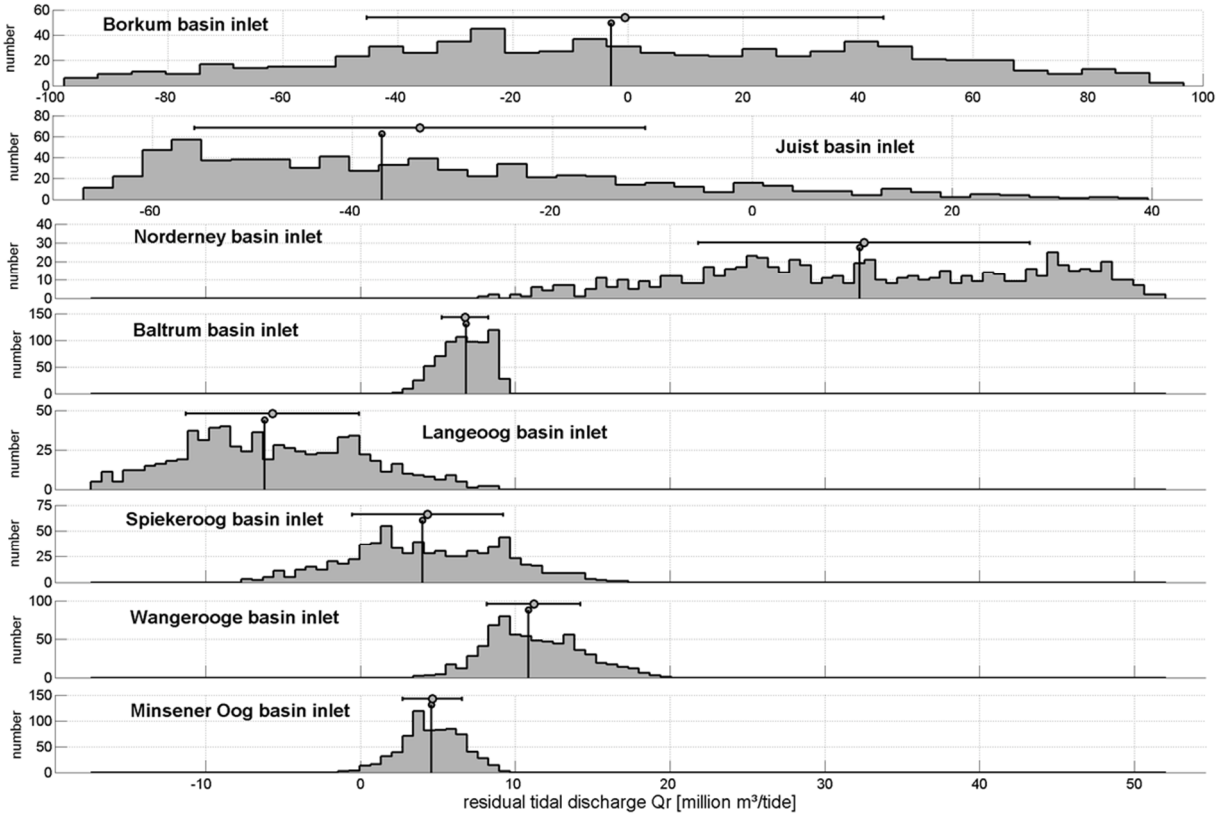

Figure 31. The histograms show the probability distribution of the annual residual tidal discharge Qr [10^6 m³/tide] for the simulation with tidal forcing only at the studied tidal inlets; the horizontal line indicates the range of the standard deviation Qr_STD with the mean value in the centre; the vertical line represents the median value. Ebb-directed residual discharges are signed positive. Note the different axis-scales.

Generally, the yearly mean values of Qr do not exceptionally deviate from the yearly median values of Qr for the tidal inlets in the study area, except for the tidal inlet draining the basin of Juist (Fig. 31). Here, the analysis of the yearlong time series of Qr reveals a mean value of -33.3 x10^6 m³/tide and a median value of -37.0 x10^6 m³/tide. The standard deviations of the residual discharge Qr_STD is a measure of the variability of the net discharge rate. With Qr_STD of 44.9 x10^6, 22.5 x10^6 and 10.7 x10^6 m³/tide at the Westerems and at the inlets of the Juist and Norderney basins, respectively, these westerly tidal inlets show a considerably larger variability of the discharge rates than the inlets more to the east (Tab. 2). The smallest Qr_STD with 1.5 x10^6 m³/tide is assessed for the basin of Baltrum. Normalized to the basin size, i.e. the ratio of Qr_STD to Pm; however, reveals a variability of the net water flux which deviates much less among the inlets.

The largest net water fluxes are identified at the lateral margins of the East Frisian Wadden Sea (Fig. 32). The riverine discharge of the Ems adds to the flood-directed net discharge through the

tidal inlet westerly of Borkum ('Westerems') resulting in net water fluxes of about 4 x10^6 m³/tide directed towards the Juist basin via the tidal divide at the island of Borkum. An annual mean Qr of 33.3 x10^6 m³/tide imports through the tidal inlet discharging the basin of Juist ('Osterems'). In between the basins of Juist and Norderney a net discharge of 37.3 x10^6 m³/tide is estimated through the tidal divide which refers to 7.1 % and 20.4 % of the mean tidal prisms of Juist and Norderney, respectively. At the eastern lateral side of the EFWS, the annual mean water volume of 16.6 x10^6 m³/tide is imported to the basin of Minsener Oog during an average tidal cycle referring to 23.7 % of the basin's mean tidal prism. As mentioned earlier, the smallest residual water exchanges with the North Sea or with the adjacent basins are determined for the basin of Spiekeroog. The normalized, annual-mean residual discharges are 2.7 % at the tidal inlet and 2.3 % and -0.4 % at the tidal divides in West and East.

By integrating the annual net surplus at the basins of Juist (QrW+Qr), Langeoog (Qr) and Minsener Oog (QrE) together with the annual net outflow at the tidal inlets of the basins of Norderney (Qr), Baltrum (Qr), Spiekeroog (Qr), Wangerooge (Qr) and Minsener Oog (Qr) the residual exchange of water between the interconnected back-barrier basins (excluding the basin of Borkum, i.e. the Ems-Dollard estuary) and the North Sea is estimated to be 60 x10^6 m³/tide averaged on a yearly time basis; the standard deviation is in the order of 70 x10^6 m³/tide.

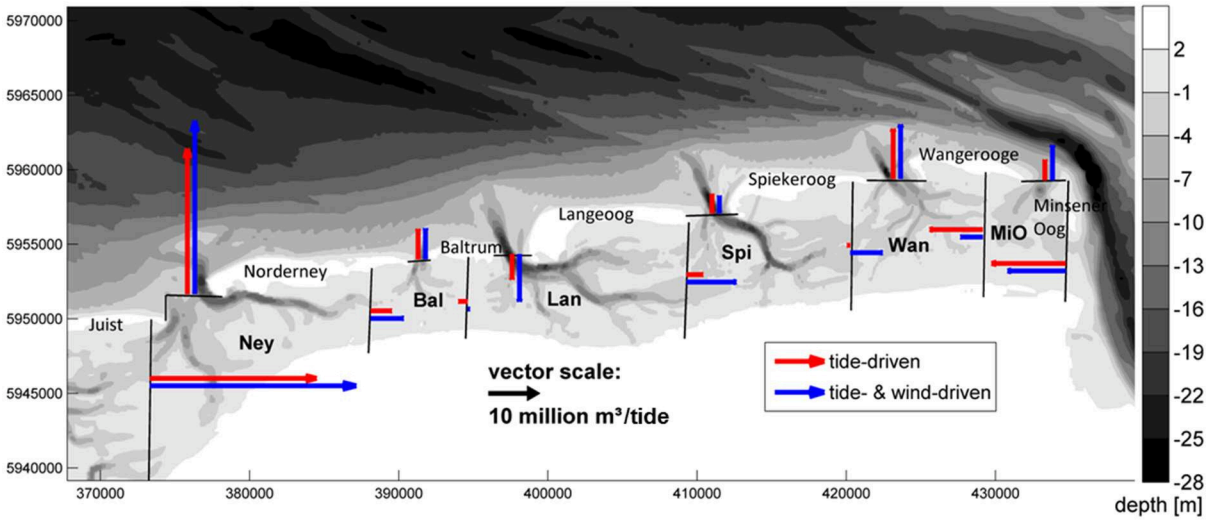

Figure 32. Scaled vectors schematize the annual-mean residual tidal discharge [m³/tide] through tidal inlets and across tidal divides for the simulations with tidal forcing only (red) and tidal and wind forcing (blue).

4.4.2. Wind effect on residual discharges

The response of the net circulation to different forcing conditions is shown by comparison of the hydrodynamics under tidal forcing only, on the one hand, and by additional forcing of an observed year-long time series of wind velocity, on the other.

At most investigated tidal inlets the annual average of residual discharges is ebb-directed, with the exception of the basins of Borkum (i.e. including the outer Ems-Dollard estuary), Juist, Langeoog and the tidal opening between the island Minsener Oog and the mainland which all reveal a net import of water masses for the simulation with and without wind (Fig. 32). The latter tidal opening south of the island of Minsener Oog at the lateral side to the east of the EFWS features the characteristic functions of a tidal inlet that connects directly to the sea and of a tidal divide that falls dry during low tide because of the shallow water depth.

The effect of the wind on the tidal inlet water fluxes is most prominent at the tidal inlet of the Langeoog basin. The annual mean residual discharge of -10.7 $x10^6$ m^3/tide for the combined tidal and wind forcing shows a relative increase of 88% related to the simulation without wind (-5.7 $x10^6$ m^3/tide). The wind forcing results in relative discrepancies of -16 %, +19 %, +2 %, +88 %, -10 %, +9 % and +70 % at the tidal inlets of the basins Jui, Ney, Bal, Lan, Spi, Wan and MiO (Tab. 2, Fig. 32).

The standard deviation is considered as a measure for the variability of the net flow at the inlet. The effect of the wind on the variability of the residual discharge at the tidal inlet, i.e. the standard deviation (Qr_STD), is least important at the basin of Baltrum with 2.2 $x10^6$ m^3/tide (Tab. 2). The ratio between Qr_STD due to the tidal and wind forcing to Qr_STD based on the tidally-driven flow alone shows how vulnerable a specific tidal inlet is to the wind effect. The largest ratios are determined for the tidal inlets of the basins of Langeoog and Minsener Oog (Tab. 3).

Table 3. The ratio of the standard deviation of Qr for tidal and wind forcing to the case of tidal forcing only at tidal inlets (Qr_STD) and tidal divides (QrE_STD), respectively, shows the increase of the variability of the net flow in response to the effect of the additional wind drift and is thus a measure for the vulnerability to the wind forcing.

	Jui	Ney	Bal	Lan	Spi	Wan	MiO
tidal inlet	1.3	2.1	1.4	2.6	1.1	1.6	4.5
tidal divide east	4.9	7.0	37.5	73.4	51.8	41.8	14.2

At the tidal divides the wind drift results in differences of the annual mean residual discharge of +14.2, +8.9, +2.6, +2.5, +7.5, +7.9, -6.7 and -3.6 million m^3/tide between the basins of Bor-Jui, Jui-Ney, Ney-Bal, Lan-Spi, Wan-MiO and at the tidal opening to the outer Jade in east of the basin MiO

(Tab. 2, Fig. 32). At the tidal divides Bal-Lan and Spi-Wan, the additional wind forcing reverses the net flow direction from westward to eastward. The standard deviations of the residual discharge (QrE_STD) are 0.2 $x10^6$ and 6.6 $x10^6$ m^3/tide for the forcing without and with wind at the tidal divide separating the basins of Baltrum and Langeoog and thus reveals the smallest variability of the net flow in the EFWS (Tab. 2). At all tidal divides, QrE_STD increase considerably under the effect of the additional wind. Considering the increase of QrE_STD as a measure for the vulnerability to the wind effect, the tidal divide at the east of the Langeoog basin located in the center of the EFWS shows the maximal ratio of 73.4 (Tab. 3). The tendency to be influenced by the wind decreases to both lateral margins of the EFWS, but prominently towards the western side.

The aforementioned ratio QrDay/PmDay normalizes the residual discharge to the respective daily mean tidal prism. The ratios of individual tidal inlets are compared in the time domain (Fig. 33). In case that QrDay/PmDay of the tide- and wind-driven simulation (blue) is larger than the ratio representing the case of tidal forcing only (red), the wind induces an additional net outflow of the basin or at least dampens the relative net inflow capacity. Pronounced differences can be identified for wind velocities exceeding approx. 8 to 9 m/s. The maximal response on residual discharges is identified for wind directions from the sector south to west and the sector north to east. Three wind scenarios are selected to show the effect on the overall net circulation.

Scenario (a) is a storm event of the duration of several days with hourly-mean peak velocities of 22 m/s on 8. Januar 2005 from south-westerly (SW) direction (Fig. 33). A surplus of up to 20% of the estuarine tidal prism is net imported through the Westerems (Pm of the Ems-Dollard estuary is approx. 865 $x10^6$ m^3 regarding the cross-section at Borkum). This generates an important residual throughflow to the neighboring basins of Juist, Norderney and Baltrum. At their tidal inlets, the residual discharge is ebb-directed with approx. 15%, 60 % and 40% of their actual lunar-day-mean tidal prisms (PmDay). At Accumer Ee, however, more than 40% of PmDay is net imported to the basin of Langeoog; for the simulation solely forced by tide it is in the order of 4 %. At the basin of Spiekeroog, the residual discharge is similar to the case without wind and reveals an export of approx. 3% of PmDay. Further to the east, the two basins of Wangerooge and Minsener Oog are characterized by a residual export of water through the tidal inlets of 25% and 60% of their respective PmDay. This qualitative pattern of the overall net circulation repeats for other periods with strong wind from the south-westerly sector and is thus considered as representative for this wind direction (Fig. 33).

The weather scenario (b) is characterized by wind directions changing from south to north over the westerly sector (Fig. 33). Wind velocities are between 10 to 17 m/s. The first part of the period is characterized by wind directions from south to west and thus comparable to the overall pattern described for scenario (a) unless net discharges are smaller in quantity. For tidal cycles with

wind directions from west-north-west to north, however, QrDay changes to the opposite direction at all tidal inlets except for the basins of Baltrum and Wangerooge. There, the residual discharges decrease and the ebb- and flood prisms are closely balanced.

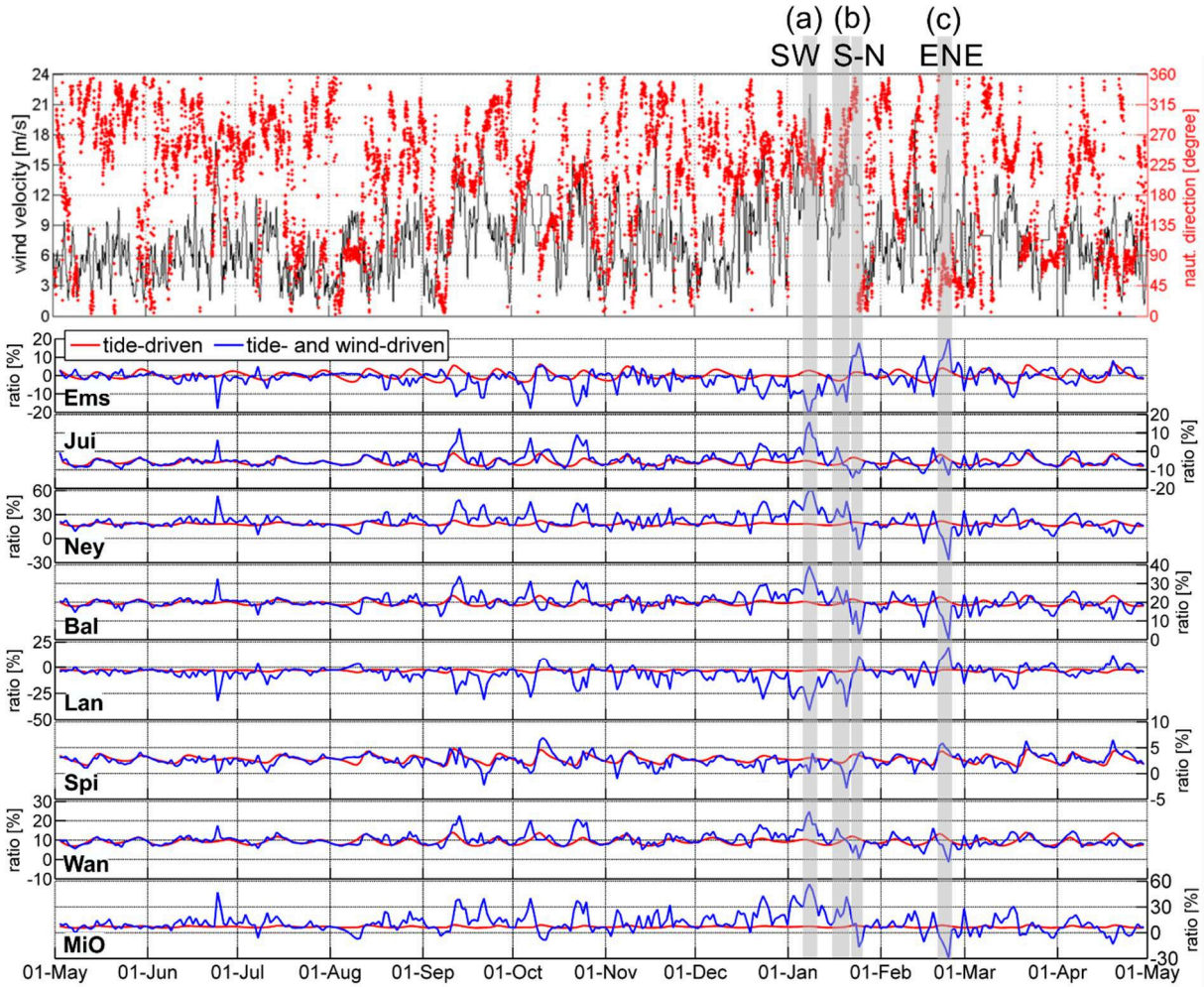

Figure 33. The lunar-daily-mean residual discharges normalized by the related lunar-day-mean tidal prisms (QrDay/PmDay) as for the solely tide-driven (red) and the tide- and wind-driven (blue) simulations show the effect of the wind on the net flow at the tidal inlets. The ratio [%] is positively defined for seaward-directed net discharges through the tidal inlets; note the different scales of the y-axis.

The scenario (c) represents strong wind from the east-north-east with magnitudes of up to 16 m/s (Fig. 33). The net flow through the tidal inlet is flood-directed for the basins of Minsener Oog, Norderney and Juist with 30%, 30% and 10% of PmDay, respectively. The basins of Wangerooge and Baltrum reveal no major residual flow through the tidal inlets. At the tidal inlets draining the basins of Spiekeroog, Langeoog and at the Westerems, ebb-directed flow is predicted with approximately 6%,

20% and 20% of the PmDay, respectively. The response of the residual tidal discharges and the net circulation in between the basins to east-north-easterly wind is comparable to the second period described for scenario (b), when wind prevails from northerly directions.

Throughout the whole year, it appears that the net flow at the tidal inlet of the basin of Spiekeroog is less influenced by the wind. Note that exceptional deviations are solely subject to a wind rotating from the sector south-west to the sector north-west (compare scenario 'b'). While the wind rotates over west, yet only then, the residual discharge at the basin of Spiekeroog is negative, i.e. flood-directed.

Another remarkable observation is related to the basins of Baltrum and Langeoog. Tidal cycles that reveal an ebb-directed residual flow to be considerably increased or decreased under the influence of a particular wind direction at the basin of Baltrum, systematically reflect a qualitative change at the adjacent basin of Langeoog, but for the flood-directed flow (Fig. 33.) The response of the net flow to the same wind is thus mirrored at these tidal inlets. The annual net flow at the tidal divide between these basins is least compared to other tidal divides at the EFWS.

4.4.3. Sensitivity study

A sensitivity study aimed to evaluate the response of the simulated residual discharges Qr to different bottom shear stresses by varying the friction coefficient on the one hand and the water depth on the other. The friction coefficient determining the bottom roughness is considered an unknown model parameter yet having an important effect on the modelled hydrodynamics. An increased water depth was tested against the background of an accelerated sea level rise that might drown back-barrier tidal flats if these are not able to keep path through enhanced accretion of sediments.

Three simulations with friction coefficients prescribed constantly over the area are tested by Manning values of 0.028, 0.023 and 0.018. (Fig. 34). The value of 0.023 is the reference value and was tested to perform best in comparison to measured water levels (sect. 4.3.4.1). A decrease of the friction coefficient reduces the bottom roughness. Independently of the Manning value, the bottom stress increases rapidly with decreasing depth. Our sensitivity study shows that the net throughflows have the same direction at the basin openings independent of the friction coefficient applied. For a decreasing Manning value, a consistently larger residual discharge is simulated through the tidal divides and tidal inlets of the interconnected system except for the tidal divide between the basins of Spiekeroog and Wangerooge. Here, the westward directed net discharge is generally low, but still decreases for a decreasing friction coefficient. Increasing the bottom friction to a value of 0.028, the residual discharge at the tidal divide between the basins of Langeoog and Spiekeroog ceases.

The water level in the model domain is increased with respect to the reference case (Manning 0.023) by adding 0.5 meters to the water level time series prescribed at the open sea boundaries (Fig. 34). As expected, the residual discharge responds in a same way as for the decrease of the bottom roughness, except at the tidal divide between the basins of Spiekeroog and Wangerooge where the behavior is inversed. The effect of the increased water level on the net discharges is generally not as large as for the case with reduced bottom friction (Manning value of 0.018).

The sensitivity study shows that the overall direction of the circulation patterns in between the basins and the coastal sea is independent of the different bottom frictions. The magnitude of the residual discharge, however, is a function of the relative bottom roughness and generally increases for a reduced friction value. The same yields for the mean tidal prism of the back-barrier basin that increases for a reduction of the bottom roughness. The mean tidal prism of the basin of Spiekeroog, for instance, either decreases by 2% or increases by 3% after increasing or decreasing the bottom friction with respect to the reference case.

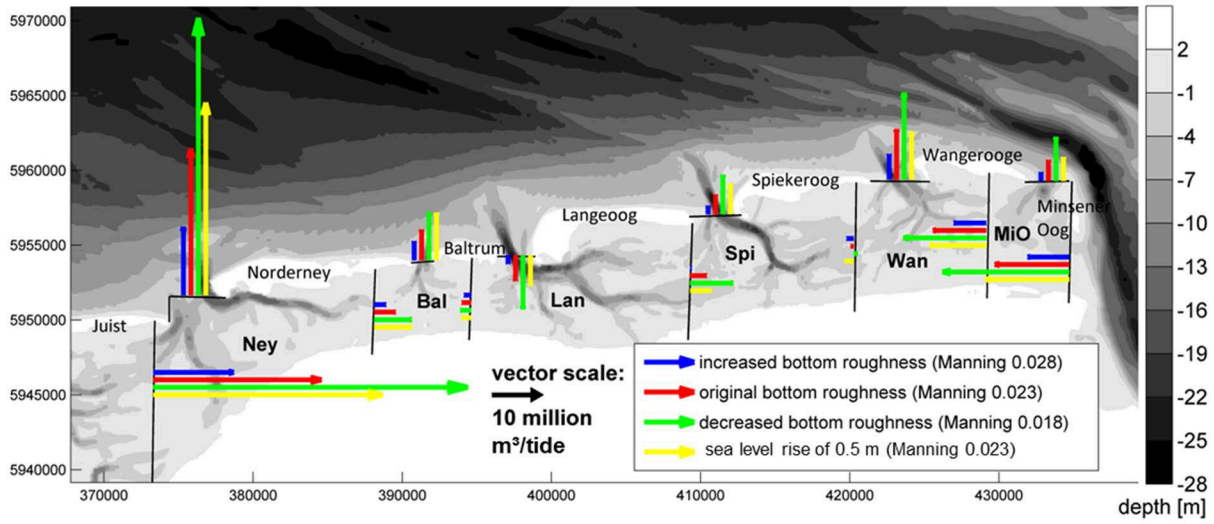

Figure 34. The sensitivity of the residual tidal discharges [m³/tide] at tidal inlets and across tidal divides is shown for varying model settings of solely tidally-driven simulations, i.e. three different bottom roughness values (Manning, 0.028, 0.023, 0.018) and a sea level rise of 0.5 m.

4.4.4. Tidal transformation along the barrier islands

Residual water fluxes through tidal inlets and across tidal divides are generated by pressure gradients resulting from the non-linear transformation of the tidal wave propagating along the complex topography of the barrier island coast. The phase shift and the difference in tidal amplitude from one tidal inlet to the subsequent quantify the alteration of the tidal signal along the length of each island.

The island length is estimated as a straight line in between the tidal inlet centers to be approx. 21.2, 16.0, 5.9, 14.1, 11.8, 10.3 and 5.7 km for the islands of Juist, Norderney, Baltrum, Langeoog, Spiekeroog, Wangerooge and Minsener Oog, respectively. Water levels simulated at the center of each tidal inlet are investigated by means of a harmonic analysis. The difference in tidal amplitude and the phase lag are shown for the semi-diurnal tidal constituents M2, S2 and N2 along the length of each island (Fig. 35). The difference of the tidal amplitude is negligible along the most westerly island Juist but gradually increases eastwards. The change in amplitude of the principal lunar semi-diurnal constituent M2 increases from 2 cm along Norderney to almost 10 cm along Wangerooge and along Minsener Oog. An opposite trend becomes apparent for the phase shift. The phase shift of the M2 tide decreases from maximal 10 degrees at the length of the island of Juist to only 2 degrees along Spiekeroog. Along the most eastward islands, the phase shift increases again moderately to almost 8 and 6 degrees at Wangerooge and Minsener Oog, respectively. Analogous trends with respect to the qualitative change of amplitude and phase shift along the barrier islands are determined for the other semi-diurnal constituents S2 and N2 (Fig. 35). These findings are consistent with co-tidal charts of the southern German Bight that were derived from water level measurements (Lassen and Siefert, 1991): the occurrence of high water is almost at the same time for the islands of Langeoog and Spiekeroog, while the tidal ranges steadily increase from west to east.

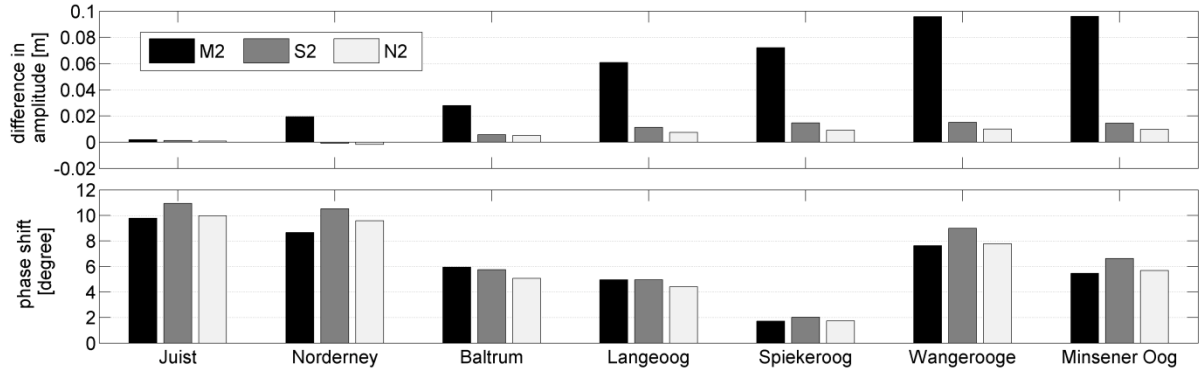

Figure 35. Tidal amplitude and phase differences between the tidal inlets from west to east of each island based on modelled water levels and shown for the semi-diurnal astronomical components M2, S2 and N2.

4.5. Discussion

4.5.1. Tidally-driven residual circulation

In a solely tidally-driven system, the flood-ebb-asymmetry of the time-integrated discharge at tidal inlets and across divides is driven by water level gradients that are due to the tidal phase lag and the tidal amplitude difference between adjacent basin openings. Likewise the geometrical asymmetry of sub-basins, i.e. ratios of width, length or depth, can generate residual flow patterns. The early study of Van der Kreeke and Cotter (1974) compared analytical and numerical model results based on idealized geometries that aided in understanding the circulation among communicating basins and between the sea. They found that residual water fluxes are in the direction of the tidal inlet where the tidal signal enters last. In case of a difference in the tidal amplitude, the net flow is directed to the inlet with the minor tidal amplitude. Furthermore, they investigated the relationship of geometrical features of neighboring basins and concluded that the resultant flow direction is from the broader to the narrower tidal inlet and from the shallower to the deeper inlet. Their generic conclusions were confirmed partly (Liu and Aubrey, 1993; Herman, 2007) or entirely (Ridderinkhof, 1988b). Ridderinkhof (1988a, 1988b) who applied a numerical model with a 'real-world' bathymetry of the Western Dutch Wadden Sea and an idealized analytical model concluded that the residual flow from the Vlie basin to the Marsdiep basin is induced by the difference in tidal amplitude as well as the depth and width ratio between the basins. The phase difference between the basins yet reveals an opposing flow which, however, is much smaller than the combined effect of the morphological asymmetry and the difference in tidal amplitude.

The physical mechanisms liable for the control of the residual circulation evaluated at the EFWS are explained likewise: At the western part of the EFWS, the residual tidally-driven flow through the basins of Juist, Norderney and Baltrum is eastward directed. Most of the surplus that inflows at the Juist basin directs towards the basins of Norderney and Baltrum, where the net flow is easterly directed across the tidal divides and seaward at the tidal inlets (Fig. 32, Tab. 2). Both, tidal and morphological asymmetries play a role and comply with the above-mentioned general conclusions: The phase difference along the islands of Juist and Norderney is largest in the study area while the difference in amplitude is very small (Fig. 35). The phase difference between the tidal inlets suggests that the tide enters first at the inlet in the west thus inducing a net flow to the east, just as predicted by our model. Furthermore, the basins' sizes (tidal prisms) decrease from Juist to Norderney and to Baltrum caused by a continuous reduction of the basins' depths, widths and lengths which likewise applies to a continuous reduction of the respective tidal inlet widths (Fig. 27, Tab. 2). This geometrical asymmetry of the funnel-shaped basins-system emphasizes the tendency of the residual flow to be

directed to the east over the tidal divides and out of the basins at the tidal inlets. Our model results confirm the study of Herman (2007) who applied both an analytical and a numerical model covering these three basins. We identified the same net flow patterns while the larger magnitudes of the residual discharges compared to her results are explained by a difference in the tidal forcing and/or bottom friction applied.

At the eastern side of the EFWS, the basins of Minsener Oog and Wangerooge represent the opposite case with a net flow directed to the west at the tidal divides yet still a seaward net flow through the tidal inlets (Fig. 32, Tab. 2). The differences in tidal amplitude along both islands are largest with respect to the entire domain. According to the linear solution established from idealized model studies, the amplitude ratio induces an overall westward directed net water flux which, however, may be superimposed by an opposing flow component generated by the elevated phase difference in between the islands (Fig. 35). Liu and Aubrey (1993) showed that the generation of residual currents in an open tidal channel is most sensitive to the mean sea-level differences, less sensitive to the tidal amplitude differences, and at least sensitive to the tidal phase differences between the two ends of the channel that they investigated by an analytical model. Noteworthy differences in the mean sea level are neither observed from the analysis of the one year observations nor from the predicted water level time series. The change in tidal amplitude is thus suggested to be the dominant physical mechanism generating the residual discharge in westerly direction at the east of the study area having an influence up to the basin of Spiekeroog. It is noted that the tidal opening between the island Minsener Oog and the mainland at the lateral side of the EFWS has to be interpreted as a tidal inlet that opens to the sea. This inlet is characterized by a very wide and shallow cross-section that directs the residual flow towards the narrower and deeper tidal inlet of the basin Minsener Oog. This complies to the analytical solution proposed by van der Kreeke and Cotter (1974) and Ridderrinkhof (1988b) with respect to width and depth ratios of adjacent tidal inlets.

The mechanism driving the net circulation at the two central tidal basins of Langeoog and Spiekeroog are less obvious to be interpreted as the nonlinearity generated by the tidal asymmetry is strongly superimposed. These basins are in between the earlier described lateral residual circulation cells with opposing net flow patterns. The net import at the tidal inlet of the Langeoog basin (Accumer Ee) is primarily directed to the basin of Spiekeroog and to a minor degree to the basin of Baltrum (Fig. 32, Tab. 2). The tidal wave propagates from west to east offshore the islands, which suggests that the change of the residual discharge regime importing water at Accumer Ee to the basin of Langeoog is explained in the relationship to the basin of Baltrum and not to the basin of Spiekeroog. The amplitude ratio and the phase ratio along Langeoog are both intermediate with respect to the ranges found along the EFWS and thus theoretically may induce opposing flows (Fig. 35). It is thus proposed that

asymmetries of the basins geometry are the determining factor here. The relationships of the tidal prisms of adjacent basins in the EFWS are all in the order of 1 to 3, except for the large basins adjacent to the small basin of Baltrum. Here, the tidal prisms of the basins of Norderney and Langeoog are both 5 times larger than the prism of the Baltrum basin. It is thus suggested to play a role in the net circulation in the way that the small basin of Baltrum imports residual discharges from both lateral margins. Herman (2007) showed that an increase in surface area ratio (and thus tidal prism ratio) emphasizes the net flow to the basin with the smaller surface area. An additional explanation to decipher the mechanisms responsible for the predicted flood-directed residual discharge at Accumer Ee is due to the inferior length of the island of Baltrum. Wang et al. (2013) describe the influence of the island length on the net flow induced by the relative phase ratio. In other words, a small distance in between the inlets reduces the relative net flow induced by a tidal phase difference and – for the given situation at Baltrum - relatively increases the opposite, westward directed flow due to the amplitude ratio. In a consequence of the surplus inside the basin of Langeoog, residual fluxes across the eastern tidal divide to the basin of Spiekeroog are expected and are hence compensated by a net outflow at the tidal inlet Otzumer Balje.

In view of the tide-induced residual circulation patterns that have been deciphered in the EFWS, we question the assumption of Li (2013) that in a purely tide-driven system the subtidal exchange flow usually does not show an obvious inward flow at one inlet and outward at another inlet. In a solely tidally-driven case, we identify three overall circulation cells where the tidal divides south of Baltrum (Bal/Lan) and south of Spiekeroog (Spi/Wan) establish a border between the individual compartments. This is emphasized by small standard deviations, i.e. a low variability of the residual discharges at these tidal divides.

It is shown that the residual discharges at all tidal inlets and at most divides are less sensitive against changes of the bed friction or against an imposed sea level rise and meteorological forcing; it means, that the annual net flow direction at the investigated cross-sections is not inverted and the identified residual circulation thus tends to be robust.

4.5.2. Wind-driven residual circulation

For the tide only forcing, the accumulation of the residual discharge reveals a linear trend at the tidal inlets and divides of the individual basins over time. Including wind stress, strong non-linear subtidal fluxes induced by changing wind directions are superimposed as shown by the responses of the net flow at eight tidal inlets of the EFWS (Fig. 33). We could find general agreement with findings of Li (2013) who investigated the influence of stationary wind forcings from varying directions on the subtidal water flux at an idealized multiple-inlet system by applying a numerical model. He postulated

that the net outward flow tends to occur at the inlet farther away in the downwind direction, when the wind direction is parallel or oblique to the alignment of the coast with three interconnected basins. This then is associated with a net inward transport at the upwind inlet and a minimum net flow at the centered inlet. The communicating basins of the EFWS reveal a related circulation pattern for example during strong northeasterly winds (Fig. 33, wind scenario ‘c’) with a corresponding inflow at the tidal inlets of the basins Minsener Oog and Wangerooge, minimum net discharge at the tidal inlet of the Spiekeroog basin and strong outward directed residual discharge at the tidal inlet of the Langeoog basin. The same response of the residual flow to this wind direction is predicted at the westerly circulation cell; inflow at the tidal inlets of the basins of Baltrum and Norderney, minimal at Juist and strong net outflow at the tidal inlet southwest of Borkum. In the opposite case, with strong south-westerly winds (Fig. 33, wind scenario ‘a’), the funneling shape of the aligned basins of Borkum, Juist, Norderney and Baltrum even emphasizes the wind-induced subtidal flow behavior with an inflow at Borkum, a net throughflow along the basins and a net ebb-directed discharge at the tidal inlets, respectively. Buijsman and Ridderinkhof (2007) who investigated subtidal flows by cross-sectional ADCP measurements at the most westerly tidal inlet of the Western Dutch Wadden Sea had drawn related conclusions: the variability in the subtidal water transports are mainly governed by local wind stress. Southwesterly winds induce a throughflow in easterly directions along the axis of the Marsdiep basin to the Vlie basin, whereas north-westerly winds force a smaller mean water transport in the opposite direction.

The standard deviation of the residual discharges quantifies the variability of the net fluxes. It is found that the variability increases more at basin divides compared to tidal inlets. The strong westerly wind regime that parallels the orientation of the island chain is responsible for the dominant net mass flux to the east which becomes apparent by comparing the yearly averaged residual fluxes based on the simulation with and without wind forcing (Fig. 32). The wind drift superimposes on the tide-induced, easterly directed net flow at the western basins and decreases the opposing net flow at tidal divides of the basins eastward of Spiekeroog island. In the idealized model domain of Li (2013) and other simplified multi-basin model geometries found in literature, the lateral boundaries and particularly the tidal divides of the marginal back-barrier basins are closed. The EFWS fringed by the East Frisian barrier islands, however, is open to the Ems-Dollard estuary to the west and the Jade Bay to the east. These lateral openings provide the exchange of substantial residual water fluxes, in particular due to wind-driven flow. On the other hand, the variability of the residual discharges tends to be largest in the center of the EFWS, i.e. at the basins of Spiekeroog and particularly Langeoog, because westward and eastward wind drifts result into important throughflows here. At the tidal divide between the basins of Baltrum and Langeoog, however, the amount as well as the variability of the

residual water flow is predicted to be minimal on a yearly time basis. This supports the assumption of the existence of two dominant circulation cells in the EFWS, with only minor throughflows from the westerly to the easterly circulation cell. The minimal inter-basin communication implies a relative increase of fine sediments at the tidal divide south of the island of Baltrum due to converging fluxes. This is further evidenced by morphological and sedimentological observations. The tidal flats at this tidal divide are more elevated (Fig. 27), while sedimentological maps based on interpolated grain-size samples show a pronounced accumulation of fine sediments in comparison to other tidal divides in the study area (Figge, 1981).

4.5.3. Relevance of the circulation to sedimentation and ecology

Facing an accelerated sea level rise, ongoing research aims to evaluate the ability of the Wadden Sea tidal flats to accumulate sediments at a progressive rate in order to keep pace (Dissanayake et al., 2012; Flemming and Bartholomä, 1997; Wang et al., 2012b). This issue is strongly linked to the uncertainties with respect to the physical mechanisms responsible for the fine-grained sediment to be deposited in the Wadden Sea, e.g. settling/scour lag effect (Postma, 1961; Van Straaten and Kuenen, 1957). Recently also density-driven flows comparable to estuarine circulations have been identified to contribute to the import of sediments to the back-barrier tidal flats (Burchard et al., 2008; Flöser et al., 2011). In view of the relatively small flow velocities induced by density gradients in the Wadden Sea, we suppose that tide- and wind-driven residual water fluxes mainly entering the back-barrier basins from the lateral margins of the EFWS have been underestimated so far. For the combined forcing, the annual-mean net inflow from the lateral margins, i.e. from the Juist basin (46 $x10^6$ m^3/tide) and the outer Jade Bay channel (13 $x10^6$ m^3/tide), is estimated to be in the order of 85% of the total residual import to the EFWS, as compared to 15% being net imported at Accumer Ee (11 $x10^6$ m^3/tide), the tidal inlet of the Langeoog basin at the center of the EFWS. The total net import of approx. 70 $x10^6$ m^3/tide corresponds to 5.5 % of the total mean tidal prism of the EFWS that we estimated to 1268 $x10^6$ m^3 excluding the basin at the mouth of the Ems-Dollard estuary. This surplus of water is residually circulated within the multi-basin system during an average tidal cycle and is supposed to carry an important amount of fine sediment in suspension. Generally, the water level is higher than mean sea level when residual discharges pass across tidal divides. The surplus of suspended sediments thus occurs around high water when intertidal flats are inundated yielding a smaller average water depth than at low water when water is confined to the deeper channels (Van Straaten and Kuenen, 1957). Higher residence times and decreased turbulence due to increased water levels favors the settling of fine sediment. Hence, during high water slack, a potentially higher amount of suspended sediments gets to settle out. Although the mechanisms responsible for the import of fine

sediments to the Wadden Sea are far more complex and interact on several spatial and temporal scales the delineated mechanism of an additional net surplus entering from the lateral margins of the EFWS and the circulation within is claimed to need more attention with respect to the governing question of sediment import mechanisms to the back-barrier tidal flats.

Residual circulations may not only influence sediment budgets, but also other suspended particulate matter (SPM) that is advected by the inter-basin residual water fluxes in the Wadden Sea. Kohlmeier and Ebenhöh (2007, 2009) and Grunwald et al. (2010) used a semi-Lagrangian box model coupled to a localized circulation model to evaluate the transformation of organic matter to dissolved nutrients in the back-barrier basin of Spiekeroog island. They consider a semi-enclosed basin where particulate organic matter is imported from the North Sea through the tidal inlet while dissolved inorganic nutrients are exported from the tidal flats. The budget is thus only established at the tidal inlet disregarding the residual mass exchanges across the tidal divides. We predicted relatively low annual mean residual discharges of 3.9 $x10^6$, 11.1 $x10^6$ and 7.2 $x10^6$ m^3/tide (3 %, 7 % and 5 % of the mean tidal prism) at the tidal inlet and across the western/eastern tidal divides of the Spiekeroog basin. The standard deviations of the residual discharge of 5.2 $x10^6$ m^3/tide at the tidal inlet and of approx. 20 $x10^6$ m^3/tide at both tidal divides, however, indicate a high variability of the net throughflow in comparison to other basins of the EFWS. These net fluxes across tidal divides of the Spiekeroog basin may have an influence on residence times and on inter-basin SPM budgets. Inter-basin communication thus needs to be considered in ecosystem studies (e.g. nutrient cycling) in the back-barrier tidal flats.

4.6. Conclusions

A process-based hydrodynamic model of the East Frisian Wadden Sea (EFWS) is applied to exemplarily study the significance of tidally- and wind-driven water exchange among communicating sub-basins of a multiple-inlet system. The residual circulation as the response to the non-linear interaction of tidal and subtidal drivers is deciphered by evaluating simulations based on tidal only and combined tidal and meteorological forcings. The accumulated tidally-driven discharge at inlet cross-sections shows a quasi-linear trend that is controlled by the lunar-daily inequality and the neap-spring cycle while being superimposed by modulations of tidal components of a longer periodicity. Annual, tidal-mean residual water fluxes reveal substantial net inflows of up to 24% of the sub-basin's mean tidal prism at the lateral margins of the multiple-inlet system. The physical mechanisms responsible for the flood/ebb-asymmetry of time-integrated discharges at tidal inlets and across divides are delineated. The tidal phase difference between adjacent tidal inlets induces the eastward directed residual fluxes in the west of the study area, while the opposing net fluxes at the eastern lateral side are due to differences in the tidal amplitude. The variability of residual discharge rates substantially increases

when wind stress is added to the tidal forcing; coast-parallel wind directions generate an inflow at the upwind inlet and an outflow at the downwind inlets. During south-westerly storms, this is compensated by inter-basin fluxes of up to 60% of the respective tidal prism. The annual residual circulation patterns in the EFWS turned out to be consistent and fairly robust against varying boundary conditions: the time-integrated flow directions at tidal inlets show the same orientation independently of an additional wind forcing, varying bed friction coefficients or an imposed sea level rise. For the solely tidally-driven case, three distinctive residual circulation cells are identified inside the back-barrier system. Under the influence of wind these merge to two largely independent circulation cells with only minor net exchanges across a tidal divide in the center of the system. Here, the observed sedimentology and morphology indicates a zone of accumulation of prominent fine-grained sediments that is suggested to be linked to the convergence of net imported substantial water fluxes from both lateral margins of the EFWS, which to our knowledge have been underestimated until now. We suppose that this inter-basin transport of suspended particulate matter may have implications on residence times and estimates of nutrient budgets among the back-barrier basins and between the North Sea and thus needs to be taken into consideration in related studies.

Acknowledgements

This study is associated to and funded by the research project WIMO (www.wimo-nordsee.de) being financed in equal parts by two ministries in Lower Saxony, Germany, the Ministry of Environment, Energy and Climate Protection and the Ministry of Science and Culture.

We gratefully acknowledge the authorities and research institutes, namely the Federal Maritime and Hydrographic Agency (BSH) and the Coastal Research Station belonging to Lower Saxony Water Management, Coastal Defense and Nature Conservation Agency (FSK-NLWKN) for furnishing bathymetrical data, the federal agencies of hydrology (BfG) and water and navigation (WSV) for water level data and the Federal Ministry for Environment, Nature Conservation and Nuclear Safety (BMU) and the Project Management Jülich (PTJ) for providing wind data measured at the offshore platform FINO1.

Chapter 5: Concluding remarks and perspectives

This thesis demonstrates process-based modelling to be a reliable tool to simulate coastal morphological evolution of different spatio-temporal scales in response to a variety of forcing conditions. Coastal dynamics driven by the interaction of the tide, waves and meteorological forcing are investigated at a barrier island system at the southern North Sea coast.

A hierarchical cascade of nested numerical models is set-up to hindcast a severe storm event in the North Sea and to study the effect of extreme wave conditions on the morphology and sedimentology at the tidal inlet Otzumer Balje. For a comparative evaluation, mid-term fair-weather conditions with low-energetic waves are simulated to determine the system's response to tide-dominant conditions. The mutual feedbacks among different morphological units are evaluated while focusing on sediment dynamics at mixed-energy tidal inlets. For the first time, multi-fractional sediment transport modelling is applied to determine the surface sediment grain-size distribution in response to distinct hydrodynamic drivers.

Conceptual models of alongshore sediment bypassing at tidal inlets are commonly established on the basis of sedimentological surveys or aerial photographs. These bypassing schemes are reviewed and discussed by means of detailed simulations of multi-grain-size sediment transport at the East Frisian barrier islands. In contrast to the sediment fluxes controlled by distinct hydrodynamic conditions, here, the residual transport pathways are shown in response to long-term representative boundary conditions. The identification of grain-size dependent sediment pathways brings together formerly contradicting theories on sediment bypassing at mixed-energy tidal inlets.

The East Frisian Wadden Sea, on a comprehensive scale, is investigated to study the tidally- and wind-driven circulation of a typical multiple-inlet system. Residual water fluxes that manifest as flood-ebb-asymmetries at tidal inlets are generated when the tide propagates over the irregular bathymetry of interconnected back-barrier basins. The complexity of the circulation further increases when the non-linear interaction with wind-driven flow is considered. The presented results contribute to the phenomenological description of the residual circulation in the system.

In the following, the main findings are summarized addressing the research questions presented in the introduction.

(1) Residual morphological and sedimentological response to distinct hydrodynamic drivers

(2) The effects of storm events and fair-weather conditions on morphology and sedimentology

Model scenario experiments allow for the synthetic separation of processes by imposing reduced boundary conditions aiming a greater understanding of the system's response. At mixed-energy tidal inlets, however, a possible model approach that reduces the forcing to either tides or waves alone would be misleading as the natural interaction is ignored. Tide- and wave-dominated forcing conditions are thus represented by realistic fair-weather and storm scenarios, respectively. In this way, the mixed-energy regime is preserved while the morphological and sedimentological response to distinct hydrodynamic drivers is evaluated. Consequently, the answers to research questions (1) and (2) are related.

During storm conditions, the ebb-tidal delta loses sand through wave erosion; this deficit is compensated by ebb-directed residual sediment transport at the inlet throat during tide-dominated fair-weather. The model satisfactorily reproduces this dynamic morphological equilibrium condition. Observed responses of sedimentology and morphology are explained in relation to distinct forcing conditions and particular drivers which, in nature, are obscured by continuous interaction.

The model approach elucidates how sediment grain-size sorting mechanisms are affected by distinct drivers. Furthermore, it is shown that the observed sediment grain-size distribution and morphological response at mixed-energy tidal inlets are the result of both, tide-dominant fair-weather and wave-dominated less frequent storm conditions. This becomes evident as solely the combined scenario forcing, i.e., alternating fair-weather and storm simulations, can result in a sediment grain-size distribution that is in agreement with measurements of surface sediment grain-size composition. Therefore, in a mixed-energy environment, a preceding redistribution of imposed grain-size fractions – particularly in response to high-energy events – is a requisite prior to performing simulations of realistic scenarios.

Simulated sediment grain-size compositions at the investigated tidal inlet show that medium-sized sand (the coarsest investigated fraction) is found at either tidal inlet channels exposed to tidal-flow-induced bottom shear or at the ebb-tidal delta shoals where winnowing of fine sand is a result of wave stirring. It is suggested that surface sediments, here, can be explained by erosional, and not depositional, processes. Morphological patterns that are prone to depositional processes and accumulation of fine sand are identified to occur in zones of reduced bottom shear as a result of opposing tidal currents and waves; e.g. demonstrated at the barrier island foreshore.

(3) Net sediment transport pathways for distinct hydrodynamic forcing conditions

The model study deciphers sediment dynamics in response to either wave- or tide-dominant forcing conditions. During fair-weather, the tide-induced sediment transport mainly focuses on the inlet throat and the marginal flood channels. As during storms, the net bed load sediment transport is

generally onshore directed on the shallower ebb-tidal delta and driven by wave-induced processes. The magnitude and seaward reach of the bypassed fluxes and the dominant grain-size are primarily controlled by wave energy, i.e. wave-induced alongshore current, that are consequently more significant for storm than for fair-weather conditions.

The study endorses the significance of the recirculation of sand at the Otzumer Balje tidal inlet and thus confirms earlier sedimentological surveys. However, it exposes that only the combination of residual sediment fluxes of both scenarios, i.e. storm and fair-weather, is able to achieve a residual sediment circulation over the eastern ebb-tidal delta shoal redirecting sand back to the inlet throat.

(4) Sediment bypassing at mixed-energy tidal inlets

Simulations of representative mid-term forcing conditions (two years) are time-integrated and show that very fine to fine sand (125 µm) mainly bypasses along the periphery of the ebb-tidal delta to the downdrift island. Fine to medium sand (250 µm) is delivered by alongshore sediment drift to the inlet throat where ebb-dominant flow directs the sand to the ebb-tidal delta lobe. From here, it is entrained by waves and oriented downdrift and bypasses either continuously or by the migration of large bar complexes to the adjacent island. It is shown that medium to coarse sand (375 µm) is largely recirculated among inlet throat and ebb-tidal delta, hence only very few amounts are bypassed. Detailed results at two tidal inlets suggest that the ratio of the totally bypassed sand directly downdrift of the ebb-tidal delta to the recirculated sediments is approximately two. The model thus confirms common theories of tidal inlet bypassing but reveals clear dependencies of the residual sediment pathways with respect to particular sediment grain-size fractions.

(5) The net circulation in the multiple-inlet system in response to the non-linear interaction of tidal and meteorological forcing

For the solely tidally-driven model scenario, three largely independent residual circulation cells are identified at interconnected back-barrier basins. Under the influence of wind these merge to two cells with only minor net exchanges across a tidal divide in the center of the system. Here, the observed sedimentology and morphology indicates a zone of accumulation of fine-grained sediments that is suggested to be linked to the convergence of net imported water fluxes from both lateral margins of the East Frisian Wadden Sea. The physical mechanisms responsible for the flood/ebb-asymmetry of water fluxes at inter-basin cross-sections are delineated: The tidal phase difference between adjacent tidal inlets induces eastward directed residual fluxes in the west of the study area, while the opposing net fluxes at the eastern lateral side are due to differences in the tidal amplitude. It is shown how the variability of residual discharge rates substantially increases when wind stress is

added to the tidal forcing; coast-parallel wind directions generate an inflow at the upwind inlet and an outflow at the downwind inlets. During south-westerly storms, this is compensated by inter-basin fluxes of up to 60% of the respective tidal prism. Despite such occasional extreme flow asymmetries, the residual pathways of annually-integrated water fluxes are consistent for meteorological forcing, an imposed sea level rise or different bed friction coefficients. It is further shown that the multi-basin system imports a substantial surplus of water from the lateral margins of the East Frisian Wadden Sea having an impact on the mass budget of the communicating basins that has been underestimated until now in hydrological, sedimentological and ecosystem studies.

In this study, interacting processes are separated in a way that the effect of a particular phenomenon can be evaluated on the basis of morphological and sedimentological responses or by means of residual transport fluxes of either sediment or water. It is shown how morphodynamics are driven at tidal inlets and at the barrier island foreshore. At the back-barrier, the net transport of water volume being subject to tidal- and meteorological forcing are exposed and quantified. The presented modeling approach can be considered as a tool that contributes to the assessment of the actual status of the system. This methodology can thus be adopted for the development of management strategies aiming for the 'Good Environmental Status'; in particular, for the definition of qualitative descriptors of morphology and sedimentology as a requirement for ongoing monitoring issues. Furthermore, all requirements are fulfilled to go the next logical step of incorporating advective and diffusive transports of very fine sand (< 125 μm) and cohesive particles (< 63 μm) into the model. The governing physical processes that need further attention are entrainment, advection-diffusion, settling and consolidation of sediments in the back-barrier basins; complex phenomena like biostabilization of surface sediments by diatom biofilms or settling whilst flocculation of cohesive particles etc. need to be parameterized. The interrelation of these processes – many of these often supposed to be secondary phenomena when considered exclusively – may be crucial to evaluate the sensitive morphological equilibrium condition that is controlled by eroding and depositional properties. This then will allow for the evaluation of exchange processes and realistic sediment budgeting between the barrier island foreshore and the back-barrier basins on a multi-decadal time scale. The achieved process-based understanding of the governing phenomena then permits an assessment of whether the Wadden Sea's intertidal flats will succeed in accumulating enough sediment to follow up the persistent and accelerated sea level rise and thus resist the consequences of anthropogenic climate change.

References

Antia, E.: Sedimentary Deposits Related to Inlet-Shoreface Storm Flow Interaction in the German Bight, Estuar. Coast. Shelf Sci., 40, 699–712, doi:10.1006/ecss.1995.0047, 1995.

Antia, E., Flemming, B. and Wefer, G.: Transgressive facies sequence of a high energy, wave-tide-storm-influenced shoreface: A case study of the east Frisian Barrier Islands (Southern North Sea), Facies, 30(1), 15–23, 1994.

Ardhuin, F., Rascle, N. and Belibassakis, K. A.: Explicit wave-averaged primitive equations using a generalized Lagrangian mean, Ocean Model., 20, 35–60, doi:10.1016/j.ocemod.2007.07.001, 2008.

Ardhuin, F. and Roland, A.: The development of spectral wave models: coastal and coupled aspects, in: Proceedings of the 7th International Conference on Coastal Dynamics, 24–28 June 2013, University of Bordeaux, France, 25–38, 2013.

Badewien, T. H., Zimmer, E., Bartholomä, A., and Reuter, R.: Towards continuous long-term measurements of suspended particulate matter (SPM) in turbid coastal waters, Ocean Dynam., 59, 227–238, doi:10.1007/s10236-009-0183-8, 2009.

Barnard, P. L., Erikson, L. H., Elias, E. P. L. and Dartnell, P.: Sediment transport patterns in the San Francisco Bay Coastal System from cross-validation of bedform asymmetry and modeled residual flux, Mar. Geol., 345, 72–95, doi:10.1016/j.margeo.2012.10.011, 2013.

Bartholomä, A., Kubicki, A., Badewien, T. H., and Flemming, B. W.: Suspended sediment transport in the German Wadden Sea-seasonal variations and extreme events, Ocean Dynam., 59, 213–225, doi:10.1007/s10236-009-0193-6, 2009.

Behre, K.-E.: A new Holocene sea-level curve for the southern North Sea, Boreas, 36(1), 82–102, doi:10.1111/j.1502-3885.2007.tb01183.x, 2007.

Bennis, A.-C., Ardhuin, F., and Dumas, F.: On the coupling of wave and three-dimensional circulation models: Choice of theoretical framework, practical implementation and adiabatic tests, Ocean Model., 40, 260–272, doi:10.1016/j.ocemod.2011.09.003, 2011.

Bertin, X., Fortunato, A. B., and Oliveira, A.: A modeling-based analysis of processes driving wave-dominated inlets, Cont. Shelf Res., 29, 819–834, doi:10.1016/j.csr.2008.12.019, 2009.

Blondeaux, P.: Sediment mixtures, coastal bedforms and grain sorting phenomena: An overview of the theoretical analyses, Adv. Water Resour., 48, 113–124, doi:10.1016/j.advwatres.2012.02.004, 2012.

Booij, N., Ris, R. C., and Holthuijsen, L. H.: A third-generation wave model for coastal regions 1. Model description and validation, J. Geophys. Res., 104, 7649–7666, doi:10.1029/98JC02622, 1999.

Brouwer, R. L., van de Kreeke, J. and Schuttelaars, H. M.: Entrance/exit losses and cross-sectional stability of double inlet systems, Estuar. Coast. Shelf Sci., 107(0), 69–80, doi:http://dx.doi.org/10.1016/j.ecss.2012.04.033, 2012.

Bruun, P. and Gerritsen, F.: By-Passing of Sand by Natural Action at Coastal Inlets and Passes, in Vol. 85, Journal of Waterways and Harbours Devision, Proc. ASCE, pp. 75–107., 1959.

Bruun, P. and Gerritsen, F.: Natural by-passing of sand at coastal inlets, Trans. Am. Soc. Civ. Eng., 126(4), 823–850, 1961.

Bruun, P.: Stability of tidal inlets, Elsevier., 1978.

BSH: Spatial Plan for the German Exclusive Economic Zone in the North Sea -Map-. [online] Available from: http://www.bsh.de/en/Marine_uses/Spatial_Planning_in_the_German_EEZ/documents2/MSP_DE_North Sea.pdf, 2014.

Buijsman, M. C. and Ridderinkhof, H.: Water transport at subtidal frequencies in the Marsdiep inlet, J. Sea Res., 58(4), 255–268, doi:http://dx.doi.org/10.1016/j.seares.2007.04.002, 2007.

Burchard, H., Flöser, G., Staneva, J. V., Badewien, T. H. and Riethmüller, R.: Impact of Density Gradients on Net Sediment Transport into the Wadden Sea, J. Phys. Oceanogr., 38, 566–587, doi:10.1175/2007JPO3796.1, 2008.

Cheung, K. F., Gerritsen, F., and Cleveringa, J.: Morphodynamics and Sand Bypassing at Ameland Inlet, The Netherlands, J. Coast. Res., 231, 106–118, doi:10.2112/04-0403.1, 2007.

Chu, K., Winter, C., Hebbeln, D. and Schulz, M.: Improvement of morphodynamic modeling of tidal channel migration by nudging, Coast. Eng., 77(0), 1–13, doi:http://dx.doi.org/10.1016/j.coastaleng.2013.02.004, 2013.

Common Wadden Sea Secretariat: Nomination of the Dutch-German Wadden Sea as World Heritage Site, Wilhelmshaven, Germany. [online] Available from: http://www.waddensea-secretariat.org/sites/default/files/downloads/whs-final-dossier08-01-16.pdf, 2008.

Cuneo, P. S. and Flemming, B. W.: Quantifying concentration and flux of suspended particulate matter through a tidal inlet of the East Frisian Wadden sea by acoustic doppler current profiling, in: Proceedings in Marine Science, Muddy Coast Dynamics and Resource Management, Elsevier, 2, 39–52, doi:10.1016/S1568-2692(00)80005-4, 2000.

Davis, R. Jr. and FitzGerald, D. (Eds.): Beaches and Coasts, 4th Edn., John Wiley & Sons, Oxford, UK, 2009. Deltares: User manual Delft-3D FLOW, online available from: www.deltares.nl (last access: December 2011), 2011.

De Swart, H. E. and Zimmerman, J. T. F.: Morphodynamics of Tidal Inlet Systems, Annu. Rev. Fluid Mech., 41, 203–229, doi:10.1146/annurev.fluid.010908.165159, 2009.

De Swart, H. E. and Volp, N. D.: Effects of hypsometry on the morphodynamic stability of single and multiple tidal inlet systems, J. Sea Res., 74(0), 35–44, doi:http://dx.doi.org/10.1016/j.seares.2012.05.008, 2012.

Deltares: User manual Delft-3D FLOW, [online] Available from: www.deltares.nl, 2011.

Dissanayake, D. M. P. K., Roelvink, J. a. and van der Wegen, M.: Modelled channel patterns in a schematized tidal inlet, Coast. Eng., 56(11-12), 1069–1083, doi:10.1016/j.coastaleng.2009.08.008, 2009.

Dissanayake, D. M. P. K., Ranasinghe, R. and Roelvink, J. A.: The morphological response of large tidal inlet/basin systems to relative sea level rise, Clim. Change, 113(2), 253–276, doi:10.1007/s10584-012-0402-z, 2012.

Dodet, G., Bertin, X., Bruneau, N., Fortunato, A. B., Nahon, A., and Roland, A.: Wave-current interactions in a wave-dominated tidal inlet, J. Geophys. Res.-Oceans, 118, 1587–1605, doi:10.1002/jgrc.20146, 2013.

Douvere, F.: The importance of marine spatial planning in advancing ecosystem-based sea use management, Mar. Policy, 32(5), 762–771, doi:http://dx.doi.org/10.1016/j.marpol.2008.03.021, 2008.

Duran-Matute, M., Gerkema, T., de Boer, G. J., Nauw, J. J. and Gräwe, U.: Residual circulation and fresh-water transport in the Dutch Wadden Sea: a numerical modeling study, Ocean Sci. Discuss., 11(1), 197–257, doi:10.5194/osd-11-197-2014, 2014.

Elias, E. P. L., Cleveringa, J., Buijsman, M. C., Roelvink, J. a. and Stive, M. J. F.: Field and model data analysis of sand transport patterns in Texel Tidal inlet (the Netherlands), Coast. Eng., 53(5-6), 505–529, doi:10.1016/j.coastaleng.2005.11.006, 2006a.

Elias, E. P. L. and van der Spek, A. J. F.: Long-term morphodynamic evolution of Texel Inlet and its ebb-tidal delta (The Netherlands), Mar. Geol., 225(1–4), 5–21, doi:http://dx.doi.org/10.1016/j.margeo.2005.09.008, 2006b.

Elias, E. P. L., Gelfenbaum, G., and Van der Westhuysen, A. J.: Validation of a coupled wave-flow model in a high-energy setting: The mouth of the Columbia River, J. Geophys. Res.-Oceans, 117, C09011, doi:10.1029/2012JC008105, 2012.

Elias, E. P. L. and Hansen, J. E.: Understanding processes controlling sediment transports at the mouth of a highly energetic inlet system (San Francisco Bay, CA), Mar. Geol., 345(0), 207–220, doi:http://dx.doi.org/10.1016/j.margeo.2012.07.003, 2013.

Escoffier, F. F.: The stability of tidal inlets, Shore and Beach, 8(4), 114–115, 1940.

Figge, K.: Karte der Sedimentverteilung in der Deutschen Bucht, Nordsee. , Karte Nr. 2900., Hamburg., 1981.

Finley, R. J.: Ebb-tidal delta morphology and sediment supply in relation to seasonal wave energy flux, North Inlet, South Carolina, J. Sediment. Res., 48, 227–238, doi:10.1306/212F743C-2B24-11D7-8648000102C1865D, 1978.

FitzGerald, D. M., Nummedal, D., and Kana, T. W.: Sand circulation pattern at Price Inlet, South Carolina, in: 15th Conference on Coastal Engineering, Honolulu, Hawaii, 1976.

FitzGerald, D. M.: Sediment bypassing at mixed energy tidal inlets, in: Proceedings of the 18th International Conference on Coastal Engineering, 14–19 November 1982, Cape Town, South Africa, 1094–1118, 1982.

FitzGerald, D. M., Penland, S., and Nummedal, D. A. G.: Control of barrier island shape by inlet sediment bypassing: East Frisian Islands, West Germany, Develop. Sediment., 39, 355–376, doi:10.1016/S0070-4571(08)70154-7, 1984a.

FitzGerald, D. M.: Interactions between the ebb-tidal delta and landward shoreline; Price Inlet, South Carolina, J. Sediment. Res., 54, 1303–1318, doi:10.1306/212F85C6-2B24-11D7-8648000102C1865D, 1984b.

FitzGerald, D. M. and Penland, S.: Backbarrier dynamics of the East Friesian Islands, J. Sediment. Res., 57, 746–754, doi:10.1306/212f8bf7-2b24-11d7-8648000102c1865d, 1987.

FitzGerald, D. M.: Shoreline erosional-depositional processes associated with tidal inlets, Lect. Notes Coast. Estuar. Stud., 29, 186–225, doi:10.1029/LN029p0186, 1988.

FitzGerald, D. M., Buynevich, I., and Hein, C.: Morphodynamics and Facies Architecture of Tidal Inlets and Tidal Deltas, in: Principles of Tidal Sedimentology SE 12, edited by: Davis Jr., R. A. and Dalrymple, R. W., Springer, Netherlands, 301–333, 2012.

Flemming, B. W. and Davis, R. A.: Holocene Evolution, Morphodynamics and Sedimentology of the Spiekeroog Barrier Island System (Southern North Sea), Senckenbergiana maritima, 24, 1994.

Flemming, B. W. and Nyandwi, N.: Land reclamation as a cause of fine-grained sediment depletion in backbarrier tidal flats (southern North Sea), Netherl. J. Aquat. Ecol., 28(3-4), 299–307, 1994.

Flemming, B. and Bartholomä, A.: Response of the Wadden Sea to a rising sea level: a predictive empirical model, Dtsch. Hydrogr. Zeitschrift, 49(2-3), 343–353, doi:10.1007/BF02764043, 1997.

Flöser, G., Burchard, H. and Riethmüller, R.: Observational evidence for estuarine circulation in the German Wadden Sea, Cont. Shelf Res., 31(16), 1633–1639, doi:http://dx.doi.org/10.1016/j.csr.2011.03.014, 2011.

Fredsøe, J.: Turbulent boundary layer in wave-current motion, J. Hydraul. Eng., 110, 1103–1120, 1984.

Gaye, J. and Walther, F.: Die Wanderung der Sandriffe vor den ostfriesischen Inseln, Bautechnik, 41, 1–13, 1935; cited in Hanisch, J.: Sand transport in the tidal inlet between Wangerooge and Spiekeroog (W. Germany), Holocene Mar. Sediment. North Sea Basin Spec. Publ. 5 IAS, 35, 175–185, 1981.

Gibbs, R. J., Matthews, M. D., and Link, D. A.: The relationship between sphere size and settling velocity, J. Sediment. Res., 41, 7–18, doi:10.1306/74D721D0-2B21-11D7-8648000102C1865D, 1971.

Grunwald, M., Dellwig, O., Kohlmeier, C., Kowalski, N., Beck, M., Badewien, T. H., Kotzur, S., Liebezeit, G. and Brumsack, H.-J.: Nutrient dynamics in a back barrier tidal basin of the Southern North Sea: Time-series, model simulations, and budget estimates, J. Sea Res., 64(3), 199–212, 2010.

Hageman, B. P.: Development of the western part of the Netherlands during the Holocene, Geol. en Mijnb., 48, 373–388, 1969.

Hanisch, J.: Sand transport in the tidal inlet between Wangerooge and Spiekeroog (W. Germany), Holocene Mar. Sediment. North Sea Basin Spec. Publ. 5, IAS, 35, 175–185, 1981.

Hayes, M. O.: Morphology of sand accumulation in estuaries: an introduction to the symposium, edited by: Cronin, L. E., Estuar. Res., 2, 3–22, 1975.

Hayes, M. O.: Barrier island morphology as a function of tidal and wave regime, in: Barrier islands, from the Gulf of St. Lawrence to the Gulf of Mexico, edited by: Leatherman, S., Academic Press, New York, 1–27, 1979.

Hench, J. L. and Luettich, R. A.: Transient Tidal Circulation and Momentum Balances at a Shallow Inlet, J. Phys. Oceanogr., 33, 913–932, 2003.

Herman, A.: Numerical modelling of water transport processes in partially-connected tidal basins, Coast. Eng., 54(4), 297–320, doi:http://dx.doi.org/10.1016/j.coastaleng.2006.10.003, 2007.

Herrling, G. and Elsebach, J.: Assessment criteria for the identification of human impacts on water bodies by morphodynamic investigations, Coast. Eng. Proc., 5(31), 4620–4632, 2008.

Herrling, G., Knaack, H., Kaiser, R. and Niemeyer, H. D.: Evaluation of design water levels at the Ems-Dollard estuary considering the effect of a storm surge barrier, Coast. Eng. Proc., 1(32), doi:http://dx.doi.org/10.9753/icce.v32.management.43, 2011.

Herrling, G. and Winter, C.: Morphological and sedimentological response of a mixed-energy barrier island tidal inlet to storm and fair-weather conditions, Earth Surf. Dyn., 2(1), 363–382, doi:10.5194/esurf-2-363-2014, 2014.

Homeier, H. and Kramer, J.: Verlagerung der Platen im Riffbogen vor Norderney und ihre Anlandung an den Strand, Jahresber. d. Forschungsst. f. Insel- u. Küstenschutz, 8, 1957; cited in Hanisch, J.: Sand transport in the tidal inlet between Wangerooge and Spiekeroog (W. Germany), Holocene Mar. Sediment. North Sea Basin Spec. Publ. 5 IAS, 35, 175–185, 1981.

Hubbard, D. K., Oertel, G., and Nummedal, D.: The role of waves and tidal currents in the development of tidal-inlet sedimentary structures and sand body geometry; examples from North Carolina, South Carolina, and Georgia, J. Sediment. Res., 49, 1073–1091, doi:10.1306/212F78B5-2B24-11D7-8648000102C1865D, 1979.

Isobe, M. and Horikawa, K.: Study on water particle velocities of shoaling and breaking waves, Coastal Engineering in Japan, 25, 109–123, 1982.

Kaiser, R., Niemeyer, H. D., Dirks, H., and Witting, M.: KFKI-Projekt DÜNEROS, Schlussbericht 03KIS063, Norderney, 2008.

Kohlmeier, C. and Ebenhöh, W.: Modelling the ecosystem dynamics and nutrient cycling of the Spiekeroog back barrier system with a coupled Euler–Lagrange model on the base of ERSEM, Ecol. Modell., 202(3), 297–310, 2007.

Kohlmeier, C. and Ebenhöh, W.: Modelling the biogeochemistry of a tidal flat ecosystem with EcoTiM, Ocean Dyn., 59(2), 393–415, doi:10.1007/s10236-009-0188-3, 2009.

Komar, P. D.: Tidal-Inlet Processes and Morphology Related to the Transport of Sediments, J. Coast. Res., 23, 23–45, 1996.

Kragtwijk, N. G., Zitman, T. J., Stive, M. J. F. and Wang, Z. B.: Morphological response of tidal basins to human interventions, Coast. Eng., 51, 207–221, doi:http://dx.doi.org/10.1016/j.coastaleng.2003.12.008, 2004.

Kwoll, E. and Winter, C.: Determination of the initial grain size distribution in a tidal inlet by means of numerical modelling, J. Coast. Res., 64, 1081–1085, 2011.

Lane, A., Riethmuller, R., Herbers, D., Rybaczok, P., Gunther, H., Baumert, H., and Riethmüller, R.: Observational data sets for model development, Coast. Eng., 41, 125–153, doi:10.1016/S0378-3839(00)00029-6, 2000.

Lassen, H. and Siefert, W.: Mittlere Tidewasserstände in der südöstlichen Nordsee - säkularer Trend und Verhältnisse um 1980, Die Küste, 52, 85–137, 1991.

Lesser, G. R., Roelvink, J. A., van Kester, J. A. T. M., and Stelling, G. S.: Development and validation of a three-dimensional morphological model, Coast. Eng.,51, 883–915, doi:10.1016/j.coastaleng.2004.07.014, 2004.

Longuet-Higgins, M. S. and Stewart, R. W.: Radiation stresses in water waves; a physical discussion, with applications, Deep-Sea Res., 11, 529–562, 1964.

Li, C.: Subtidal water flux through a multiple-inlet system: Observations before and during a cold front event and numerical experiments, J. Geophys. Res. Ocean., 118(4), 1877–1892, doi:10.1002/jgrc.20149, 2013.

Liu, J. T. and Aubrey, D. G.: Tidal Residual Currents and Sediment Transport Through Multiple Tidal Inlets, in Formation and Evolution of Multiple Tidal Inlets, pp. 113–157, American Geophysical Union., 1993.

Luck, G.: Inlet Changes of the Eastfrisian Islands, Coast. Eng. Proc., 1(15), 1976.

Luck, G.: Der Einfluss der Schutzwerke der ostfriesischen Inseln auf die morphologischen Vorgange im Bereich der Seegaten und ihre Einzugsgebiete, Mitt. Leichtweiss Inst., Braunschweig, 47, 1–22, 1975; cited in Hanisch, J.: Sand transport in the tidal inlet between Wangerooge and Spiekeroog (W. Germany), Holocene Mar. Sediment. North Sea Basin Spec. Publ. 5 IAS, 35, 175–185, 1981.

Ludwig, G., Müller, H. and Streif, H.: New Dates on Holocene Sea-Level Changes in the German Bight, Holocene Mar. Sediment. North Sea Basin, 211–219, 1981.

Nahon, A., Bertin, X., Fortunato, A. B., and Oliveira, A.: Process-based 2DH morphodynamic modeling of tidal inlets: A comparison with empirical classifications and theories, Mar. Geol., 291, 1–11, doi:10.1016/j.margeo.2011.10.001, 2012.

Niedoroda, A. W., Swift, D. J. P., Hopkins, T. S., and Ma, C.- M.: Shoreface morphodynamics on wave-dominated coasts, Mar. Geol., 60, 331–354, doi:10.1016/0025-3227(84)90156-7, 1984.

Noormets, R., Ernstsen, V. B., Bartholomä, A., Flemming, B. W., and Hebbeln, D.: Implications of bedform dimensions for the prediction of local scour in tidal inlets: a case study from the southern North Sea, Geo-Mar. Lett., 26, 165–176, doi:10.1007/s00367-006-0029-z, 2006.

Nummedal, D. and Penland, S.: Sediment dispersal in Norderneyer Seegat, West Germany, Sedimentology, 5, 187–210, 1981.

O'Brien, M. P.: Estuary tidal prisms related to entrance areas, Civ. Eng., 1(8), 738–739, 1931.

O'Brien, M. P.: Equilibrium flow areas of tidal inlets on sandy coasts, Coast. Eng. Proc., 1(10), 1966.

Oertel, G. F.: Processes of sediment exchange between tidal inlets, ebb deltas and barrier islands, in Hydrodynamics and sediment dynamics of tidal inlets, pp. 297–318, Springer., 1988.

Onken, R., Callies, U., Vaessen, B., and Riethmüller, R.: Indirect determination of the heat budget of tidal flats, Cont. Shelf Res., 27, 1656–1676, doi:10.1016/j.csr.2007.01.029, 2007.

Outzen, O., Herklotz, K., Heinrich, H., and Lefebvre, C: Extreme waves at FINO 1 research platform caused by storm 'Tilo' on 9 November 2007, DEWI Mag., 33, 17–23, 2008.

Pawlowicz, R., Beardsley, B. and Lentz, S.: Classical tidal harmonic analysis including error estimates in MATLAB using TDE, Comput. Geosci., 28, 929–937, doi:10.1016/S0098-3004(02)00013-4, 2002.

Postma, H.: Transport and accumulation of suspended matter in the Dutch Wadden Sea, Netherlands J. Sea Res., 1(1), 148–190, 1961.

Ridderinkhof, H.: Tidal and residual flows in the Western Dutch Wadden Sea I: Numerical model results, Netherlands J. Sea Res., 22(1), 1–21, doi:http://dx.doi.org/10.1016/0077-7579(88)90049-X, 1988a.

Ridderinkhof, H.: Tidal and residual flows in the Western Dutch Wadden Sea II: an analytical model to study the constant flow between connected tidal basins, Netherlands J. sea Res., 22(3), 185–198, 1988b.

Ris, R. C., Holthuijsen, L. H., and Booij, N.: A third-generation wave model for coastal regions 2. Verification, J. Geophys. Res., 104, 7667–7681, doi:10.1029/1998JC900123, 1999.

Rodi, W.: Turbulence models and their application in hydraulics, a state of the art review, International Association of Hydraulics Research, Delft, the Netherlands, 1984.

Roelvink, J. A.: Coastal morphodynamic evolution techniques, Coast. Eng., 53, 277–287, doi:10.1016/j.coastaleng.2005.10.015, 2006.

Rupert, D., Aden, L. and Maarfeld, S.: Ermittlung von Abflüssen über Siel- und Pumpmengen in Ostfriesland, Aurich., 2004.

Salles, P., Voulgaris, G. and Aubrey, D. G.: Contribution of nonlinear mechanisms in the persistence of multiple tidal inlet systems, Estuar. Coast. Shelf Sci., 65(3), 475–491, doi:http://dx.doi.org/10.1016/j.ecss.2005.06.018, 2005.

Schneggenburger, C., Günther, H., and Rosenthal, W.: Spectral wave modelling with non-linear dissipation: Validation and applications in a coastal tidal environment, Coast. Eng., 41, 201–235, doi:10.1016/S0378-3839(00)00033-8, 2000.

Sha, L. P.: Variation in ebb-delta morphologies along the West and East Frisian Islands, The Netherlands and Germany, Mar. Geol., 89, 11–28, doi:10.1016/0025-3227(89)90025-X, 1989.

Sha, L. P.: Surface sediments and sequence models in the ebb-tidal delta of Texel Inlet, Wadden Sea, The Netherlands, Sediment. Geol., 68, 125–141, doi:10.1016/0037-0738(90)90123-B, 1990.

Sha, L. P. and Van Den Berg, J. H.: Variation in Ebb-Tidal Delta Geometry along the Coast of the Netherlands and the German Bight, J. Coast. Res., 9, 730–746, 1993.

Smith, S. D. and Banke, E. G.: Variation of the sea surface drag coefficient with wind speed, Q. J. R. Meteorol. Soc., 101(429), 665–673, 1975.

Smith, J. B. and FitzGerald, D. M.: Sediment Transport Patterns at the Essex River Inlet Ebb-Tidal Delta, Massachusetts, USA, J. Coast. Res., 10, 752–774, 1994.

Son, C. S., Flemming, B. W., and Bartholomä, A.: Evidence for sediment recirculation on an ebb-tidal delta of the East Frisian barrier-island system, southern North Sea, Geo-Mar. Lett., 31, 87–100, doi:10.1007/s00367-010-0217-8, 2010.

Soulsby, R. L., Hamm, L., Klopman, G., Myrhaug, D., Simons, R. R., and Thomas, G. P.: Wave-current interaction within and outside the bottom boundary layer, Coast. Eng., 21, 41–69, 1993.

Stanev, E. V., Wolff, J.-O., Burchard, H., Bolding, K. and Flöser, G.: On the circulation in the East Frisian Wadden Sea: numerical modeling and data analysis, Ocean Dyn., 53(1), 27–51, doi:10.1007/s10236-002-0022-7, 2003.

Van de Kreeke, J.: Can multiple tidal inlets be stable?, Estuar. Coast. Shelf Sci., 30(3), 261–273, doi:http://dx.doi.org/10.1016/0272-7714(90)90051-R, 1990a.

Van de Kreeke, J.: Stability analysis of a two-inlet bay system, Coast. Eng., 14(6), 481–497, doi:http://dx.doi.org/10.1016/0378-3839(90)90031-Q, 1990b.

Van de Kreeke, J.: Equilibrium and cross-sectional stability of tidal inlets: application to the Frisian Inlet before and after basin reduction, Coast. Eng., 51(5–6), 337–350, doi:http://dx.doi.org/10.1016/j.coastaleng.2004.05.002, 2004.

Van de Kreeke, J., Brouwer, R. L., Zitman, T. J. and Schuttelaars, H. M.: The effect of a topographic high on the morphological stability of a two-inlet bay system, Coast. Eng., 55(4), 319–332, doi:http://dx.doi.org/10.1016/j.coastaleng.2007.11.010, 2008.

Van de Kreeke, J. and Cotter, D. C.: Tide-induced mass transport in lagoon-inlet systems, Coast. Eng. Proc., 1(14), 1974.

Van der Wegen, M. and Roelvink, J. A.: Reproduction of estuarine bathymetry by means of a process-based model: Western Scheldt case study, the Netherlands, Geomorphology, 179, 152–167, doi:10.1016/j.geomorph.2012.08.007, 2012.

Van der Wegen, M., Dastgheib, A., Jaffe, B. E., and Roelvink, D.: Bed composition generation for morphodynamic modeling: case study of San Pablo Bay in California, USA, Ocean Dynam., 61, 173–186, doi:10.1007/s10236-010-0314-2, 2011a.

Van der Wegen, M., Jaffe, B. E., and Roelvink, J. A.: Process-based, morphodynamic hindcast of decadal deposition patterns in San Pablo Bay, California, 1856–1887, J. Geophys. Res.-Earth, 116, F02008, doi:10.1029/2009JF001614, 2011b.

Van der Westhuysen, A. J.: Advances in the spectral modelling of wind waves in the nearshore, Delft University of Technology, Delft, the Netherlands, 207 pp., 2007.

Van der Westhuysen, A. J.: Spectral modeling of wave dissipation on negative current gradients, Coast. Eng., 68, 17–30, doi:10.1016/j.coastaleng.2012.05.001, 2012.

Van Lancker, V., Lanckneus, J., Hearn, S., Hoekstra, P., Levoy, F., Miles, J., Moerkerke, G., Monfort, O., and Whitehouse, R.: Coastal and nearshore morphology, bedforms and sediment transport pathways at Teignmouth (UK), Cont. Shelf Res., 24, 1171–1202, doi:10.1016/j.csr.2004.03.003, 2004.

Van Rijn, L. C.: Principles of sediment transport in rivers, estuaries and coastal seas, Aqua publications, Amsterdam, the Netherlands, 1993.

Van Rijn, L. C.: General view on sand transport by currents and waves: data analysis and engineering modelling for uniform and graded sand, Report Z28, Deltares (WL), Delft, the Netherlands, 2000.

Van Rijn, L. C.: Sand transport by currents and waves; general approximation formulae, in: Proceedings of the International Conference on Coastal Sediments, 18–23 May 2003, Clearwater Beach, Florida, USA, vol. 3, 2003.

Van Rijn, L. C., Walstra, D. J. R., and Van Ormondt, M.: Description of TRANSPOR2004 and implementation in Delft3D-ONLINE, Interim Rep. Prep. DG Rijkswaterstaat, Rijksinst, voor Kust en Zee, Delft Hydraul. Institute, Delft, the Netherlands, 2004.

Van Straaten, L. M. J. U. and Kuenen, P. H.: Accumulation of fine grained sediments in the Dutch Wadden Sea, Geol. en Mijnb., 19, 329–354, 1957.

Verboom, G. K., de Ronde, J. G., and van Dijk, R. P.: A fine grid tidal flow and storm surge model of the North Sea, Cont. Shelf Res., 12, 213–233, doi:10.1016/0278-4343(92)90030-N, 1992.

Walstra, D. J. R., Roelvink, J. A., and Groeneweg, J.: Calculation of Wave-Driven Currents in a 3D Mean Flow Model, in: Coastal Engineering, American Society of Civil Engineers, Reston, VA, 1050–1063, 2000.

Walton, T. L. and Adams, W. D.: Capacity of Inlet Outer Ears to Store Sand, Coast. Eng. Proc., 1(15), 1976.

Wang, Z. B., Hoekstra, P., Burchard, H., Ridderinkhof, H., De Swart, H. E. and Stive, M. J. F.: Morphodynamics of the Wadden Sea and its barrier island system, Ocean Coast. Manag., 68, 39–57, doi:10.1016/j.ocecoaman.2011.12.022, 2012.